TERAHERTZ PHOTONIC CRYSTAL MICROFLUIDIC SENSORS

By

Laura Cecilia Acosta Silveira

A THESIS

Submitted to
Michigan State University
in partial fulfillment of the requirements
for the degree of

Electrical Engineering – Master of Science

2014

ABSTRACT

TERAHERTZ PHOTONIC CRYSTAL MICROFLUIDIC SENSORS

By

Laura Cecilia Acosta Silveira

Challenges associated with meeting needs in the pharmaceutical industry, environment monitoring and food safety are in the interrogation of small volumes of samples with high sensitivity and specificity. The use of terahertz (THz) sensors is of significant interest due to its rich spectral content. The key focus of this research is to demonstrate THz microfluidic sensors for use in continuous flow monitoring that provide high sensitivity while using small volumes of samples. In order to achieve high sensitivity, photonic crystal (PC) based structures operating at the THz spectral region, are examined. One dimension (1D) PC devices are designed for continuous flow characterization of liquids and vapors. The same type of structure is then slightly altered with a defect layer and its effect is studied. For further improvement of the sensing capabilities a 3D PC sensor is also designed and examined. The devices are built using alternating high and low permittivity materials with characteristics (material properties and thicknesses) that regulate the THz wave through transmission. When the air region is filled with a higher permittivity sample such as a liquid or vapor, the THz wave transmission through the PC is altered. In contrast to conventional sample holders, the use of PC enhances the change in transmitted signal due to the sample being loaded into the air gaps in the PC. This sensing configuration allows for high sensitivity while using a small volume of samples. A material characterization method is developed for 1D PC based sensor in order to extract the corresponding samples dielectric properties. Details of design, fabrication and characterization of photonic crystal terahertz microfluidic sensors are presented in this thesis.

To my family for their unconditional support throughout.

ACKNOWLEDGMENTS

This journey has only been possible with the help and support of my advisor Dr. Prem Chahal, and mentor Dr. Jose Hejase, without their invaluable guidance this thesis would not have been possible, thank you for the many hours of mentoring, assistance, encouragement and support. They did not only help me through the program they were also the reason I joined the Master's program at Michigan State University. Also, a special thanks to my committee members Dr. Nelson Sepulveda and Dr. Evangeline Alocilja for their helpful discussion and for challenging me on this research topic. I am also particularly thankful to Dr. Pierce Pierre for the financial support and especially the great and valuable day to day and career advice; I will take them with me everywhere I go. Likewise, I wish to acknowledge the help provided by my peers in the research EM group, the useful discussions and assistance throughout my classes and research always influenced the outcome of both.

TABLE OF CONTENTS

LIST OF TABLES

LIST OF FIGURES

CHAPTER 1

INTRODUCTION

1.1.1 Terahertz and its Applications

Terahertz (THz) is equivalent to 10^{12} Hz, the THz spectral region ranges from 0.1 to 10 THz [1], lying in between microwaves and infrared frequencies as shown in Figure 1.

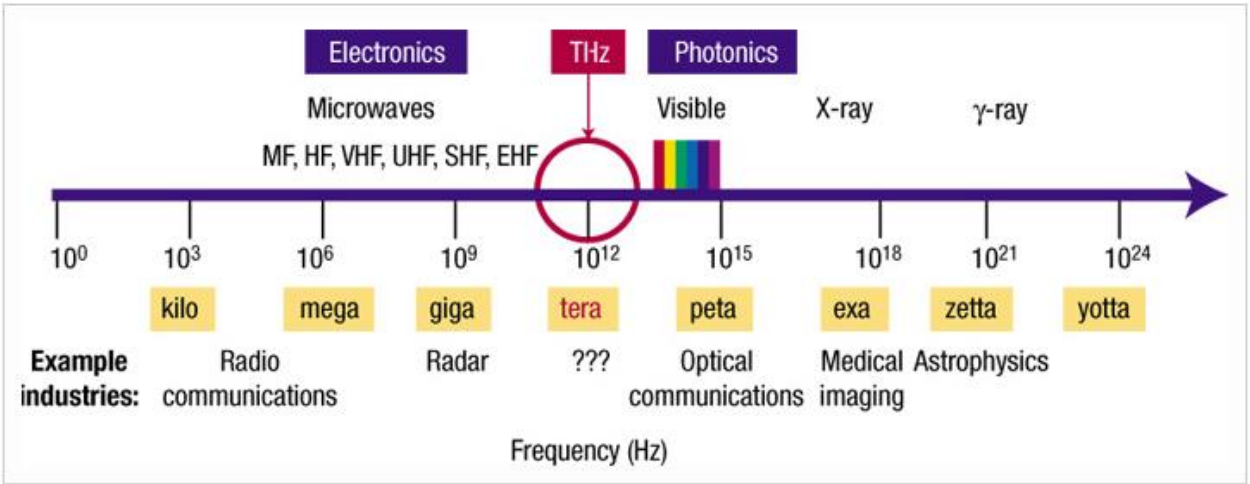

Figure 1. Frequency spectrum [1]

The THz frequency band is one of the least explored regions of the electromagnetic spectrum [2], due to the relatively recent development of the technologies used for THz radiation and detection. In part, this region of the spectrum is of interest due to its spectroscopy advantages, in particular its richness with material spectral fingerprints [2]. Other advantages include its ability to penetrate most materials, with metal and absorbing materials, like water being exceptions [3]. THz radiation is non-ionizing, thus is non-damaging to biological samples when used for their characterization [3]. Additionally, it allows for higher resolution imaging when compared to

microwaves because of its smaller wavelength [3]**.** These advantages make the THz region an ideal candidate to design a sensor capable of tracking dielectric properties in small quantities. Studies have been performed with Terahertz photons and DNA and it has been found that THz radiation is not energetic enough to break chemical bonds or ionize atoms or molecules and ordinary resonant effects will not achieve expansion of double stranded DNA, although, nonlinear resonances and extended exposure will lead to bond breakage [4-5]. However, since nonlinear stability is very unlikely due to low power generation, it has been concluded that THz is not damaging to our health. This conclusion is agreeable since the natural environment we live in is full of terahertz waves. The safety associated with the terahertz radiation, when it comes to the human body, is another reason why terahertz technology became important to understand and develop. Commercial uses for terahertz began approximately 20 years ago as the technology enabled new instrumentation and measurement systems [5-6]. The benefits that could arise in the medical and biomedical community and the opportunity of making the field available to the general public helped with the growth and study of devices that work in the terahertz spectral region [5, 7]. Other areas that will benefit from terahertz are security, pharmaceuticals, communications, defense, environment, food quality control as well other industries with the need to identify or detect unknown materials and perform nondestructive analysis [2, 5, 8]. Due to all the potential benefits with THz technology, there have been developments to overcome its limitations, those being the lack of source power (1nW-1μW) [2] and sensor technologies [9]. One approach has been the development of THz time-domain spectroscopy (TDS), TDS uses femtosecond pulse laser technology to produce and sense pulses of THz radiation as a function of time [9]. This means that the dielectric constant of a material can be measured and its frequency dependent conductivity can be found. This technology allows for the examination of

spectroscopic data as a function of depth in materials. In THz TDS, a pulse is transmitted in free space, and then the electric field of this pulse is detected, when a sample is placed between the transmitter and receiver there is delay and an attenuation seen by the receiver [9] and this is how THz technologies can be used as sensors. Tracking the delay and attenuation of the signal is the key to several sensors [10-14]. Terahertz sensors are based in transmission or waveguide techniques [15]. The time domain results can easily be converted to frequency domain by performing a Fourier transform of the data obtained in the time domain [9], allowing for the investigation of results at each frequency point. THz technology is widely used in scientific spectroscopy and commercial applications. As the power of THz sources increases this area will continue to grow, this is due to the power increase generating a higher signal to noise ratio which in turn increases the THz bandwidth, making the technology more usable to many new applications, in particular sensing [9]. Terahertz with all its advantages is a great technology that eventually will take off and help ease many aspects of medicine, security, and pharmaceutical amongst others, but as of right now the biggest disadvantage of this technology is cost and the bulkiness of the systems [2], and as mentioned before the difficulty that low power sources entail. There is work in progress to help shrink the systems as well as making them more cost effective [2] and more powerful [8].

1.1.2 Terahertz Time Domain Systems

Most terahertz sources use mode-locking femtosecond lasers to excite photoconductive switches that in turn generate THz radiation [1, 2]. The system used for measurements in this paper is one of these devices. The system has two photoconductive switches, one placed at the emitter and one at the receiver [16]. In order for the emitter to generate radiation, it needs to be excited with

a pump laser with very short pulse [16]. The receiver switch then detects the radiation, when triggered by another gate laser pulse delivered through the time delay fixture [16]. Measurements of transmission and reflection mode can be achieved by switching the locations of the transmitter and the receiver [16], in other words, TDS enables the calculation of complex refractive index as well as complex dielectric properties of materials by obtaining both the amplitude and the phase spectrums of the terahertz wave [2]. A typical Terahertz time domain system has reliable data between 100GHz and 2.5THz [16]. Figures 2 and 3 show the measurement setup of reflection mode and transmission mode respectively.

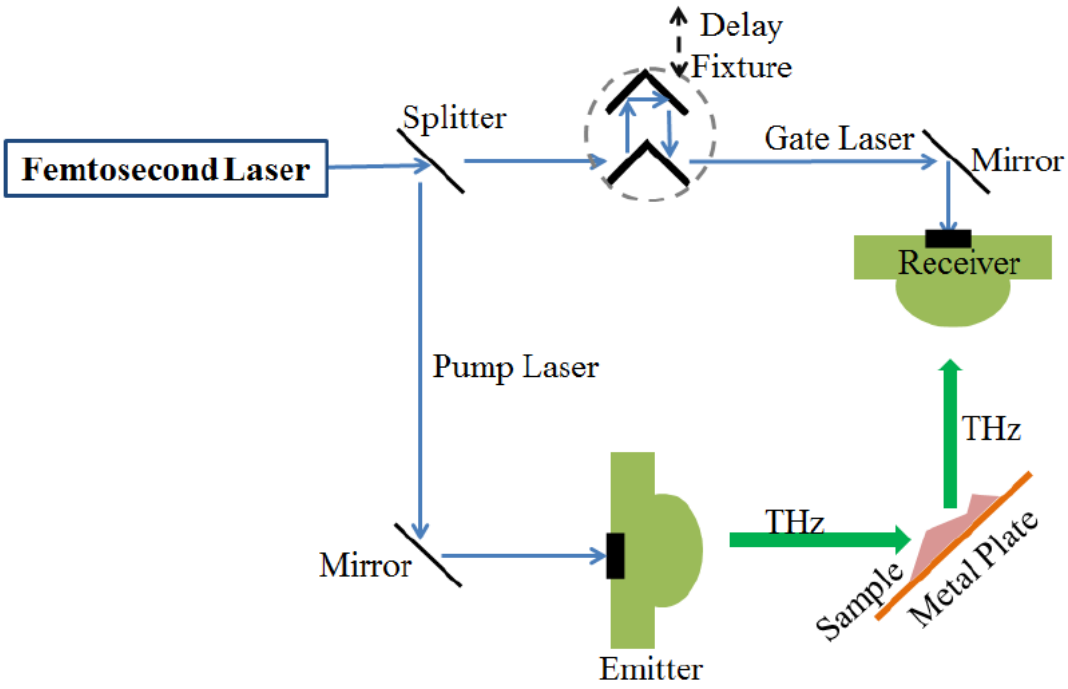

Figure 2. THz time domain system setup for reflection mode [16]

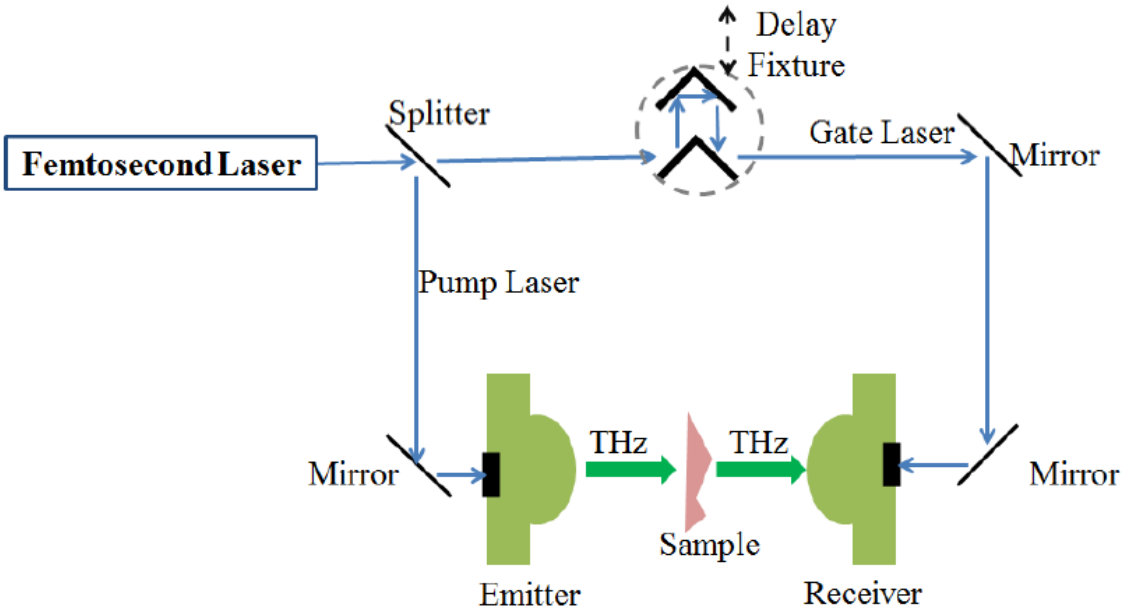

Figure 3. THz time domain system setup for transmission mode [16]

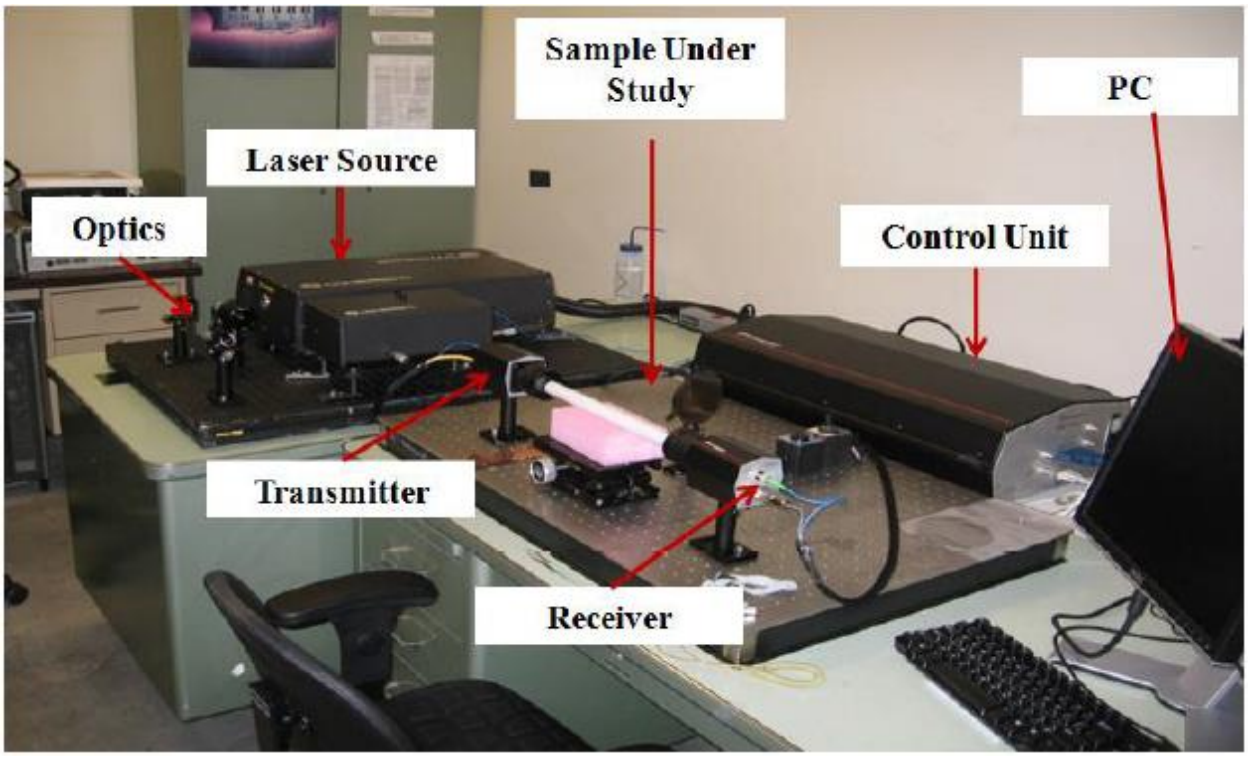

Figure 4. T-ray 2000 time domain THz system [16]

Throughout this paper all measurements are done using the T-ray 2000 machine shown above in Figure 4 and using the transmission mode technique shown in Figure 2.

1.2.1 Photonic Crystal

A crystal is a set of atoms or molecules that are arranged periodically [17]. The crystal conductivity is determined by two different factors, the lattice, which is the organization of the atoms, and the periodic potential of the crystal to an electron propagating through it [17]. In a conductive crystal, electrons travel as waves and do not scatter unless there is a defect in the periodicity or impurity in the material. The lattice of the crystal can also impede the propagation of some waves, forming a gap in the energy band of the crystals [17]. At times this constraint could cause a complete band gap, inhibiting electron propagation [17]. A Photonic Crystal (PC) band gap has the same principle, it occurs by alternating microscopic dielectric materials that are low loss. The periodicity on the material slows down the light but does not reflect it [18]. If the electromagnetic wave absorption is minimal then the refraction and reflection of the wave will produce the same phenomena with light modes as the atomic potential produces for electrons in a semiconductor [17]. These light modes or photons are the basic units of light and of other electromagnetic radiation, photons carry electromagnetic force. The behavior of the electromagnetic wave transmission, due to the photonic crystal devices, is examined in order to study properties of materials, and these devices can be used as sensors. A mode is the wavelength of light that can pass through a medium; a photonic bang gap is then a band of wavelengths that are not allowed to pass through this medium.

One of the advantages of photonic crystals is that they can be manipulated to travel at certain frequencies and direction by using the right materials and periodicity to block the light, or

electromagnetic waves in this case. The second advantage is that there is no limitation to the designs, unlike lattices of atoms which are fixed, here any design will produce a photonic crystal band gap as long as there is periodicity [19] only restricted by the materials used and frequency range of study. The third and fourth advantage is real time detection, cost reduction [20].

Photonic crystals can be one dimensional, two dimensional or three dimensional, this means there are periodic low loss dielectrics contained in one, two or three directions [17], see Figure 5 for reference. In other words, the periodicity contained in one of the x, y or z axis, with other axes being homogenous institutes of a one dimensional (1D) photonic crystal, while in a two dimensional (2D) photonic crystals, the periodicity is contained in the x and y axis, x and z axis or y and z axis while the remaining axis is homogenous. For a three dimensional photonic crystal the periodicity is contained in all three x, y and z axes.

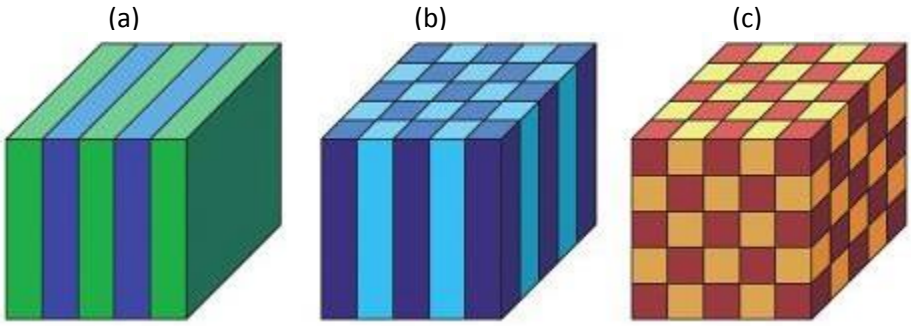

Figure 5. Examples of 1D (a), 2D (b) and 3D (c) photonic crystals. Defined by their periodicity along one or more axis [17]

A one dimensional structure can simply be stacked layers of high and low permittivity materials in only one direction [13, 20, 21-25], a 2D structure can be accomplished by either making periodic holes or by adding periodic rods to a solid surface structure [20, 26-32]. A 3D PC structure can be constructed by using a woodpile like structures [26, 33-36] or some form of Yablonovite structure [19].

In the case of a 1D PC the wavelength travels differently inside and outside of the band gap. In a 1D PC, within the band gap the wave entering the material will constructively destruct, while the wavelength outside the band gap will propagate through the material [19]. In a 2D PC each unit cell produces reflected waves will combine to cancel out the incident wave in two directions, while the same behavior is observed in a 3D structure but in all three directions [19].

By introducing defects or imperfections into the periodicity of the layers or by changing the dielectric medium in place of air photonic crystals can be used as sensors [14, 20, 23-25]. In the case of defects, the movement of the defects in the signal with respect to frequency is used for sensing when different liquids or gasses are introduced into the structures in place of the air medium (low dielectric constant). This can be achieved by using properties of cavity, waveguides, dielectric mirrors, spectroscopic absorption, resonance property, surface electromagnetic waves, diffraction characteristics and photonic bandgap properties and displacement [17, 37-38].

Photonic crystals can be designed to work in different frequency ranges, including microwave, terahertz and optics. Some applications of photonic crystals are healthcare, defense, security, automotive, aerospace, environment, food quality control amongst other [20]. Microfluidics integrated photonic crystals are devices that can be characterized lab on cheap, they are highly sensitive and selective, stable and immune to electromagnetic interference, they are also compact, low cost and allow for real time fast detections [20]. Photonic crystal sensors can detect particles, gases, chemical and biological molecules, proteins viruses and liquids amongst others [20].

After having a basic understanding of photonic crystal and its application in a wide range of frequencies, it is time to turn our attention to sensors based on the characteristics explained

above. The behavior of the photonic crystals can be used for many different sensor applications [13-14, 21-22, 26-28, 33-34, 37-39]. For the design of sensors there is a need to achieve high signal to noise ratio. In a photonic crystal structure the band stop region is sensitive to dielectric constant ratio between the high and low dielectric constant values of the layers. Contrast in dielectric constants directly affects the center frequency of the PC filter. It also directly affects the rejection ratio.

It can be concluded that photonic crystal is very advantageous due to its flexibility in design, and range of frequencies where it can be used, while one of the main disadvantage is the current difficulty constructing 3D photonic crystal devices. Photonic crystals can be used as resonant cavities by trapping lights in a defect, as waveguides by adding a defect in which the light or electromagnetic wave will be guided through, as devices by combining the resonant cavity and the waveguide and they can be used as sensors by tracking changes in transmission when materials are introduced into the PC device.

Photonic crystal sensors are usually compact, sensitive, quick response, biocompatible if the right material is used and have good resolution [25, 38, 40]. The most common PC sensors work by measuring the output power and the wavelength shift in transmission [20] spectrum with introduction of material (liquid, gas, biomaterial).

The 1D structures in this thesis are all based on quarter wave stack, constructed by alternating high and low dielectric materials with low loss. The designs consist of choosing a range of frequency which needs to block the waves from passing at certain frequencies in the terahertz range and designing $v/f = \lambda/4$ with $v = c/\sqrt{\varepsilon}$, in which v is the velocity, f is the frequency, λ the wavelength and c the speed of light ($c = 3x10^8 m/s$). The 3D sensor design

was based on [33] and scaled to work at approximately 290GHz and to use the material properties needed for fabrication with 3D printing.

1.2.2 Photonic Crystal Devices

Microfluidic devices for studying chemical samples under continuous flow are particularly useful in the pharmaceutical (drug discovery), security and chemical industries [41]. In these industries, chemicals and agents are mixed in the process of discovery over many trials. Thus, the ability to monitor small quantities of chemical mixtures under continuous flow would prove to be cost and space saving amongst other benefits mentioned above. The principals behind these sensors are the ability to measure output power and wavelength shift in transmission spectrum [38]. Sensors that use the characteristics of displacement include pressure, switching and actuation sensors [38]. By minimally displacing the photonic slabs, the transmission and reflection coefficients through the structure will change, tracking these changes is one of the sensing principle used in photonic crystal devices [38]. Surface Plasmon resonance happens when the energy transfer between the surface Plasmon's and a wave resonates, producing large response in the output energy [38]. Most biosensors are based on the tracking changes in the refractive index, when air is replaced by another material, i.e. by changing speed of light by $1/\sqrt{\varepsilon}$, with ε being the dielectric constant of the material properties of the substance being used [30]. Photonic crystal devices are very sensitive to changes in the empty medium of the device [25, 38, 42].

Different photonic crystal sensors have been studied [13, 27, 31, 38-39, 42-44]. These sensors are designed to be used at different ranges in frequency from microwave to optics. Some of the challenges encountered are how to improve sensitivity, sensing with smaller volume materials

(i.e microfluidic, nanofluidic quantities), fast response, compactness and low cost and depending on the application the design needs to be chosen to work at the right frequency spectra.

All of these challenges combined with constant new needs and discoveries have permitted researchers to have novel designs. A good sensor design will mean that the device is always sensitive to what is being measured and insensitive to any outside influence. A second property of a well-designed sensor is that the device will never influence the materials being tested. Keeping these characteristics in mind we proceeded to design 1D and a 3D sensor that are discussed in chapter 2 and 3.

Until now there is limited research done with photonic crystal sensor that work at the terahertz spectra [13-14, 25, 39], however there has been more focused research done in 1D [13, 23-24], 2D [29-32, 45] and 3D [35-36] photonic crystal structures at this frequency spectra that with a little more work could be applied to PC sensors in the THz spectral region.

1.3 Motivation and Objectives

The motivation behind this thesis in general and this sensor design activity in specific is multifaceted. There is a need to design a micro-fluidic sensing device that will work in one of the least explored frequency ranges of the electromagnetic spectrum, THz. Though many micro-fluidic sensing devices already exist [46-50], amongst others, one goal of this thesis was to make functional sensors characterized by easy to fabricate designs, compactness and cost effectiveness. In addition to this, the sensors need to be microfluidic in order to use only small amounts of samples to carry out the testing. The use of small amounts of samples has great potential benefits to many industries, in particular chemical and pharmaceutical for cost saving due to the wide scope testing carried out there. 1D devices will be designed and improved upon

each other for proof of concept, this devices will not only behave as a sensor (forward problem solution) but the collected data can be turned around and used for material characterization at individual frequencies. The material characterization will be done using several liquids and gasses (inverse problem solution). This design is fabricated, tested, and its performance analyzed from simulated and measured data.

Building upon the demonstrated 1D solution; a further sensor improvement is presented in the form of a 3D photonic crystal sensor. A 3D photonic crystal sensor adds more features to the design performance thus making it a more sensitive structure. Another advantage to this design is in the ease of its fabrication using 3D printing. The 3D device is designed and its expected behavior is shown through simulations. The device was fabricated and experimental results are shown and discussed. The novelty of this design lies in the use of 3D printing to fabricate a highly sensitive photonic crystal based micro-fluidic THz sensor. In this thesis we are investigating the blends of newly explore fronts: Terahertz and 3D printing, combined with the well-known and useful photonic crystals and microfluidics applications.

1.4 Thesis Layout

This thesis proceeds as follows. Chapter 2 presents two different 1D photonic crystal sensors with one being an improvement over the other. The background theory, forward and inverse problem solutions from simulated and measured data, fabrication and measurement results are presented for each of the sensors. Chapter 3 shows an improved 3D sensor along with its background theory, the sensor performance forward problem solution from calculated (simulated) and measured data and its limitations. In chapter 4, the conclusion and future work are presented.

CHAPTER 2

1D MICROFLUIDIC PHOTONIC CRYSTAL SENSORS

In this study 1-D photonic crystal (PC) designs were used to build a microfluidic sensor for the THz spectral range. The layers of the structure are approximately a quarter wavelength thick alternating between high and low permittivity materials. The wave transmission through a 1D PC experiences a band gap in a certain frequency range. In the band gap, the wave entering the material will partially reflect off each layer. The two different 1D sensor were designed, fabricated and tested. The first sensor material is BK-7 glass and air and the second sensor being an improvement over the first is fabricated using Polyethylene Terephthalate (PET). Bk7 and air, and PET and air represent the materials used as high and low permittivity layers, respectively. The introduction of samples in the air gap regions changes the wave transmission characteristics through the PC which results in change of blocked frequency band. This is the basis of the sensing operation of the device. In this paper the background theory, design and fabrication procedure of the sensor will be discussed. The sensing operation and limitations were examined through the forward problem solution (sensing) from calculated and measured data. Additionally, the inverse problem analysis was carried out using calculated and measured sensing data (in the case of the PET sensor), through the introduction of a material characterization method which extracts the dielectric material properties of the sample being analyzed.

2.1 Theory

The sensor design consists of a multilayer system of non-magnetic dielectric materials as shown

in Figure 6. Equation 1 describes the relationship between the transmitted signal through the multilayer system, $E_t(\omega)$, and the normally incident plane wave on the multilayer system, $E_i(\omega)$, as a function of angular frequency ω. The transmission coefficient, $T(\omega)$, is defined by the following equations [51]:

$$T(w) = \frac{E_t(w)}{E_i(w)} = \prod_{j=1}^{N-1} e^{ik_{j,z}t_j} S_{j,j+1}\ , \tag{1}$$

where, $k_{j,z} = \omega\sqrt{\mu_o \varepsilon_o}\sqrt{\varepsilon_{r,j}}$, j indicates the layer, t_j indicates the thickness of the layer, $\varepsilon_{r,j} = \varepsilon'_j + i\varepsilon''_j$ is the complex relative permittivity of the layer and z indicates the direction of propagation of the wave [51]. Additionally, $S_{j,j+1}$, is a combination of terms described by

$$S_{j,j+1} = \frac{T_{j,j+1}}{1 - R_{j+1,j}\hat{R}_{j+1,j+2}e^{2ik_{j+1,z}(t_{j+1})}}, \tag{2}$$

where, $\hat{R}_{j,j+1}$ is a recursively calculated global reflection coefficient described by,

$$\hat{R}_{j,j+1} = \frac{R_{j,j+1} + \hat{R}_{j+1,j+2}e^{2ik_{j+1,z}(t_{j+1})}}{1 + R_{j,j+1}\hat{R}_{j+1,j+2}e^{2ik_{j+1,z}(t_{j+1})}}, \tag{3}$$

where $T_{j,j+1}$ and $R_{j,j+1}$ are the interfacial transmission and reflection coefficients respectively between any two layers j and $j+1$ described by,

$$T_{j,j+1} = \frac{2\sqrt{\varepsilon'_{j+1} + i\varepsilon''_{j+1}}}{\sqrt{\varepsilon'_{j+1} + i\varepsilon''_{j+1}} + \sqrt{\varepsilon'_j + i\varepsilon''_j}}, \tag{4}$$

and

$$R_{j,j+1} = \frac{\sqrt{\varepsilon'_{j+1} + i\varepsilon''_{j+1}} - \sqrt{\varepsilon'_{j} + i\varepsilon''_{j}}}{\sqrt{\varepsilon'_{j+1} + i\varepsilon''_{j+1}} + \sqrt{\varepsilon'_{j} + i\varepsilon''_{j}}}. \quad (5)$$

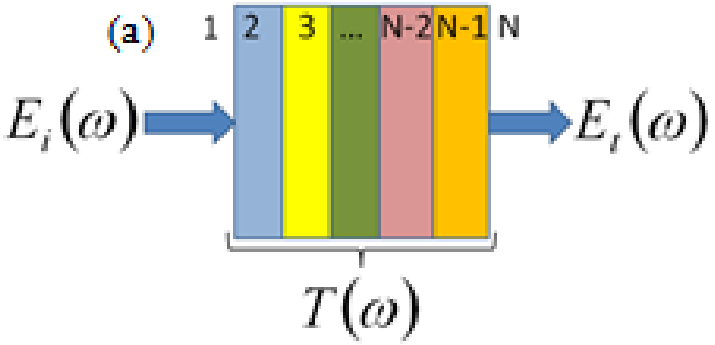

Figure 6. Multiple layer structure: theoretical model sketch [52]

2.2 BK7 Sensor Design and Analysis

2.2.1 Forward Problem Solution

As mentioned above, optimally a PC structure is composed of approximately quarter wavelength thick high and low permittivity materials. A one dimensional photonic crystal filter was designed to operate in the lower THz range (center frequency = 222 GHz). The photonic crystal is composed of 9 layers of 150μm thick BK7 glass ($\varepsilon_r \approx 6.25 + i0.274$ at 222 GHz) separated from each other by 300μm air gaps. The layer thicknesses were chosen to be approximately quarter wavelength. Figure 7 shows the fabricated photonic crystal structure.

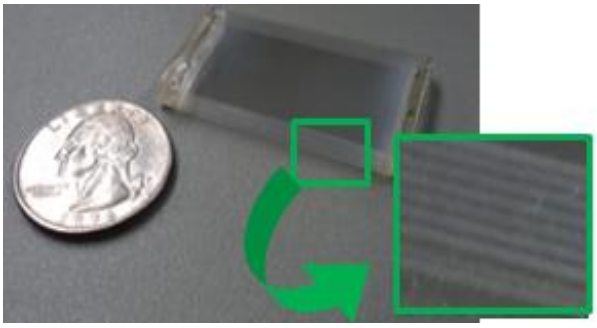

Figure 7. Photomicrograph of a fabricated photonic crystal structure

Figure 8 shows the calculated (using Eq. (1)) and measured transmission coefficients of the photonic crystal structure. It can be clearly seen that the stop band lies almost in the same frequency band. Differences in the responses might be due to fabrication imperfections, such as the layers not being parallel, the glue used to keep the glass together expanding and contracting as well as measurement issues that will be discussed later in this chapter.

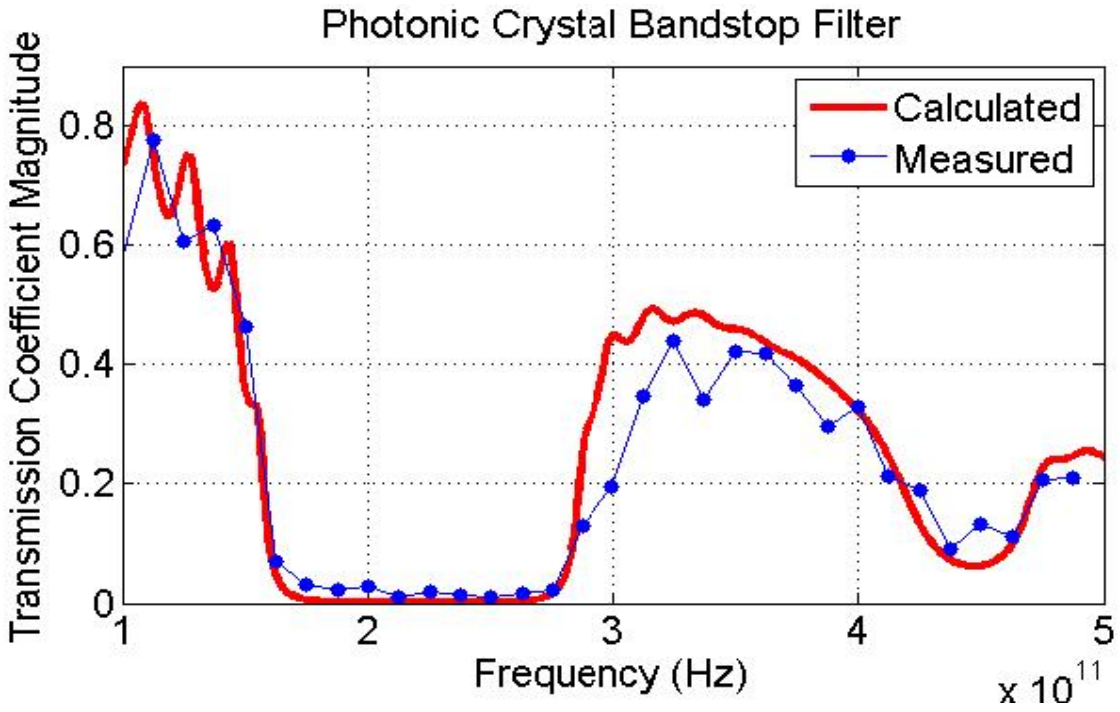

Figure 8. Calculated and measured transmission coefficients

In order to examine the sensing capability of the designed photonic crystal structure, the transmission coefficient was calculated for three different perturbations of the dielectric constant of the air regions ($\varepsilon_r = 1 + 0i$ before perturbations) using Eq. (1). The permittivities of the three different samples were chosen to be: $\varepsilon_{r1} = 1.1 + 0i$, $\varepsilon_{r2} = 2 + 0.2i$, and $\varepsilon_{r3} = 2 + 0i$. Figure 9 shows the transmission responses using ε_r, ε_{r1}, ε_{r2}, and ε_{r3}, respectively.

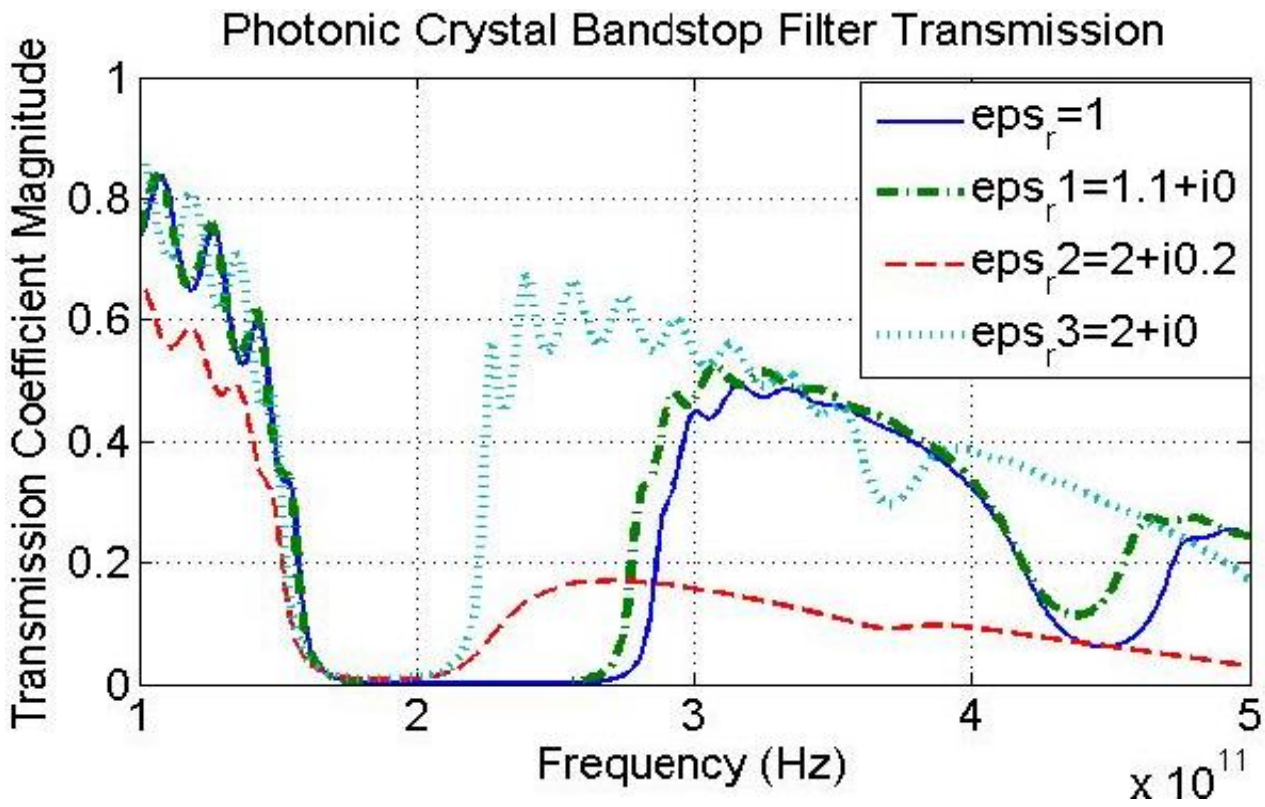

Figure 9. Transmission for different layers fillings

The traces in Figure 9 show that the filter response changes as a result of replacing air with samples of different permittivity. From the graph it can be seen that the left side of the band stop is dominated by the glass dielectric and the right side of the band stop is dominated by the air dielectric. By replacing the air with different medium dielectrics, the right side of the band stop

begins to change. From this it can be noted that the change in signal in the band stop region is significant and can easily be detected. The band bap region begins to close as the dielectric medium replacing air has a dielectric constant closer to glass medium.

It is also seen that slight differences in the dielectric constant cause only slight changes in the transmission response outside the band stop region and in part in the band stop region. The limitation of the measurement system i.e signal to noise ratio (SNR) will become an issue when trying to sense for such small differences in material properties in an actual experimental setup in these frequency regions. In order to enhance signal change due to the presence of sample, a modification is made to the photonic crystal by removing the 5^{th} glass layer thus making a central empty layer with 750μm thickness. This introduces a defect in the photonic crystal structure. This in turn introduces a notch to the transmission response. This notch can be used in characterizing the samples with high sensitivity over a narrow band. Figure 10 shows the transmission characteristics of such a structure in which the low-permittivity layers are filled with materials with $\varepsilon_r = 1 + 0i$ and $\varepsilon_{r1} = 1.1 + 0i$. The magnitude (transmitted signal) of the notch can be increased by using low loss glasses such as Pyrex or Quartz instead of BK-7 which is used here, leading to an increase in sensitivity and higher SNR.

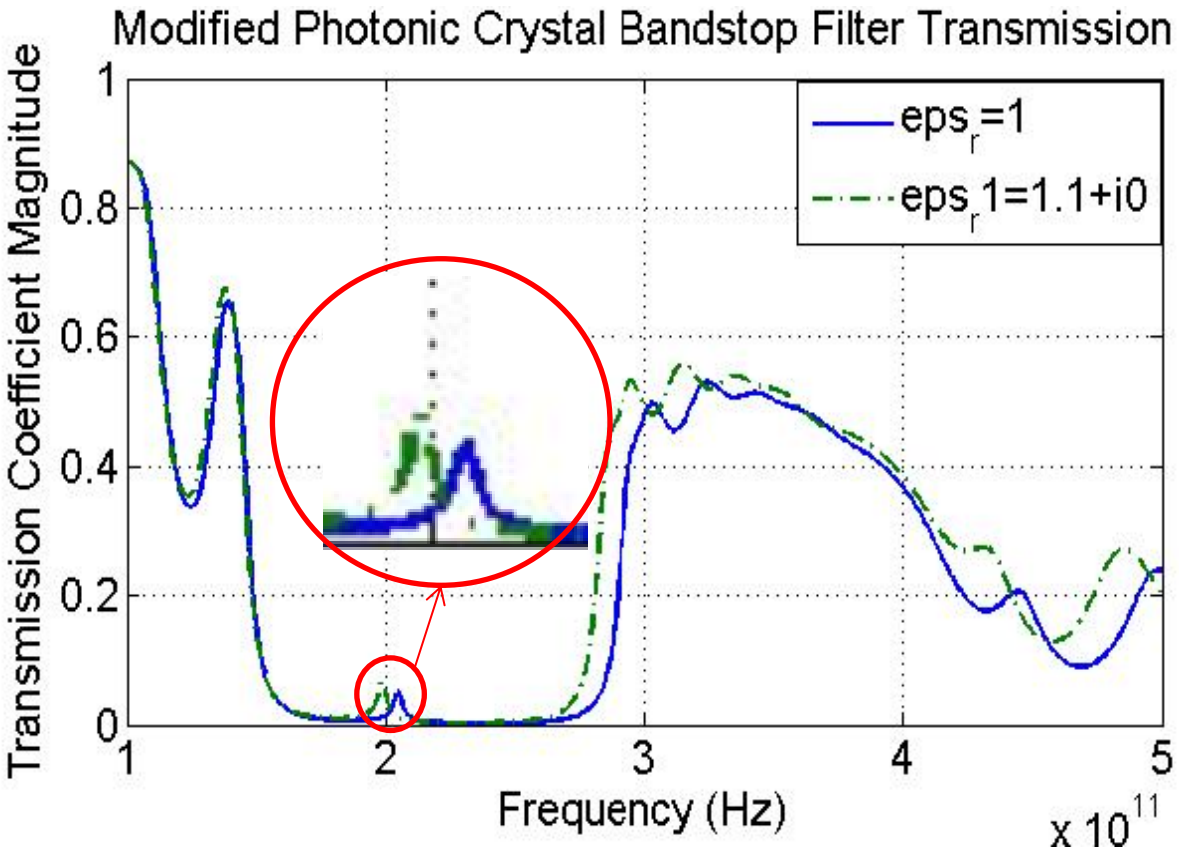

Figure 10. Transmission for different layer fillings

With this device it has been shown that theory of the design works as seen in Figuree 8 and 9. It has also been shown that this type of device could possibly be improved by adding a defect to the photonic crystal as seen in Figure 10. However, there were a few challenges encountered in this design, these challenges were mainly fabrication issues and accessibility to the empty layers with continuous flow of material. The glass used was very thin and easy to break, the glue holding the pieces together would expand and contract changing the orientation of the layers which makes constant flow of material for testing very difficult, if not impossible. Therefore, the next step is to build on this design, the new device is also a 1D photonic crystal designed to further test its sensing capabilities of a device based on the same principles and expand its used from sensing to

material characterization based on the data recovered using its sensing capabilities with the sensor, as well as try to overcome the challenges listed above.

2.3 PET Sensor Design and Analysis

Expanding on the design shown above, a second 1D photonic crystal sensor is designed in order to overcome a few challenges and expand its functionality as mentioned above.

In this study, the alternating layers were picked to be PET (9 total layers, $\varepsilon_r \approx 3.00 + 0.05i$ at 300 GHz) and air (8 total layers) arranged as shown in Figure 11(c). The thicknesses that were used to design and build the filter were 127μm nominal thickness for PET and approximately 284μm nominal thickness for air. The fabricated device is shown in Figure 11(b). It is worthy to note that due to manufacturing and fabrication imperfections, the actual thicknesses of the PET and air layers may vary slightly affecting the wave transmission through the sensor.

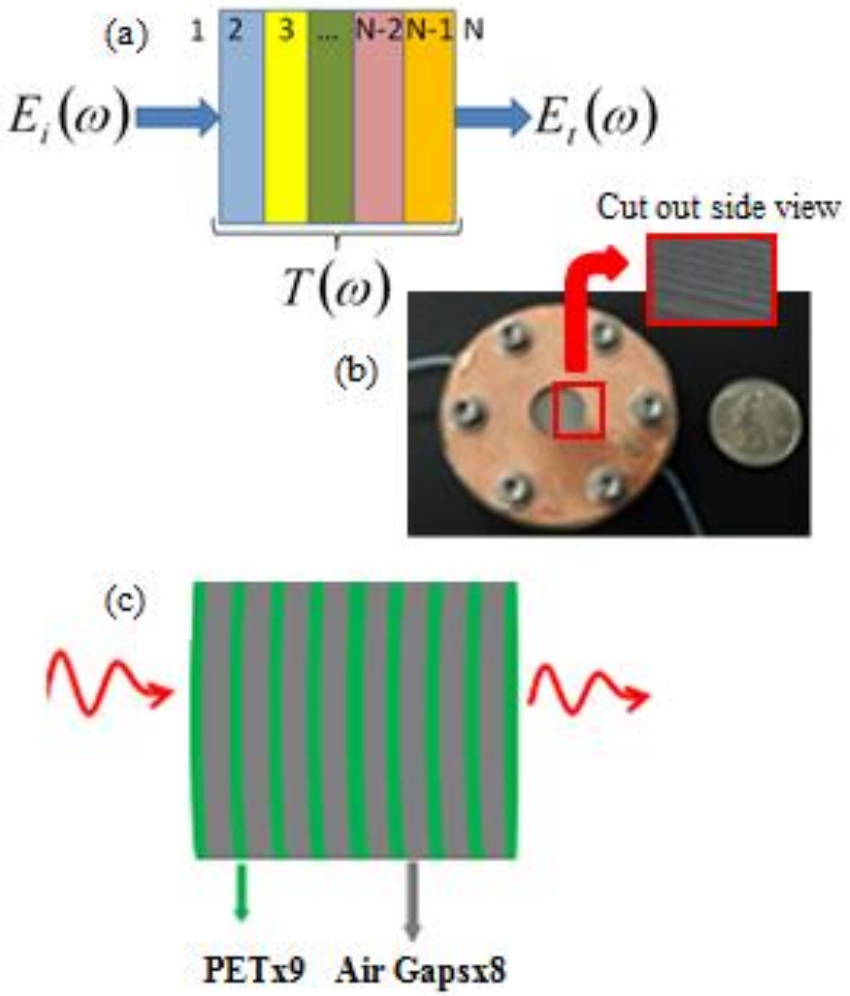

Figure 11. (a) Multiple layer structure: theoretical model sketch [52], (b) Fabricated photonic crystal structure(c) Wave entering and leaving multiple layer structure

Figure 12 shows the amplitudes of the calculated and measured transmission coefficients of the fabricated device using Eq. (1). It can be observed that both transmission coefficients' stop bands lie in the same frequency range centered at approximately 297 GHz. The differences between the calculated and the experimental results can be attributed to multiple reasons including: (1) the individual PET layers being not perfectly parallel to each other, (2) layer thickness variations due to manufacturing and fabrication imperfections including warping of the non-rigid PET layers and (3) THz source instabilities, drift in delay line and noise. The increased mismatch levels

incurred at higher frequencies are due to the fact that defects and discrepancies become more apparent due to smaller wavelengths.

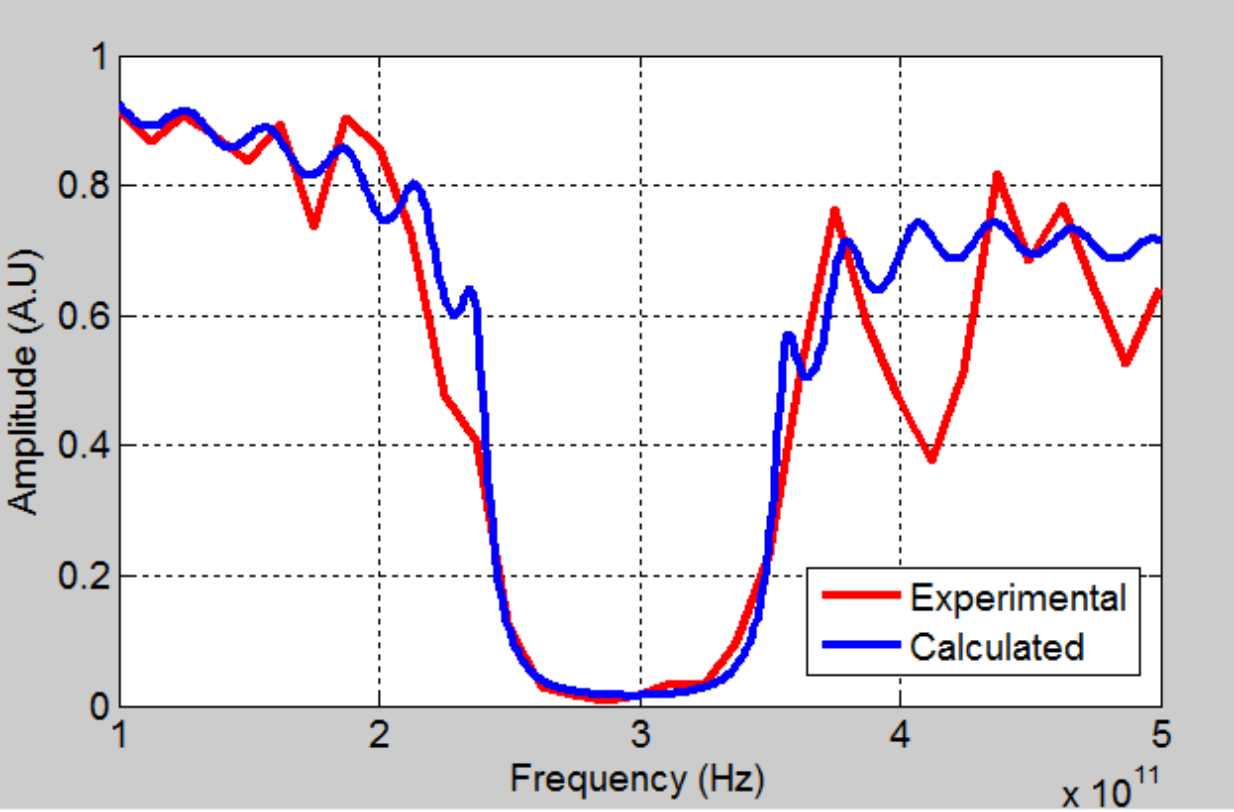

Figure 12. Calculated and measured transmission coefficients' amplitudes of the fabricated device

In order to examine the effect of the thickness non-uniformity on the sensor transmission coefficient, an alternative transmission coefficient was calculated for a structure having 127μm thick PET layers and 254μm thick air gaps for comparison. Figure 13 shows the amplitudes of the two different calculated transmission coefficients. It is worth noting that the band gap center frequency slightly shifts to the right and the band frequency range decreases with the thinner air gap layers. On a more general note, it can be anticipated that if errors in fabrication occur, due to spacing, the filter would still work but the center frequency could be slightly shifted and the stop band region size may increase or decrease.

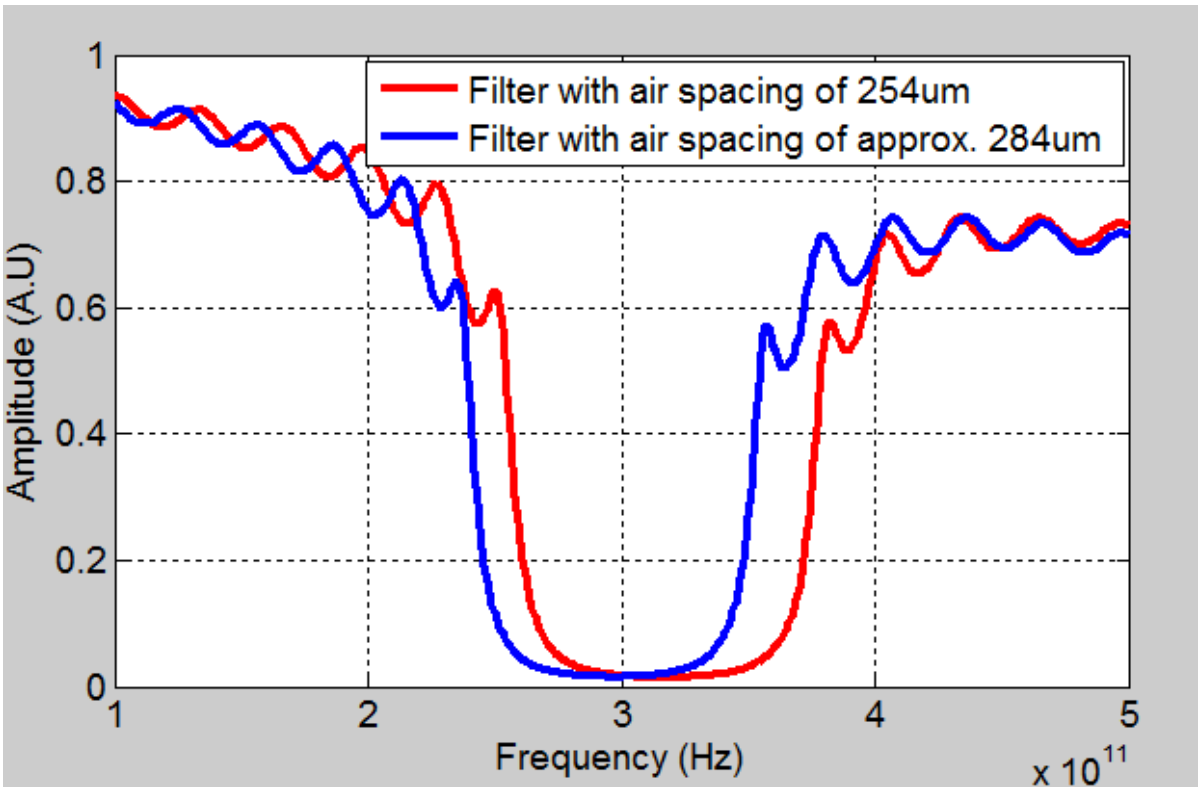

Figure 13. Calculated transmission coefficients' amplitudes of sensor for 254μm and 284μm air thickness

2.3.1 Calculated Transmission Coefficients for Different Materials in the Gap Regions

The sensing capability of the structure was examined using three different sets of varying dielectric materials replacing the air gap regions of the sensor. These varying dielectric material groups are: (1) slight variations in the real part of the dielectric constant for lossless materials, (2) large variations in the real part of the dielectric constant for lossless materials, and (3) varying loss for non-changing real part of the dielectric constant. The transmission coefficient for each variation was calculated using Eq. (1).

With respect to lossless materials with slight variations in the real part of the dielectric constant, the dielectric properties used are as follows: $\varepsilon_r = 1.00 + 0i$, $\varepsilon_r = 1.02 + 0i$, $\varepsilon_r = 1.04 + 0i$, $\varepsilon_r = 1.06 + 0i$, $\varepsilon_r = 1.08 + 0i$, and $\varepsilon_r = 1.10 + 0i$. Figure 14 shows the amplitude of the

transmission coefficient obtained for each case. From Figure 14 it can be noted that as the real part of the dielectric constant increases, the transmission coefficient stop band size decreases with its right side moving to the left.

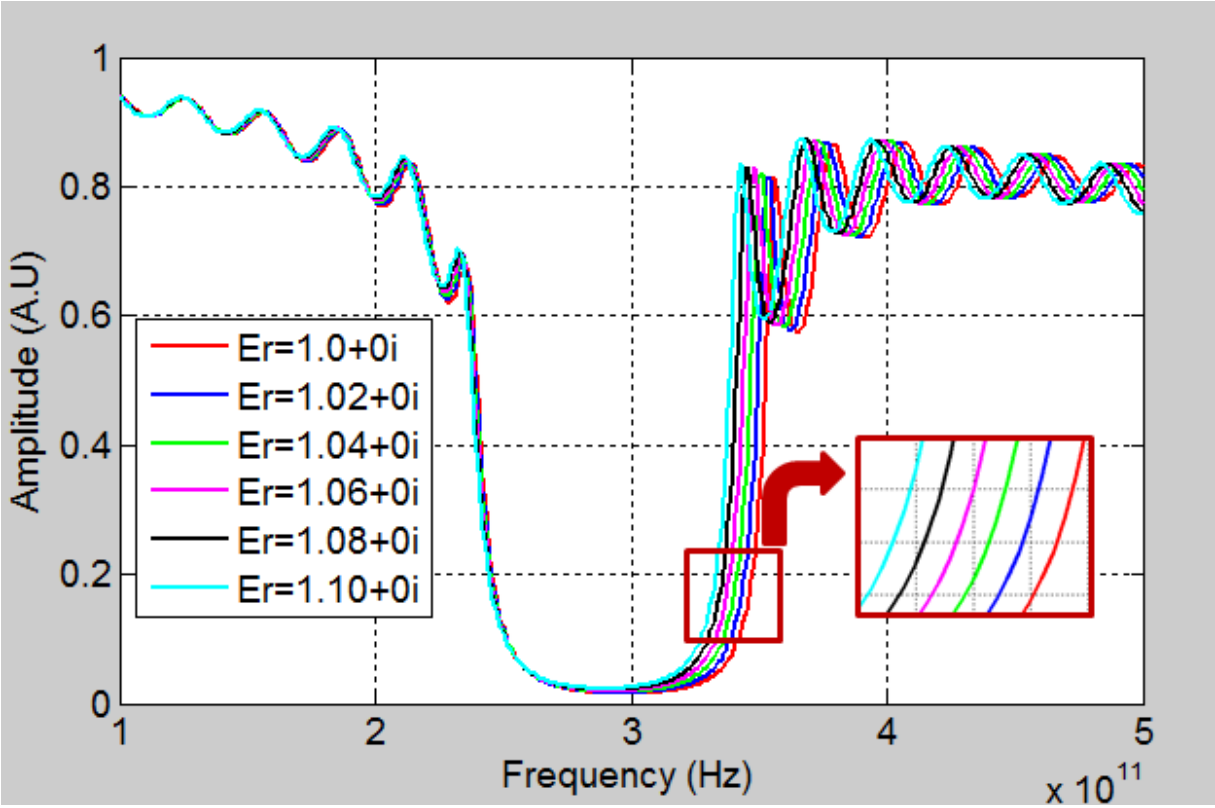

Figure 14. Calculated transmission coefficients' amplitudes for gap region dielectric filling variation between $\varepsilon_r = 1.00 + 0i$ and $\varepsilon_r = 1.10 + 0i$

Figure 15 shows the results obtained by varying the real part of the dielectric constant of a lossless material in large intervals. The cases examined range between $\varepsilon_r = 1.00 + 0i$ and $\varepsilon_r = 2.50 + 0i$ with steps of $\varepsilon_S = 0.50 + 0i$. As can be predicted from the previous results, shown in Figure 14, the stop band size of the transmission coefficient decreases with its right side shifting to the left as the dielectric constant real part increases. The decrease in the stop band size however is much more substantial with large increases in the dielectric constant real part.

This is true as well for the ground level of the stop band which goes up much more with larger variations in the dielectric constant real part as opposed to slight ones. It was also observed that as the real part of dielectric constant increases, the subsequent higher frequency band gap becomes closer to the first band gap.

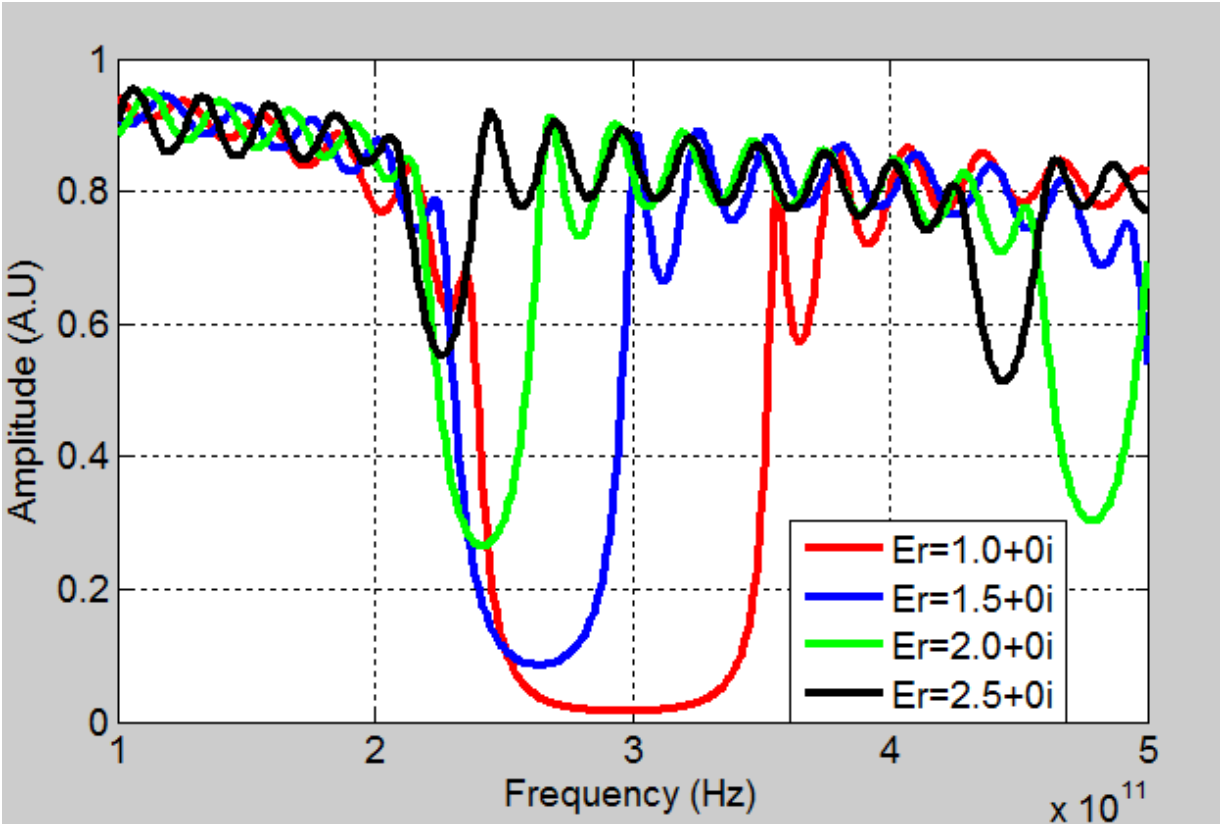

Figure 15. Calculated transmission coefficients' amplitudes for gap region filling variation between $\varepsilon_r = 1.00 + 0i$ and $\varepsilon_r = 2.50 + 0i$

Lastly, the effect of increasing dielectric loss is examined by changing the imaginary part of the dielectric constant while keeping the real part constant. It was observed that as the imaginary part of the dielectric constant increases the loss also increases. Figure 16 shows the change in amplitude of transmission coefficients' when the dielectric properties of sample are varied between $\varepsilon_r = 1.10 + 0i$ to $\varepsilon_r = 1.10 + 0.2i$, i.e. at $0i$, $0.02i$, $0.05i$, $0.1i$ and $0.2i$. It can be

observed that as the loss increases, the transmitted signal intensity in the pass band decreases. It can also be seen that the bang gap location is not affected.

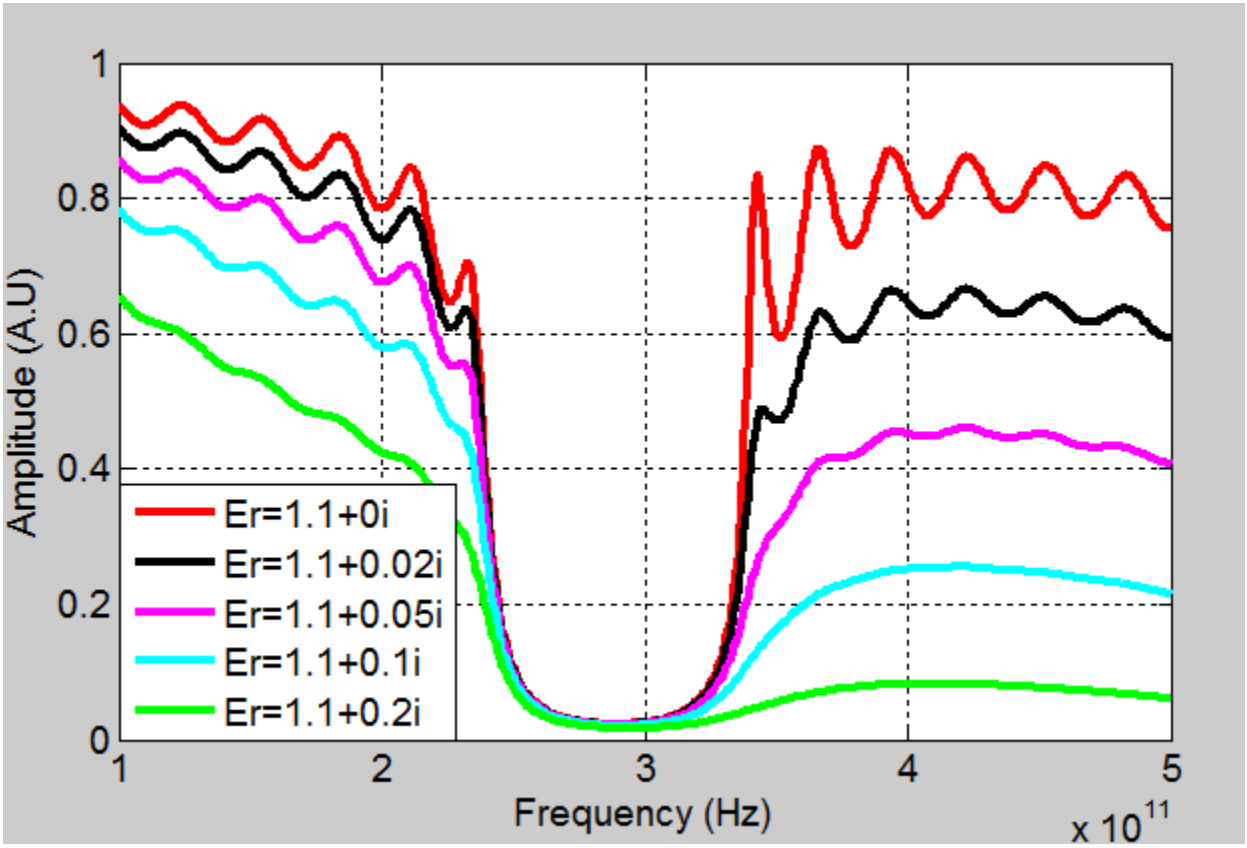

Figure 16. Calculated transmission coefficients' amplitudes for gap region dielectric filling variation between $\varepsilon_r = 1.10 + 0i$ and $\varepsilon_r = 1.10 + 0.2i$

With these calculations it can be concluded that the filter response changes as a result of replacing air with different permittivity samples. Most importantly, it is observed that increasing real part of the dielectric constant decreases the transmission coefficient stop band width and raises the amplitude of the ground level of the stop band while an increase in loss decreases the transmitted signal intensity especially in the pass band. These characteristic changes in the filter response properties, especially in the stop band, are easy to detect and can be used in the characterization of materials filling the gap regions of the PC.

2.3.2 Calculated Transmission Coefficients for Defect Yielding Sensor

Using PET we now show the alternate design described above to improve the sensitivity of the structure is examined in this subsection. This design, again, entails the removal of the 5th PET layer from the design shown in Figure 1(c). Prior to removing the PET layer, all 8 air gaps were 254μm thick. The removal of the fifth layer leaves a center gap of around 635μm thick and thus a defect is introduced in the PC structure. This defect results in a notch in the transmission response [38]. By tracking the changes of this notch more information is available in order to better distinguish between samples under test. Figure 17 shows the difference between the amplitudes of the transmission coefficients with the defect introduced in the structure versus without the defect. It can indeed be observed that the defect in the structure does introduce a notch in the transmission coefficient band gap as expected.

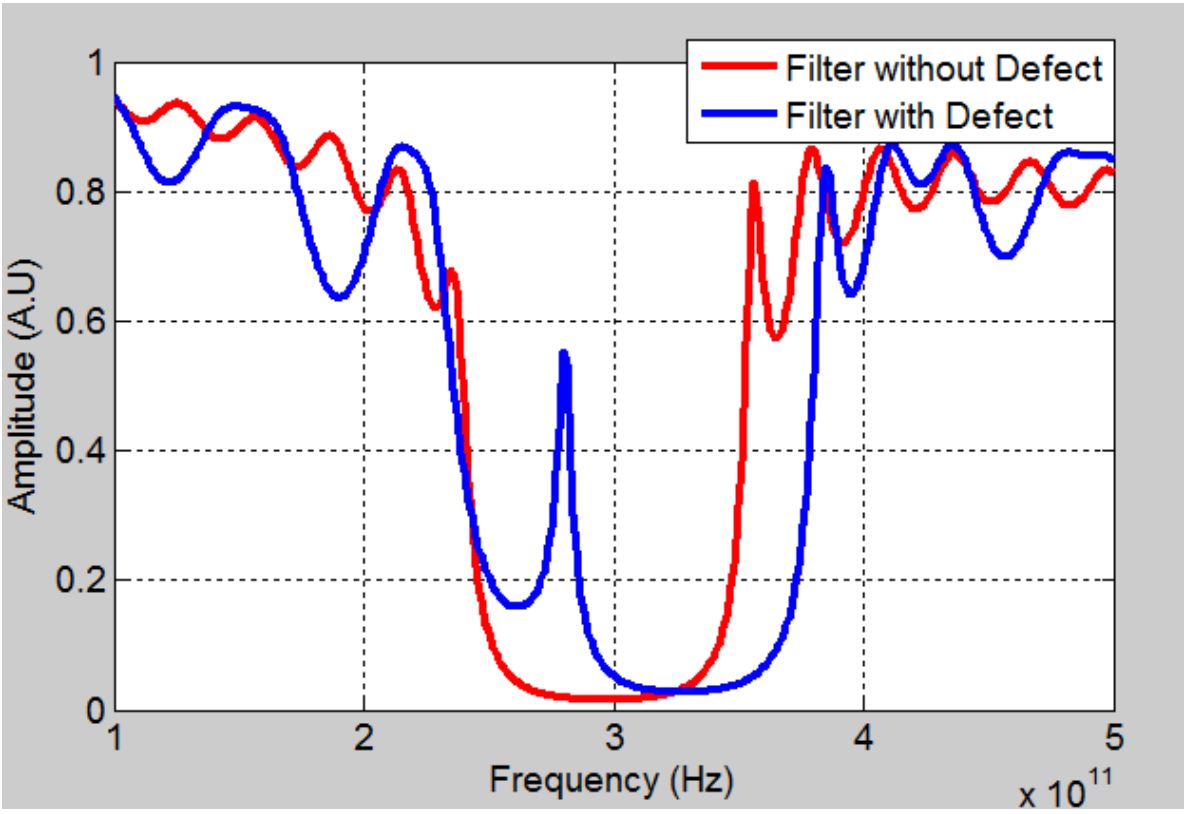

Figure 17. Calculated transmission coefficient's amplitudes for filters with and without defect

Figure 18 shows the transmission coefficient variations when small changes in the real part of the dielectric constant are introduced into the filter designed with a defect. For this test, only the central gap had material introduced. This was done in order to examine the effect of using less sample volume. In this case the materials tested are: $\varepsilon_r = 1.00 + 0i$, $\varepsilon_r = 1.001 + 0i$, $\varepsilon_r = 1.01 + 0i$ and $\varepsilon_r = 1.10 + 0i$. As the real part of the dielectric constant increases, the notch of the transmission coefficient band gap shifts to the left. This is in addition to the previously observed phenomena seen with the design having no defect. The added information (notch) further assists in differentiating between samples with infinitesimally different material properties.

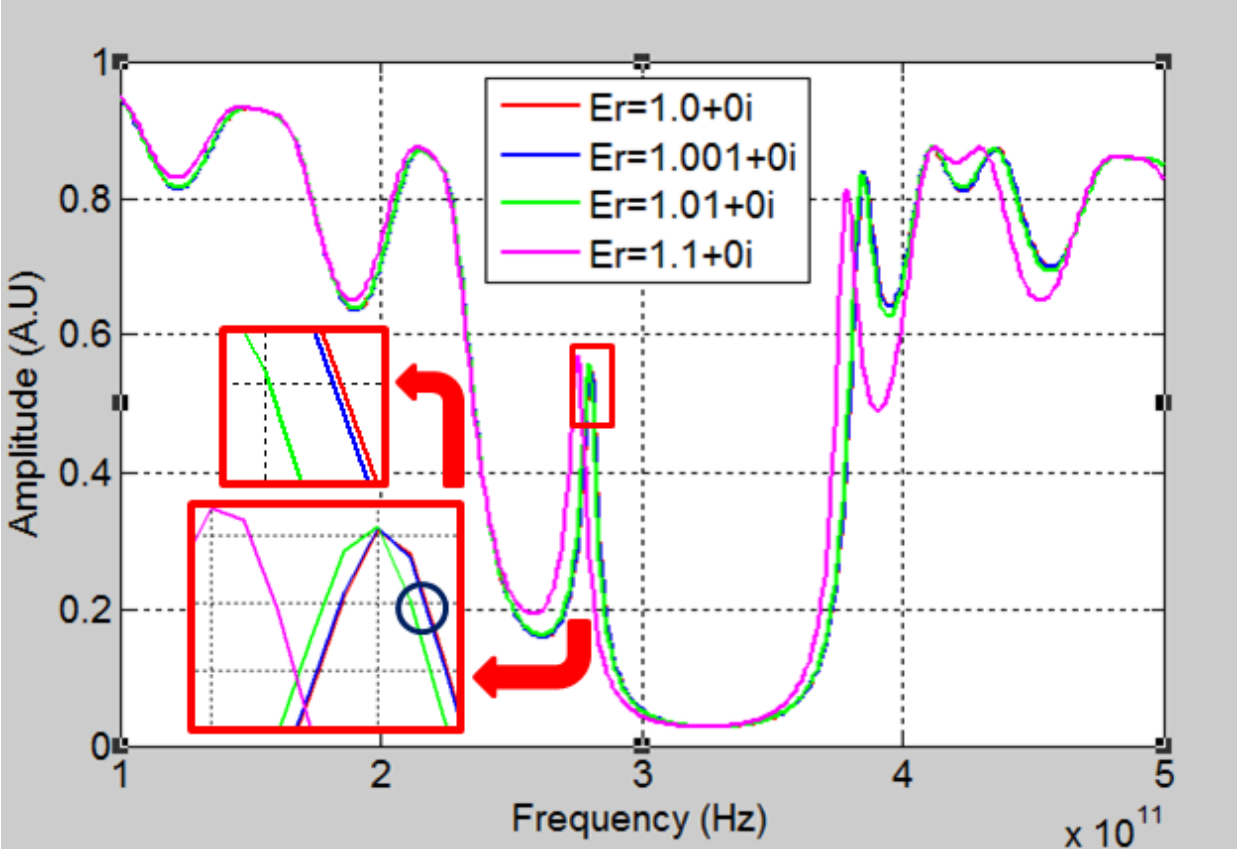

Figure 18. Calculated transmission coefficients' amplitudes for central gap dielectric filling variation between $\varepsilon_r = 1.00 + 0i$ and $\varepsilon_r = 1.10 + 0i$

In this section, the sensing capability is examined through calculation. The transmission coefficients are calculated for different materials filling the air gaps. Additionally, the performance of a slightly modified sensing structure is examined. The modified design was carried out by removing one of the PET layers from the stack and replacing it with air in order to introduce a defect in the PC structure.

2.4.1 Fabrication and Experimental Setup

The sensor was fabricated with low cost material and utilizing a relatively simple procedure. PET layers were cut using a Full Spectrum laser cutter. Two different sets of PET cuts were made. One set had nine 127μm nominal thickness circles. Each of these circles had 6 holes on the edges for holding screws to be used upon assembly of the multiple layer sensing structure as well as 2 channels to allow for entry and exit of liquids and gaseous materials as seen in Figure 19(b) (low center). The second set of cuts were eight 254μm nominal thickness circles with a large hole in the center as well as the 6 holding screw holes on the edges. The second set of cuts are used as spacers upon assembly with each large hole representing a gap layer. Figure 19(a) shows the full spectrum cutter, Figure19(b) shows the cut pieces including the outer support, and Figure 19(c) shows the assembled final product including the capillaries for entry and exit of the sample materials to be tested. The outer metal holder has dual functionality; it holds the device in place and it prevents the electromagnetic waves from entering the device outside a 14mm diameter which is the size of the opening shown on the upper right of Figure 19(b).

Figure 19. (a) CO_2 laser cutter (b) Upper left: filter piece, upper right: holder, low center: spacer (c) Final assembled PC sensor including the capillary inlet and outlet of samples

This design is advantageous because it is inexpensive, easy to fabricate and assemble. It is highly sensitive and due to PET being a relatively low loss material the signal loss in the transmission through the sensor is low. One disadvantage of this design is that the spacing between the PET layers can be altered due to the melting of PET caused by the laser cutter on the plastic, in this case the melting was measured and it was 280μm thick, this is the reason why the frequency is a little shifted from the original 254μm design, all simulations were calculated using a nominal thickness of 280μm. Laser cuts lead to edge beading of plastic (PET). This effect was minimized by air jet cooling during the cutting process. Additionally, due to lack of rigidity of the PET layers, warping is likely to happen, thus altering the spacing and parallelism between the layers. Moreover, the lack of rigidity makes the device sensitive to pressure. The preceding disadvantages affect the transmission of the signal through the sensor. In order to avoid any changes due to pressure, the samples are introduced at a constant rate of 20ml/min. Gaseous and liquids mixtures are introduced into the device via attached capillaries. In between measurements of different samples, the sensor is cleared of any residuals by blowing air and nitrogen through the capillaries and PC for approximately 10 minutes. All measurements are carried out at room temperature. Figure 20 shows the experimental setup. The sensor is located in between the transmitter (Tx) and receiver (Rx) of a Picometrix Tray-2000 THz system. The syringe pumper

is connected to the sensor via capillaries in order to inject materials for testing at a constant flow rate.

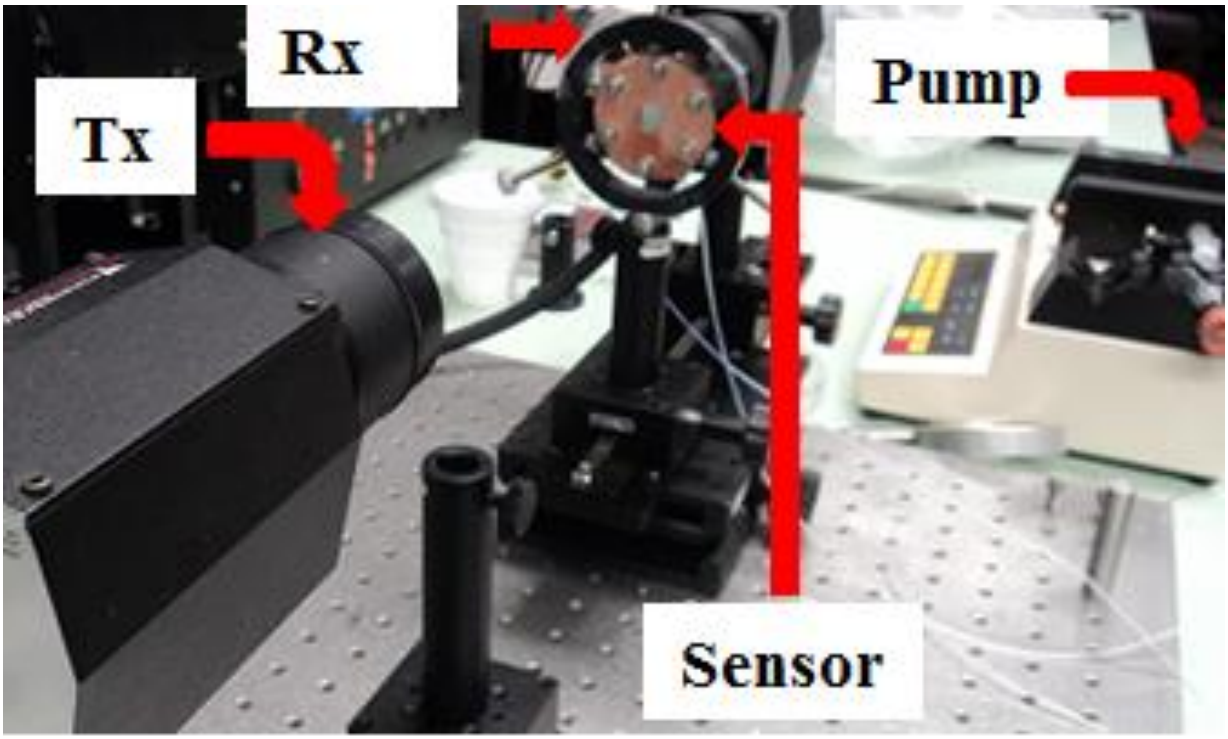

Figure 20. Experimental setup for measurement

2.4.2 Measurement Procedure

A collimated beam of a linearly polarized THz time domain electromagnetic pulse normally impinges on the sensor as shown in Figure 20. By placing the sensor in between the Tx and Rx, different transmitted signals are gathered depending on the substance introduced into the sensor gaps. Like [40], the transmission information is used to characterize the samples under-test. As mentioned previously, the samples characterized using this sensor, are liquids and gases.

For the purpose of evaluating the performance of the fabricated sensor, different frequency dependent measured transmission coefficients, $T_m(\omega)$, are required as the material in the empty gaps of the filter changes. In order to obtain $T_m(\omega)$ two measurements and post-processing of

data are required.

First, a time domain transmitted signal, $E_{tm}(t)$, through the sensor is measured. $E_{tm}(t)$ can be described as

$$E_{tm}(t) = T_m(t) * E_{im}(t-a), \tag{6}$$

where $E_{im}(t)$ is the system generated time domain incident signal, a is the time delay total due to the wave travelling from the Tx to the sensor input and then from the sensor output to the Rx and $T_m(t)$ is the time domain transmission coefficient of the PC sensor. Second, a time domain reference signal, $E_{rfm}(t)$, is measured while maintaining the same physical distance, d, between the Tx and Rx as when $E_{tm}(t)$ was measured. The reference measurement is the signal from the Tx travelling through air (with no sensor presence) to the Rx. In others words, it is a time delayed version of the system generated time domain incident signal, $E_{im}(t)$. $E_{rfm}(t)$ can be described in terms of $E_{im}(t)$ as,

$$E_{rfm}(t) = E_{im}(t-b), \tag{7}$$

where b is the time delay due to the signal travelling the distance d between the Tx and Rx of the THz system. The difference between a and b is the delay the wave encounters due to travelling through the sensor layers (see Figure 11(a) layer 2 to layer N-1).

The Fourier transforms of both, $E_{tm}(t)$ and $E_{rfm}(t)$, are then calculated to obtain $E_{tm}(\omega)$ and $E_{rfm}(\omega)$. Upon dividing $E_{tm}(\omega)$ by $E_{rfm}(\omega)$, the following can be deduced,

$$\frac{E_{tm}(\omega)}{E_{rfm}(\omega)} = \frac{E_{im}(\omega)T_m(\omega)\exp\left[i\frac{\omega}{c}(d - t_{sum})\right]}{E_{im}(\omega)\exp\left[i\frac{\omega}{c}d\right]} = T_m(\omega)\exp\left[-i\frac{\omega}{c}t_{sum}\right], \quad (8)$$

where t_{sum} is the sum of layer thicknesses of the PC sensor (layers 2 to N-1 in Figure 11(a)). Rearranging terms, $T_m(\omega)$ can be described as

$$T_m(\omega) = \exp\left[i\frac{\omega}{c}t_{sum}\right]\frac{E_{tm}(\omega)}{E_{rfm}(\omega)}. \quad (9)$$

2.5 Experimental Results

2.5.1 Forward Problem Solution – Sensing

The sensor was experimentally evaluated by measuring the transmission coefficient of the signal going through it as a result of introducing several liquids and mixture of gases as described in the previous section (Eq. (9)). First, the gaseous mixtures are tested. Small amounts of chemicals are introduced into a syringe containing air. The chemicals utilized have the characteristic of evaporating at room temperature. After evaporation is complete, the fluid in the sealed syringe becomes a gaseous mixture of air and the chemical vapor. The gaseous mixture is pushed into the sensor using the syringe pump at a rate of 20mL/min. Figure 21 shows the transmission responses as a result of introducing the following vapors into the air region of the sensor: Isopropanol (IPA), Toluene, Cyclopentanone, and a chemical mixture composed of 50% Cyclopentanone and 50% Toluene compared to air's transmission response. Small variations are observed in the transmission coefficients obtained as a result of introducing the different gaseous mixtures. This is expected as the gaseous mixtures only result in small variation in dielectric constant from air. This measured result goes in line with the calculated results for small variations in the dielectric constant seen in Figure 14.

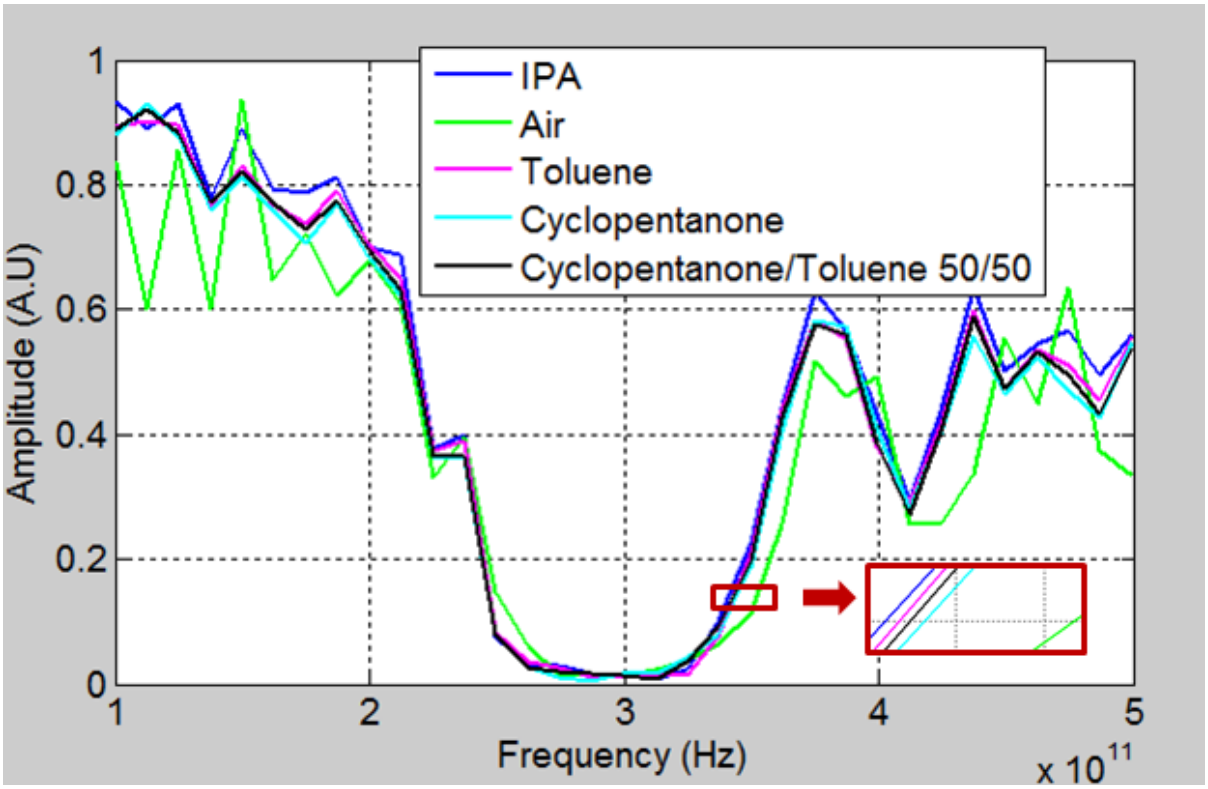

Figure 21. Measured transmission coefficients for different gaseous mixtures

Next, liquid mixtures were examined. Figure 22 shows the transmission responses when the following liquids were introduced: Methanol, IPA and Toluene, compared to air. It can be seen that the variation in the transmission response is much larger than that seen with gaseous mixtures. This is expected because of the larger variation in the dielectric properties. Another observation is that for some samples the transmission intensity decreases more than others thus providing information about the loss of the sample. These observations from measurement are similar to those seen from the calculated data shown in the previous section. From Figure 22, it is observed that the transmission coefficient amplitude of Toluene is higher compared to Methanol, indicating that Methanol has higher loss characteristics in the THz frequency range. It can also be deduced that the dielectric constant of Toluene is closer to that of air than the other liquids, as a stop band still appears in the frequency band unlike the other liquids tested. Also, it can be seen

that the stop band as a result of using Toluene in the empty gaps becomes smaller than that of air with its right side moving to the left and its ground level increasing in amplitude level. This goes in line with results shown in Figure 15 as the real part of the dielectric constant increases.

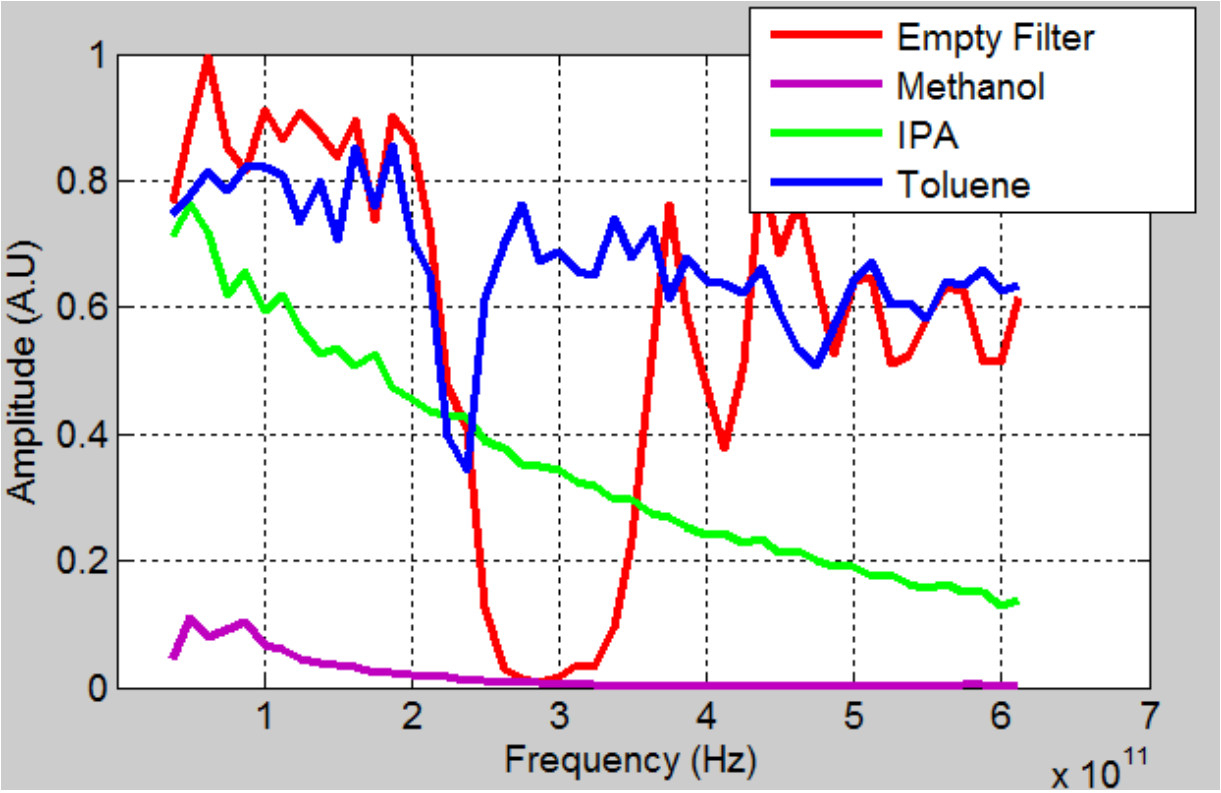

Figure 22. Measured transmission coefficient for different liquids and empty filter (air)

Furthermore, upon measuring the transmission coefficients through the sensor, as a result of introducing different mixtures of Toluene and Methanol, it is observed that the intensity of the transmission decreases as the concentration of Methanol increases (see Figure 23). This is an expected result as Toluene is a low loss liquid and Methanol is a high loss liquid as can be deduced from Figure 22. It is known that the dielectric constant of the mixture will be in between those of Toluene and Methanol subject to their concentrations. As a result, it can be concluded from Figure 23 that the real parts of the dielectric constants of Methanol and Toluene in the band

gap region are not too far off from each other; because the stop band size and location don't change much as the concentration of Methanol changes in the mixture.

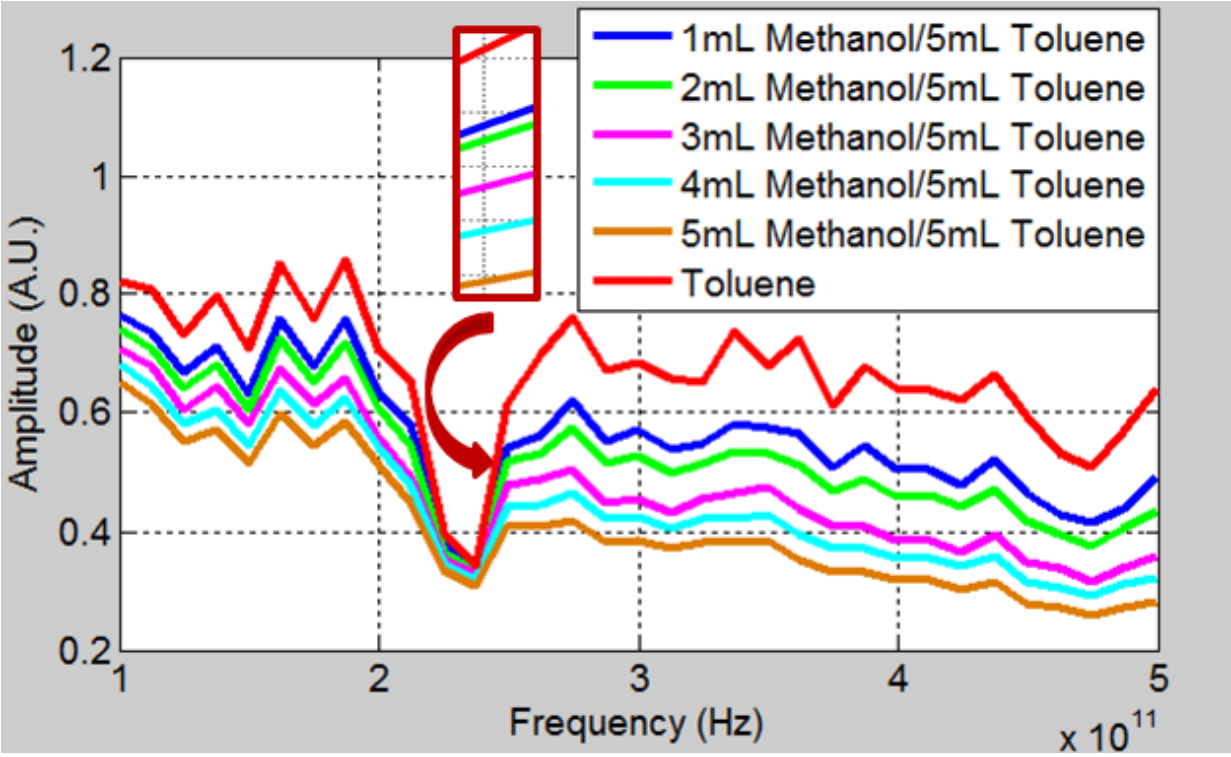

Figure 23. Measured transmission coefficient for combinations of Methanol and Toluene

2.5.2 Inverse Problem Solution -Material Characterization

The motivation behind the inverse problem solution is to extract the dielectric properties of the samples being tested. Material characterization studies for different materials such as glasses, oils and polymers have been done using THz Time Domain Spectroscopy (TDS) [53-57]. In this paper a material characterization method is devised to extract properties of liquids and vapors tested with the aforementioned sensor. This technique borrows some of the same principles of previous material characterization methods and analysis, including those used in [53-57]. This

material characterization technique has been previously introduced in [52] and is further elaborated upon and validated in this paper.

The goal of the inverse problem solutions procedure is to match calculated sensor transmission coefficient, $T_C(\omega)$ with measured sensor transmission coefficient $T_m(\omega)$ [52]. $T_m(\omega)$ is found using the measurement procedure described earlier as a result of introducing some liquid or gas sample into the sensor air gaps where the transmitted. The matching is achieved by optimizing for the properties of the sample being interrogated. The material properties optimized for are used to obtain $T_C(\omega)$. $T_C(\omega)$ is a function of the complex relative permittivity of the unknown material as seen in Equations (1) through (5). The optimization method used is the Nelder-Mead method [49, 53, 58-61], which is a multivariable unconstrained search algorithm [53]. The optimization was carried out at each frequency as done in [53]. Through the optimization the extracted dielectric properties (representing the unknown material) which are used to calculate $T_C(\omega)$ should result in the following fitness function [16]:

$$F = \left|\left|T_m(\omega)\right| - \left|T_C(\omega)\right|\right| + \left|\angle\left(T_m(\omega)\right) - \angle\left(T_C(\omega)\right)\right| \quad (10)$$

tending to 0.

To demonstrate its validity, the material characterization method was tested using synthesized data calculated for a dielectric material having the dielectric properties: $\varepsilon_r = 2.00 + 0.01i$. Figure 24(a) and 24(b) shows the Frequency dependent dielectric properties extracted as a result of the material characterization method implementation.

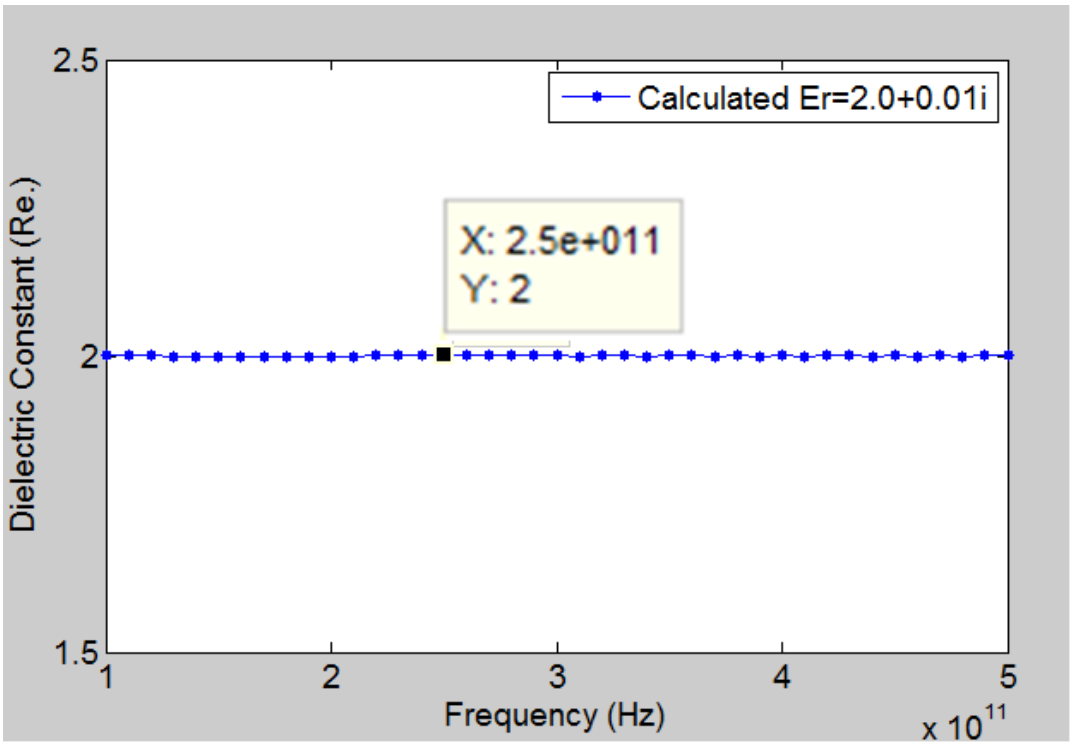

Figure 24(a). Frequency dependent dielectric constant (real part) extracted for synthesized data

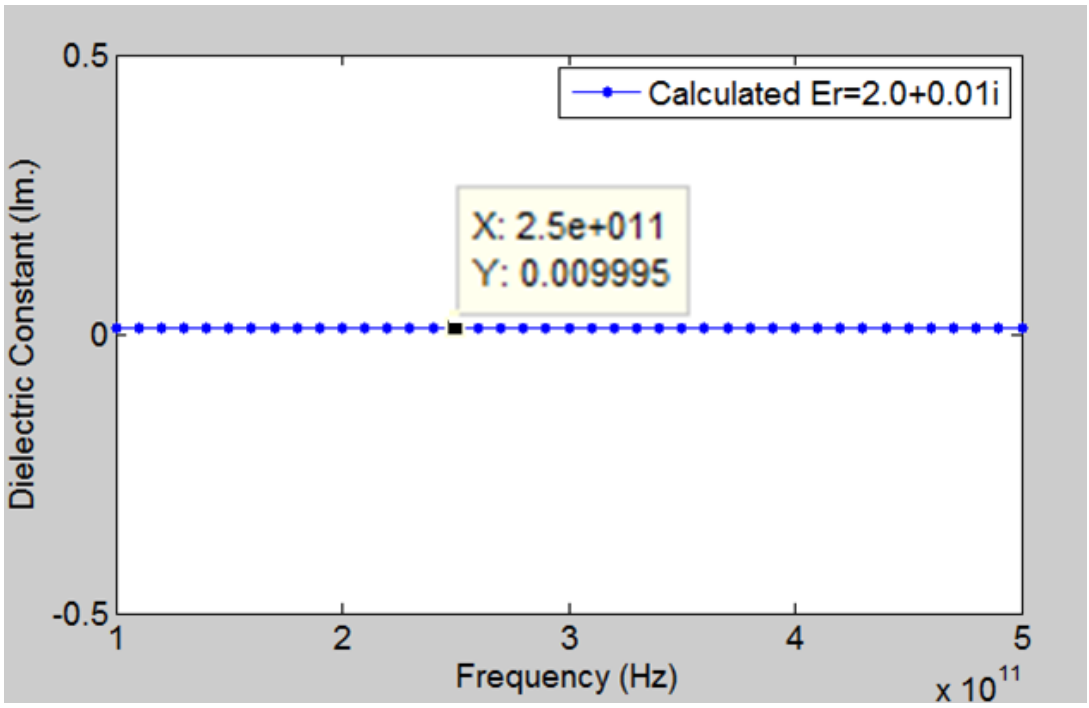

Figure 24(b). Frequency dependent dielectric constant (imaginary part) extracted for synthesized data

The extracted results match the material properties used to generate the synthesized data, giving an average of $\varepsilon_r = 2.00 + 0.01002i$. This validates the material characterization method operation and shows that the PC structure model in the inverse problem solution contributes to good convergence.

Next, the material characterization method is tested using measured data obtained as a result of introducing different liquids in the gap regions of the sensor. Table 1 shows the materials for which measurements were obtained for in this manuscript. The table lists the dielectric properties of these materials found in the literature at different frequencies for the purposes of discussion of the extracted material properties in this manuscript.

Material	Frequency	Dielectric
IPA [58]	500GHz	1.64 (no imaginary information provided)
Methanol [62]	70GHz	4.66+2.43i
Toluene [63]	250GHz	2.25+0.015i
Cyclopentanone [64]	70GHz	2.07+0.047i

Table 1. Dielectric properties of IPA, Methanol, Toluene and Cyclopentanone at corresponding frequencies (from the literature)

Figures 25(a) and (b) show the material properties extracted for Toluene as a result of the material characterization method implementation. The result obtained are comparable to the dielectric properties found in the literature. As seen in Table 1 at 250GHz Toluene has an

$\varepsilon_r = 2.25 + 0.015i$, while the results obtained in this paper show an $\varepsilon_r = 2.269 + 0.02123i$ at 249.8GHz. The difference between material properties from the literature and those obtained in this paper may be attributed to different reasons, including the errors in fabrication mentioned earlier, systems fluctuation when measuring the transmission coefficients and the optimization method convergence limitations.

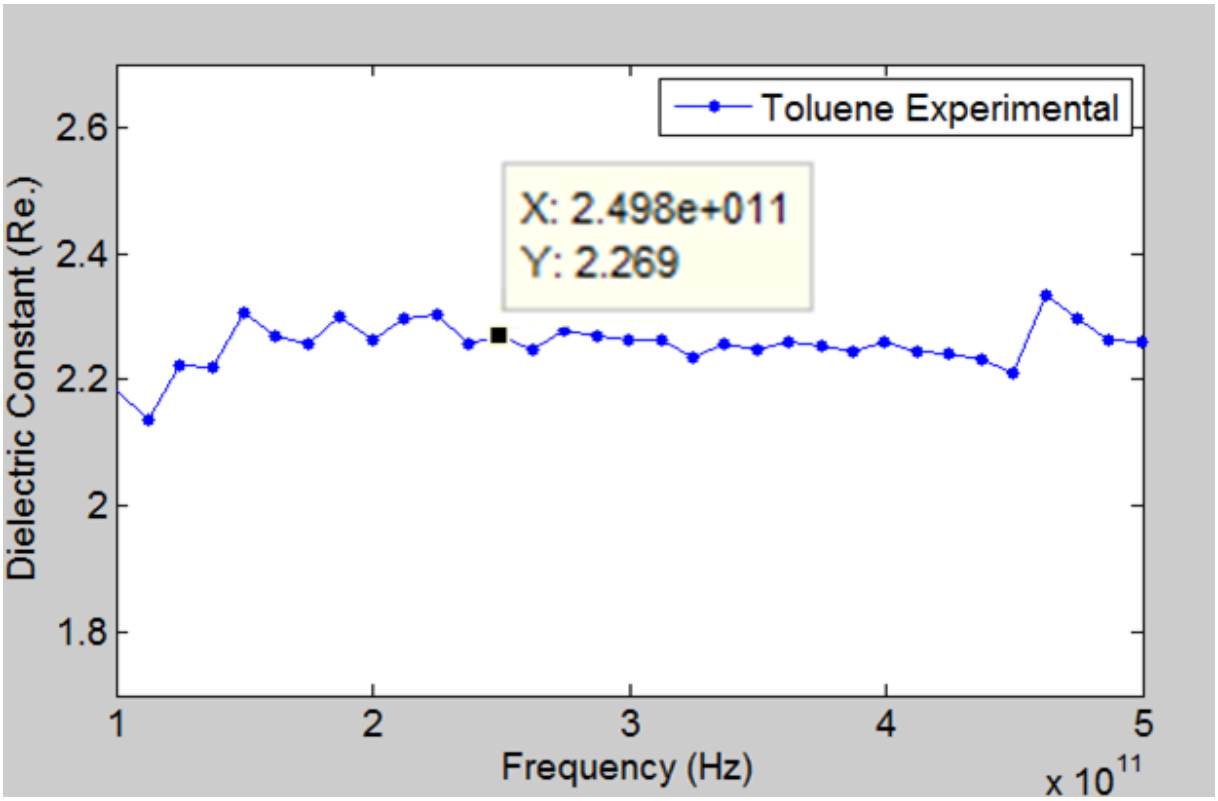

Figure 25(a). Toluene extracted dielectric constant (real part)

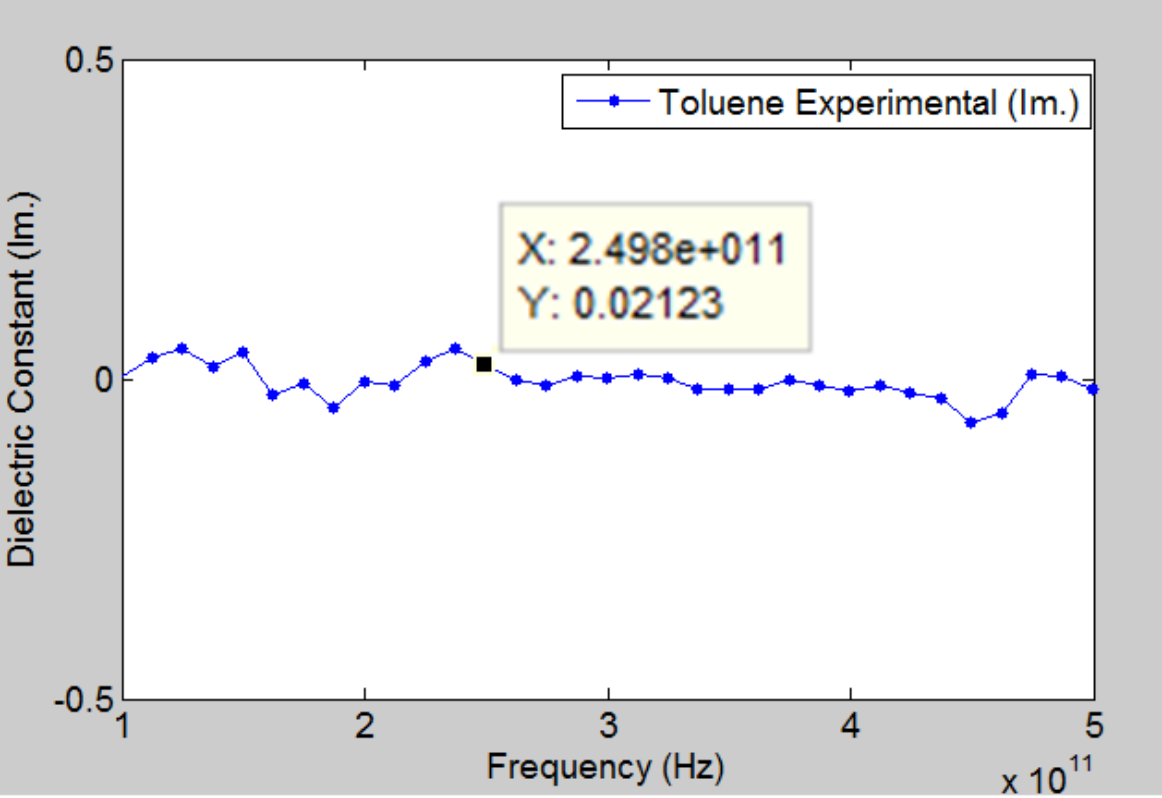

Figure 25(b). Toluene extracted dielectric constant (imaginary part)

Figures 26(a) and (b) show the dielectric properties extracted for a mixture of Toluene and Methanol (50% each). In the previous subsection, the measured transmission coefficients of the sensor as a result of injecting Toluene and Methanol were obtained separately (see Figure 22). The conclusion drawn was that Toluene is a low loss material while Methanol is a high loss material. Therefore, it is expected that the mixture would have a higher dielectric loss than Toluene alone. The Toluene dielectric properties obtained earlier, shown in Figures 25(a) and (b), show an $\varepsilon_r = 2.269 + 0.02123i$ at 249.8GHz while the extracted dielectric properties obtained for the Toluene and Methanol mixture (50% each) are $\varepsilon_r = 2.426 + 0.129i$ at 249.8GHz which has a higher loss than Toluene alone. Also, the relatively minor variation in the real part of the dielectric constant of the mixture compared to Toluene alone does explain the effect seen earlier in Figure 23 where the stop band size and location only slightly changed for

the different Toluene-Methanol mixtures compared to Toluene alone. From this it can be deduced that the real part of the dielectric constant of Methanol at about 250 GHz is considerably less than that seen at 70 GHz listed in Table 1.

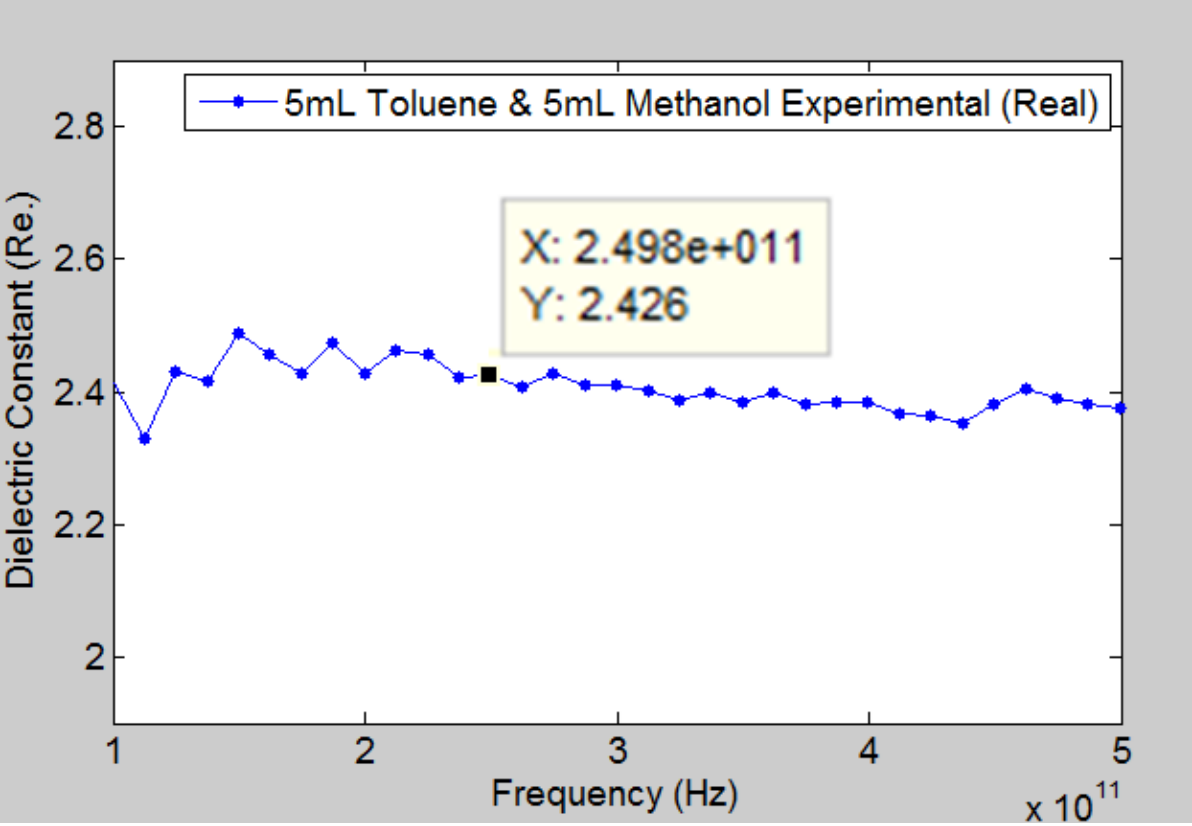

Figure 26(a). Toluene-Methanol mixture extracted dielectric constant (real part)

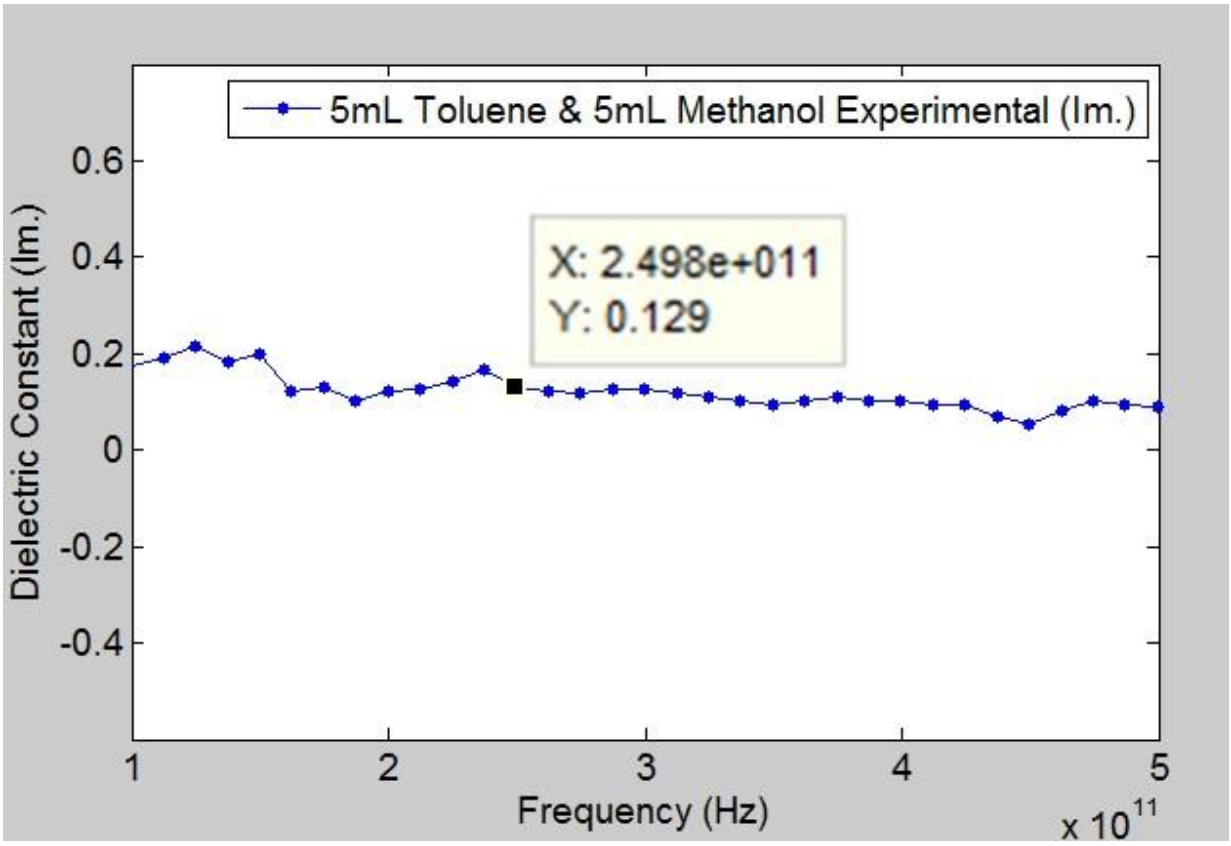

Figure 26(b). Toluene-Methanol mixture extracted dielectric constant (imaginary part)

Figures 27 (a) and (b) present the extracted material properties of IPA. It is seen that the real and imaginary parts of the dielectric constant decrease as a function of frequency between 200GHz and 500GHz. It is well known that many materials have considerable variation in the dielectric constant, throughout the frequency spectra. In this case, at 500GHz the extracted result for the real part of the dielectric constant is 1.652 which is close to that seen in literature at 1.64 [58]. The difference may again be attributed to the measurement system fluctuations and sensor fabrication disadvantages.

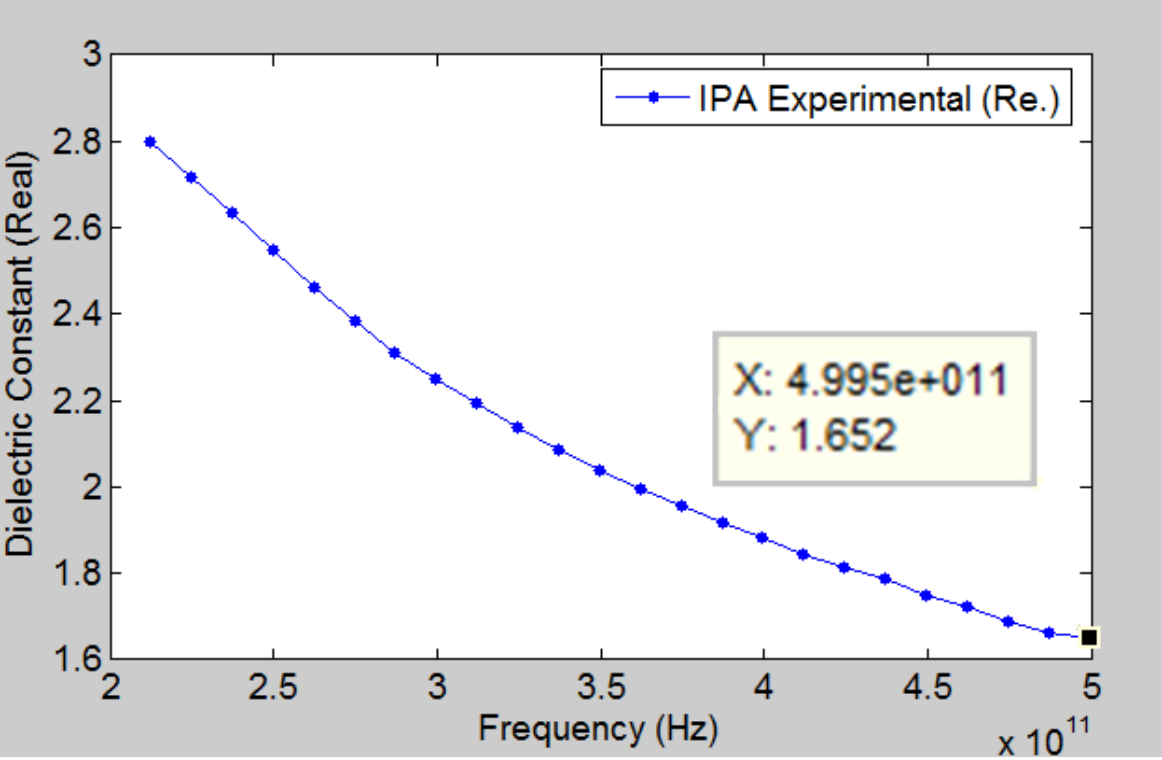

Figure 27(a). IPA extracted dielectric constant (real part)

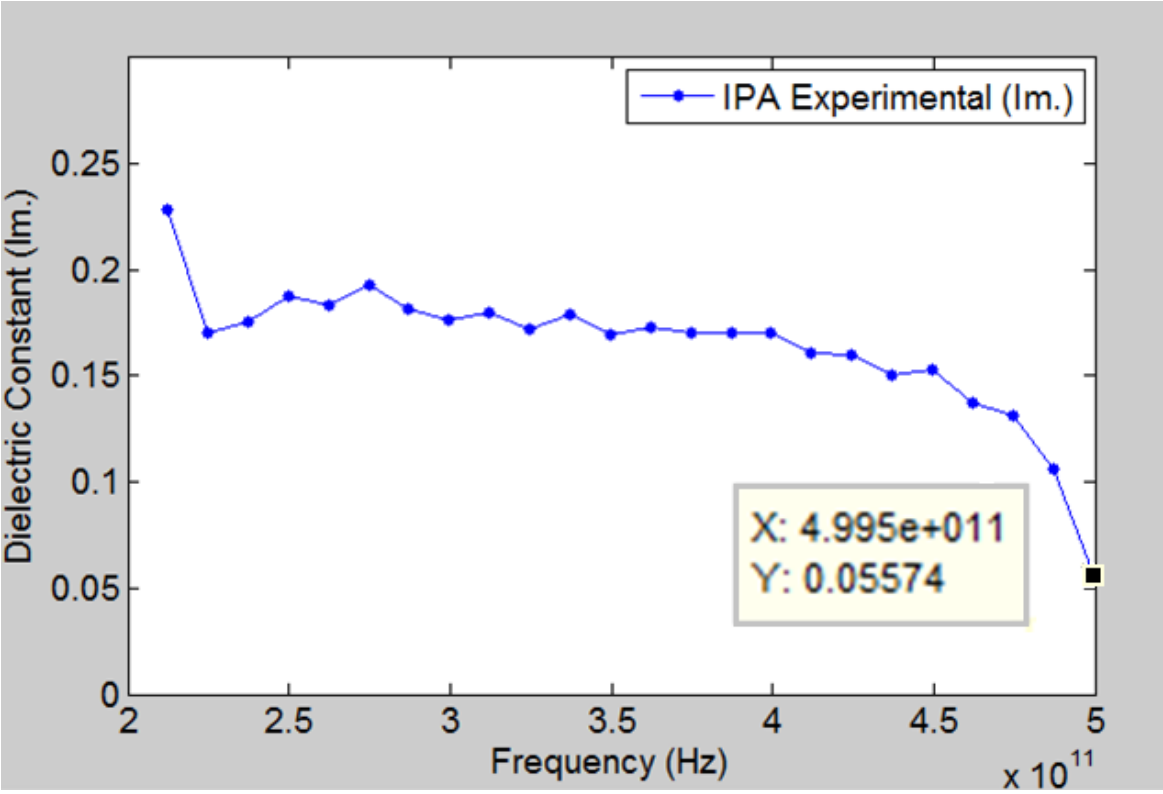

Figure 27(b). IPA extracted dielectric constant (imaginary part)

Overall it can be concluded that the material characterization method succeeds in extracting the dielectric properties of material samples accurately and can be used for future material characterization of unknown liquids and gases.

2.6 Conclusion

Two THz photonic crystal sensing structures have been demonstrated. The sensors are inexpensive, compact, highly sensitive, and allows for real time monitoring and characterization of materials. The goal is to expand on this design and find one that will be more compact and sensitive, will require less volume sample to be used and will be relatively easy and inexpensive to fabricate, therefore a 3D design is investigated in the next chapter. The use of PC structure as a sensor allows in large change in transmitted signal due to introduction of samples in the air region of the PC. This change is easily detected and leads to accurate measurement of dielectric properties of samples.

CHAPTER 3

3D PHOTONIC CRYSTAL

A 3D photonic crystal (PC) has the ability to confine and control light in all three dimensions as mentioned in chapter 1. This property allows for a 3D PC based sensor to be more sensitive than its 1D or 2D counterparts. A photonic band gap in 3D is produced by the waves blocked in all directions. As mentioned before, the bang gap is determined mainly due to contrasts in dielectric properties of the materials used. In 3D photonic crystals complete band gaps are rare; in order to achieve it the gap has to oppress the complete 3D Brillouin zone [17]. In order to achieve a complete band gap, the right design dielectric contrast as well as the right design dimensions need to be selected. The first 3D PC with a complete band gap at micron scale was designed in 1994 and this was the woodpile structure [17]. A woodpile structure is a series of stacked logs in different directions. It was found that the best woodpile structure is the ABCDABCD type structure with A representing one log orientation and B and orthogonal orientations and C and D are the same directions as A and B but offset by half the distance between two rods in one layer [17]. When comparing the woodpile structure with other 3D lattice structures, it can be seen that the woodpile will generate higher quality band gaps in wider bandgaps [65-67]. Until now, these designs have been fabricated using lithographic techniques, femtosecond laser direct writing, micromachining and wafer fusion techniques [17, 68-70] but to our knowledge there hasn't been a 3D photonic crystal design fabricated with a 3D printer.

3.1.1 Advantages and Disadvantages of 3D Photonic Crystal Microfluidic Sensor

One advantage of a 3D photonic crystal design is its high sensitivity and smaller sample volume use when compared to the 1D design. The more constraints in the device (3D versus 1D) when sending the THz wave through, the better results that can be achieved. In other words, the presence of more distinguishing features in the transmission coefficient, as a function of frequency, due to the same materials inserted in the gaps of the 3D device result in higher sensitivity in comparison to the 1D device. The main disadvantages of the current design are in its fabrication due to the low resolution of the 3D printing method in addition to the measurement limitations discussed earlier in chapter 2.

3.1.2 Woodpile Structure Design

In this thesis a periodic woodpile structure is designed. The logs in this design are parallel to each other having a pitch of 946µm. The width and height of each rod is 173µm with a length of 2cm. The layers are repeated 20 times, giving five repetitions of a unit cell adding up to a 3.46mm total height. Figure 28 depicts the first six layers of the structure design. At the top and bottom of the woodpile structure designed in this thesis there is a 400µm thick sheet covering the entire sensor (2cm x 2cm) not shown in Figure 28, this was added in order to be able to hold liquids inside if liquids are added to be tested.

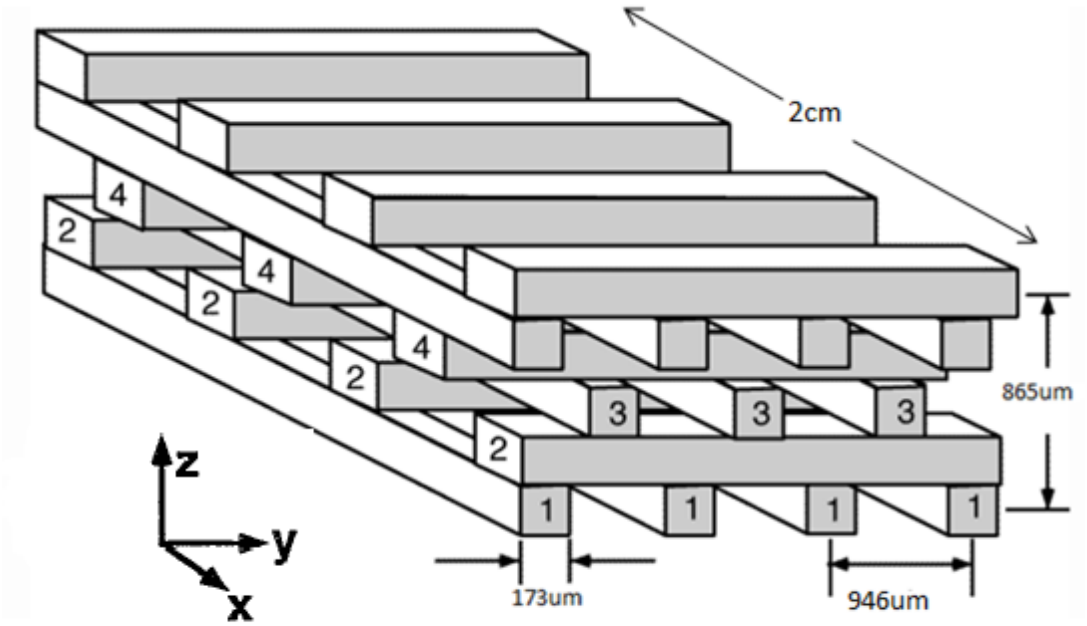

Figure 28. Woodpile structure [71] with dimensions for design in this chapter

This design, not including the top and bottom sheet was borrowed from [33] and scaled to yield a photonic band gap with resonance at approximately 290GHz using an Acrylic type material. The Acrylic material was selected due to its compatibility with 3D printing. The bang gap produced by the photonic crystal design is based on the dielectric differences between the materials being used [17, 71], in this case air and an Acrylic type material with dielectric properties of $\varepsilon_r = 2.79$ and $\tan(\delta) = 0.026$ or $\varepsilon_r = 2.79 + 0.725i$ [72]. Using these dimensions, the volume sample needed for this design would be 460µL which is less than the 952µL volume needed for a 1D design of similar dimensions.

3.2 Simulation of Filter designed

This design has been simulated using HFSS (high frequency structural simulator) by Ansys, using Floquet's theorem. As the design is a periodic structure, that can be defined by a unit cell and it has uniform periodic spacing this theorem applies [73]. Based on these simulations the design was analyzed assuming it was infinitively large in the x and y direction and limited to the number of layers in the z direction. The greater the number of layers in the woodpile structure, the more the band gap effect is enhanced [39]. As mentioned above, the design is borrowed from [33] and scaled to fit our needs. To achieved this results a woodpile structure of 20 layers was simulated with the measurements mentioned above w=h=173µm and pitch of 946µm. The simulation is shown in Figure 29 below.

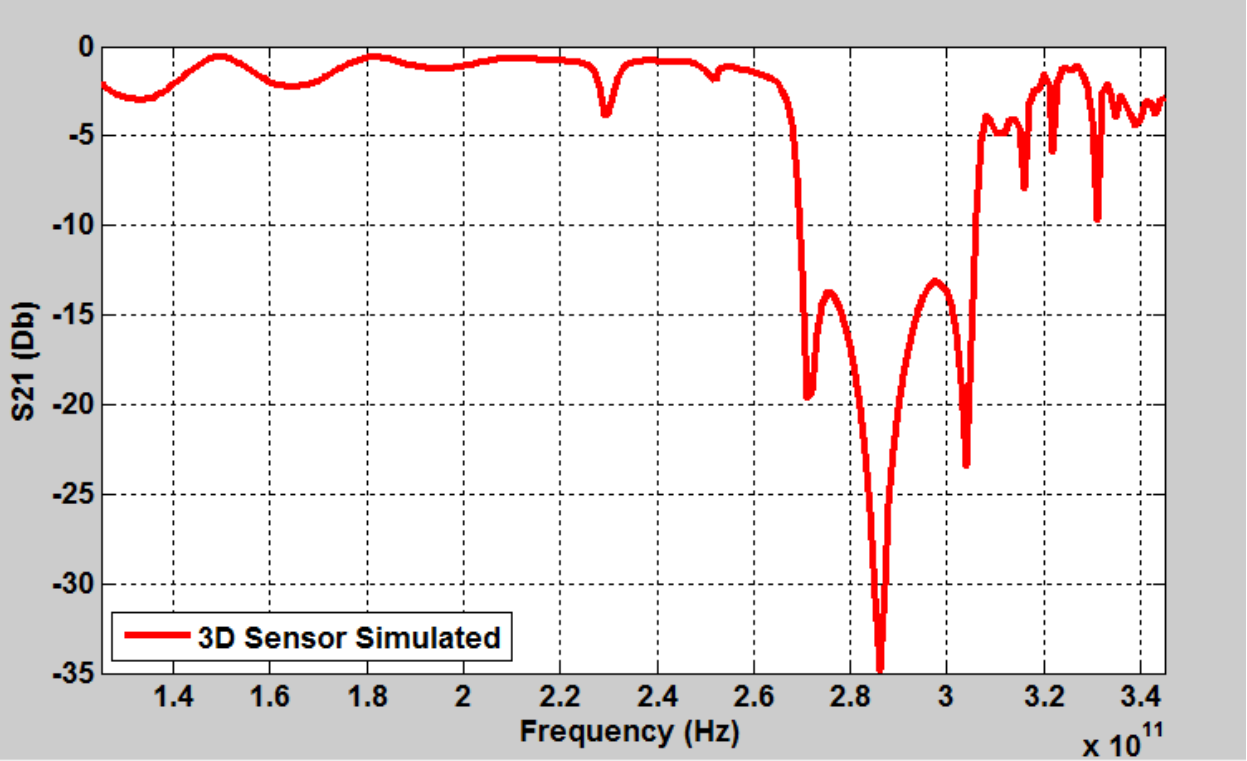

Figure 29. Transmission Coefficient Magnitude of the 3D Simulated Design with $\varepsilon_r = 1 + 0i$

In this design, the resonant frequency is observed at approximately 286GHz at depth of -35dB in the band gap. The band gap width was about 36.1GHz with maximum amplitude of -13dB. This fact is important due to the challenges in measurement, in particular the resolutions of the Terahertz machine 12GHz, only allowing for three points to be picked up in this design. Although, normally the bandwidth is analyzed at half power of -3dB, in this case being approximately 65GHz, it is important in this analysis to look below -10dB to account for errors in fabrication, measurements and simulations later in the chapter.

Figure 30 the changes in transmission due to the changes of the width of the rods composing the design is analyzed. In this simulation it is seen that when changing the width of the rods from 150µm to 173µm the resonant frquency decreases by 0.05GHz and the amplitude of the bandgap decreases by 3dB, while the bandwitdh decreases by 1GHz. When comparing the design with rods of 173µm and 200µm it is observed that the resonant frequency decreases by 6GHz from 286GHz to 281GHz and the bandwitdh increases by 2GHz, while the amplitude of the bandgap increases by approximately 1dB. Comparing the rods at 173µm to of 250µm, the bandwidth increases by 6GHz with 250µm and the resonant frequency decreases by 13GHz, while the amplitude of the bangap increased by 2.5dBs.

These calculations showed that the greater the witdth of the rods the higher the amplitude of the bandgap and the greater the bandwith the of the design. It can also be observed that the resonant frequency is decreased as the rods size is increased.

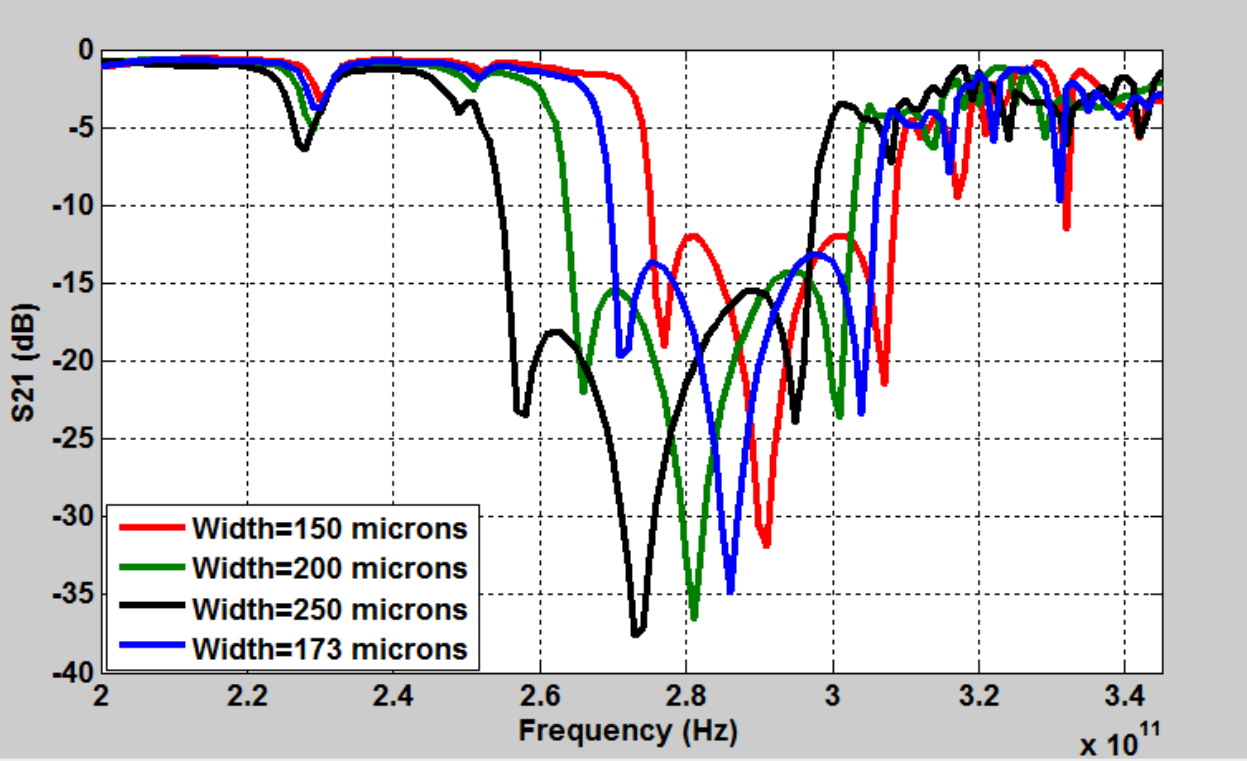

Figure 30. Transmission coefficient magnitudes as a result of various sensor rod widths

In this evaluation it is seen that there are better designs than the one used in this thesis in the sense of greater bandwidths with more intensity in the bandgap, but the resonant frequency would be lower. Also, another detail as to why the design of 173μm was chosen has to do with fabrication issues that will be explained in the next section.

In order to investigate changes in transmission due to the changes in the dielectric properties in the empty gaps of the filter, different materials of $\varepsilon_r = 1.5 + 0i$ and $\varepsilon_r = 2 + 0i$ were added in addition to air $\varepsilon_r = 1 + 0i$ and the result is shown in Figure 31 below.

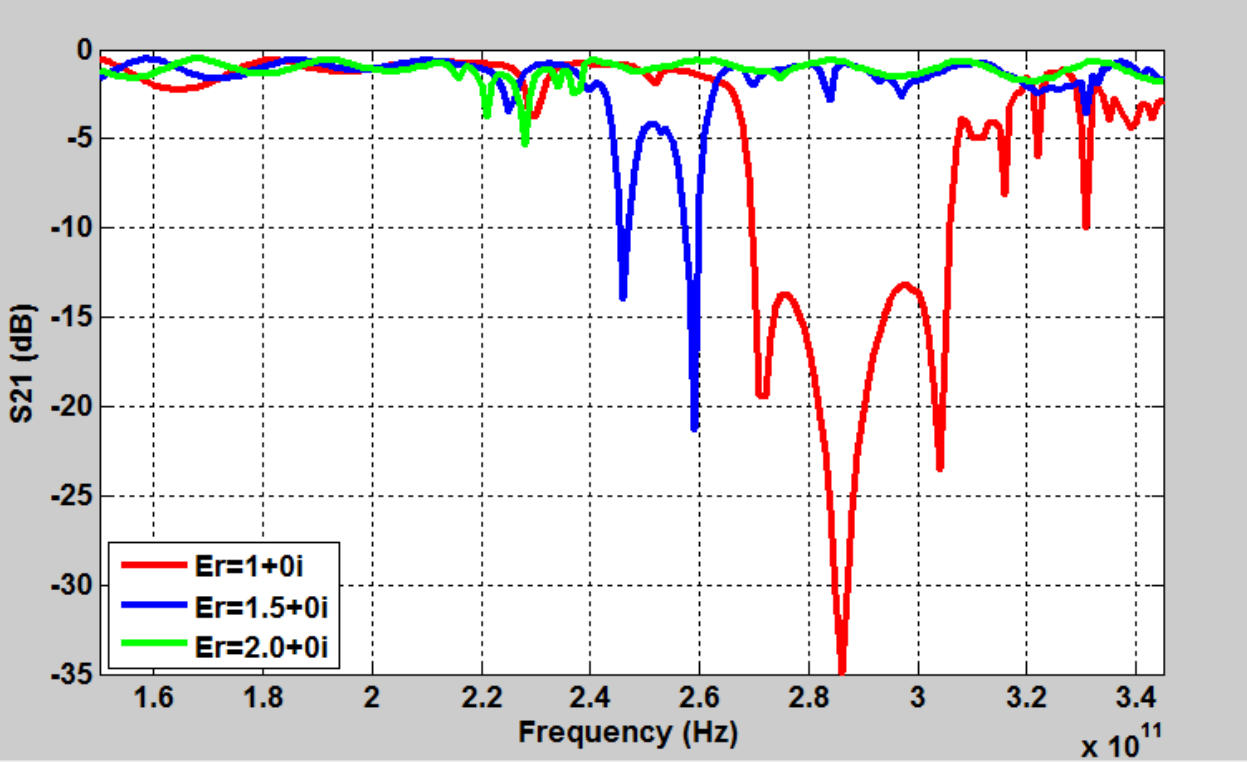

Figure 31. Transmission coefficient magnitudes as a result of introducing materials with large changes in the real part of the dielectric constant

In this case it is noticed that when the material used is changed from $\varepsilon_r = 1 + 0i$ to $\varepsilon_r = 1.5 + 0i$, the intensity of the band gap reduces by approximately 12dBs and the resonant frequency shifts to the left by approximately 12GHz. It is also observed that the three picks (resonances) conforming the bandgap shown with an air sample is now converted to two picks when using this new material ($\varepsilon_r = 1.5 + 0i$) in the simulation resulting in a shrinkage of the band gap by approximately 16GHz. Likewise, when a material of $\varepsilon_r = 2 + 0i$ is placed in the air medium of the device, it is observed that the resonant frequency again shifts to the left by approximately 30GHz and the intensity is reduced by approximately 8dBs (from the previous discussed sample). Using this calculation (simulation) it can be concluded that by largerly varying the real part of the dielectric constant the greater the dielectric constant the lesser the bandgap becomes

and the resonant frequency is shifted to the left. In the case of materials with a dielectric constant of $\varepsilon_r = 2 + 0i$ or greater the bandgap does not show below -10dBs, indicating a limitation to this design, it will only work for lossless materials that have a real part of the dielectric constant of less than $\varepsilon_r = 2$. Contrasting Figure 31 to Figure 15, it can be stated that there is significantly large change in transmitted signal for a 3D structure as opposed to a 1D photonic crystal structure. Thus, it confirms the assumption that a 3D PC provides higher sensitivity.

Figure 32 shows the same type of variation in the empty spaces but this time the dielectric change in minute amounts, here it is observed that the sensor is highly sensitive as previously thought, this can be seen by analyzing the change in transmission due to very small changes in the material properties being used, in the case below a change from $\varepsilon_r = 1 + 0i$ to $\varepsilon_r = 1.001 + 0i$. In this calculation the change between $\varepsilon_r = 1 + 0i$ to $\varepsilon_r = 1.001 + 0i$ and $\varepsilon_r = 1.01 + 0i$ is much more noticeable than it was when changing the same amounts in the 1D sensor shown in chapter 2, in order to see this changes in the 1D sensor a defect needed to be added.

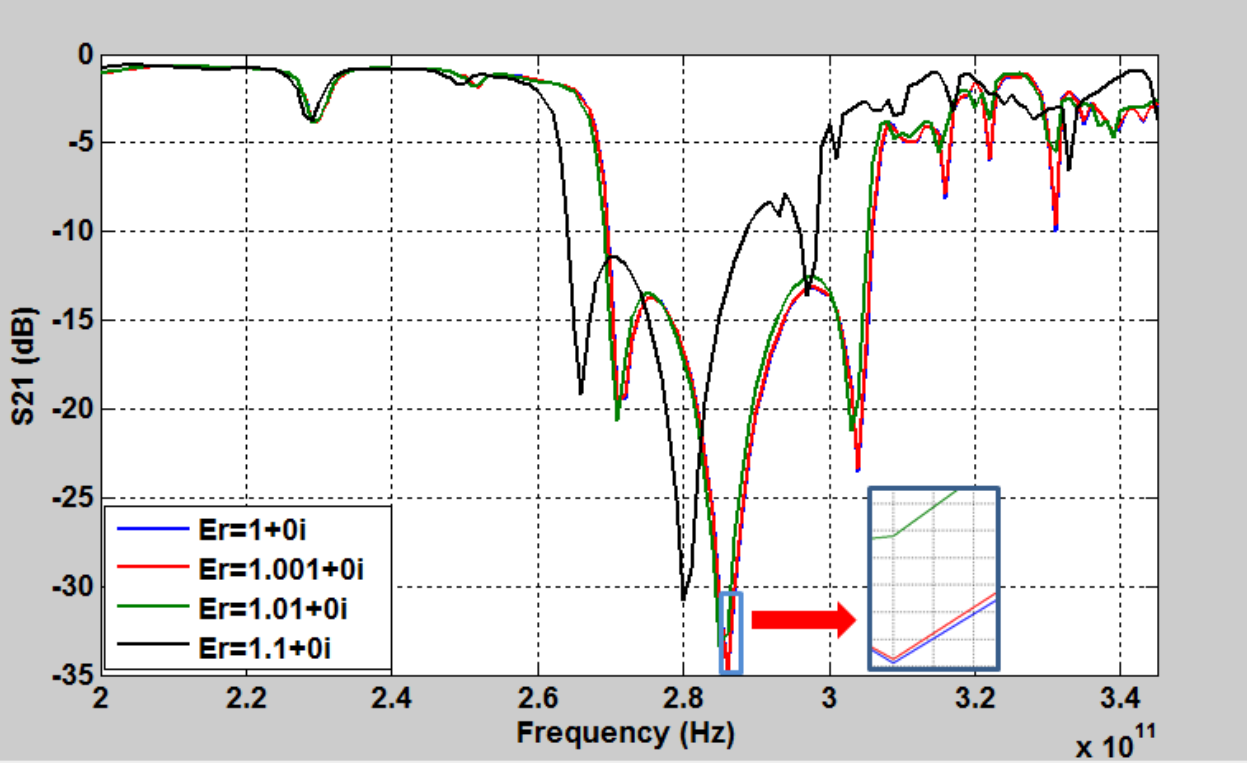

Figure 32. Transmission coefficient magnitudes as a result of introducing materials with small changes in the real part of the dielectric constant

As seen in the previous figure, here again, the resonance frequency shifts (in changes greater than 10^{-4}) to the left and the amplitude of the bandgap decreases. When changing the dielectric material from $\varepsilon_r = 1.0 + 0i$ to $\varepsilon_r = 1.001 + 0i$ it is observed a very slight decrease in the amplitude, 0.05dB and there is no shift in the resonant frequency. When the dielectric medium is changed from air to $\varepsilon_r = 1.01 + 0i$ the affect on the transmission is more clearly seen, the shift in frequency by 1GHz to the left while the intencity is reduced by approximetly 2.5dB. In both this cases the change in the bandgap is not very substancial either, less than 1GHz decrease. As the material is changed to $\varepsilon_r = 1.1 + 0i$ now the effects is much more notizable, the resonant frequency was reduced by 6GHz while the intensy was reduced by approximetly 4dBs and the bandgap at -10dB is now approximetly 25GHz. This indicates that as shown with a 1D sensor,

the increase in the real part of the dielectric property or increases in the empty spaces of the filter, the resonance frequency decreases as does the bandwith and the intensity of the bandgap. However, it also demonstrate the higher sensitivity of this sensor when compared to the 1D sensor in chapter 2 and limitation in lossless materials, but since there is not such a thing as a lossless material, that limitation is not an important part of this conclusion.

In order to get a more in depth understanding of the behaviour of the design, a simulation showing changes in the imaginary part of the dielectric constant is analyzed, see Figure 33 for details.

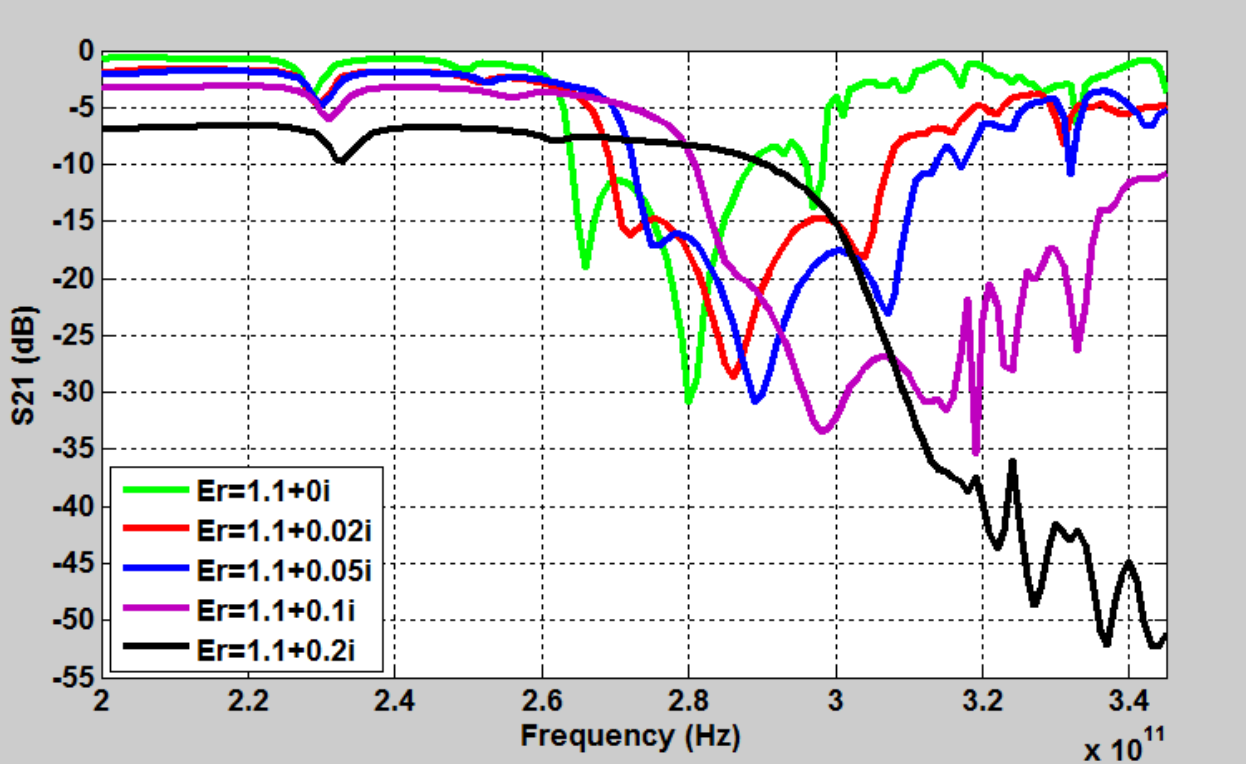

Figure 33. Transmission coefficient magnitudes as a result of introducing materials with small changes in the imaginary part of the dielectric constant

Here it is observed that when changing the properties from $\varepsilon_r = 1.1 + 0i$ to $\varepsilon_r = 1.01 + 0.02i$ and $\varepsilon_r = 1.01 + 0.05i$ the resonant frequency increases by 6GHz and approximatly 8.5GHz respectively. In the case of $\varepsilon_r = 1.01 + 0.1i$ and $\varepsilon_r = 1.01 + 0.2i$ the sample becomes too lossy for analysis. In this case it is noted that the higher the imaginary part of the lower the intensity of the signal as shown with the 1D desing in chapter 2. The other similarity is that the materials resosnant frequency is only picked up until the material becomes too lossy to show it and the signal completelly disapears into the floor level. Lastly, it is observed, not in accordance to the 1D design, that while the resonance frequency can be seen, it will increase as the loss of the material increases.

Overall, it has been demonstrated that changes in materials properties in the original air medium will produce changes in the transmission, indicating the device can be used as a sensor. Its sensitivity and limitations due to materials used has been shown. Now that we have a design we will proceed to the fabrication details in the next section.

3.3 Fabrication

Figure 34 a) and b) show the fabricated 3D PC sensor. This design was fabricated using a 3D printer, the material used is an Acrylic (ABS) type material (named Verowhite) with dielectric properties of $\varepsilon_r = 2.79 + 0.0725i$ as mentioned above.

a) b)

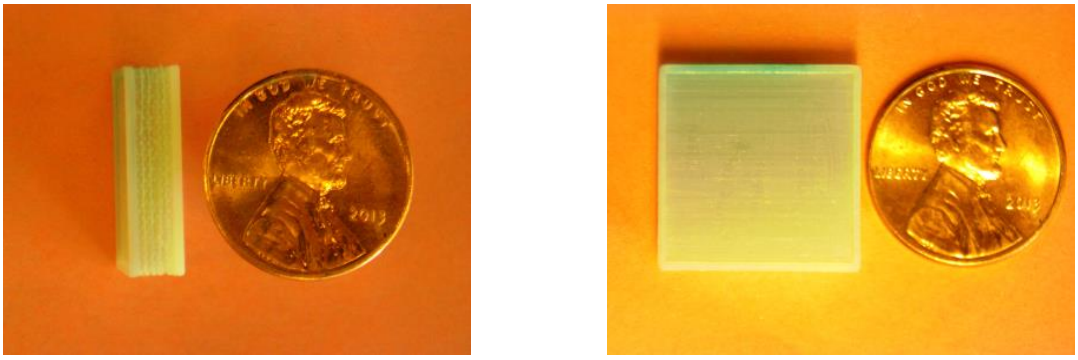

Figure 34. a) Side view of sensor, b) Frontal view of sensor

The printer prints the dielectric layer by layer. The hollow regoin is temporary filled with non-cross linked material to provide mechanical stability during the deposition of the subsequent layers. The non-cross linked layers are later washed out. One of the greatest advantages of this fabrication technique is the ease and speed in which it can be accomplished. A limitation of this fabrication method is the relatively low resolution of the printer in comparison to the design. Although the device seems to be propertly printed, it was encountered through measurements and experiments that the inside of the device is not as accurate as necessary for the design of a sensor. As mentioned above, this design is 173µm in the y direction and the printer resolution in this direction is only of 100µm. The resolution in the Z axis is 30µm, not leaving a lot of room for error. However the decision was made to use this size in order to leave a greater empty space volume to be able to clean all the residues left in the sensor by the printer. Adding to that, as seen in figure 28, the layers are offset to each other, therefore cleaning inside the airgaps is very difficult with such small features of the PC. In order to clean the residue from within the sensor, after it was printed, water and IPA were used as well as lightly blowing nitrogen through the filter to prevent breaking the delicate rods and trying to clear out residue. Additionally, the

device was placed in a vacuum oven overnigtht to remove all moisture content from the material prior to measurements. Even all of these steps were taken it appears that the inside of the filter was not completed cleared out, affecting results when measuring transmission response, which will be analyzed later in this chapter.

3.4 Experimental Results

The result was measured in a 14mm diameter window, using the holder seen in figure 19b, upper right, as it was for the sensor in chapter 2. Figure 35 shows the calculated versus measured results, here it is observed that although a bang gap it is seen, the resonant frequency is much lower than expected as well as the intensity of the band gap being decreased and the material seeming to be more lossy than expected. All of these discrepancies are explained with by the limitation in measurement and fabrication mentioned before. As it was discussed, the greater the width of the rods, the further to the left the resonance frequency will shift and the greater the bandwidth of the bandgap, since the printer resolution was low in comparison it was suspected that the extra material was not completely removed from the inside of the sensor, resulting in wider rods. This result seems to be in accordance with that assertion.

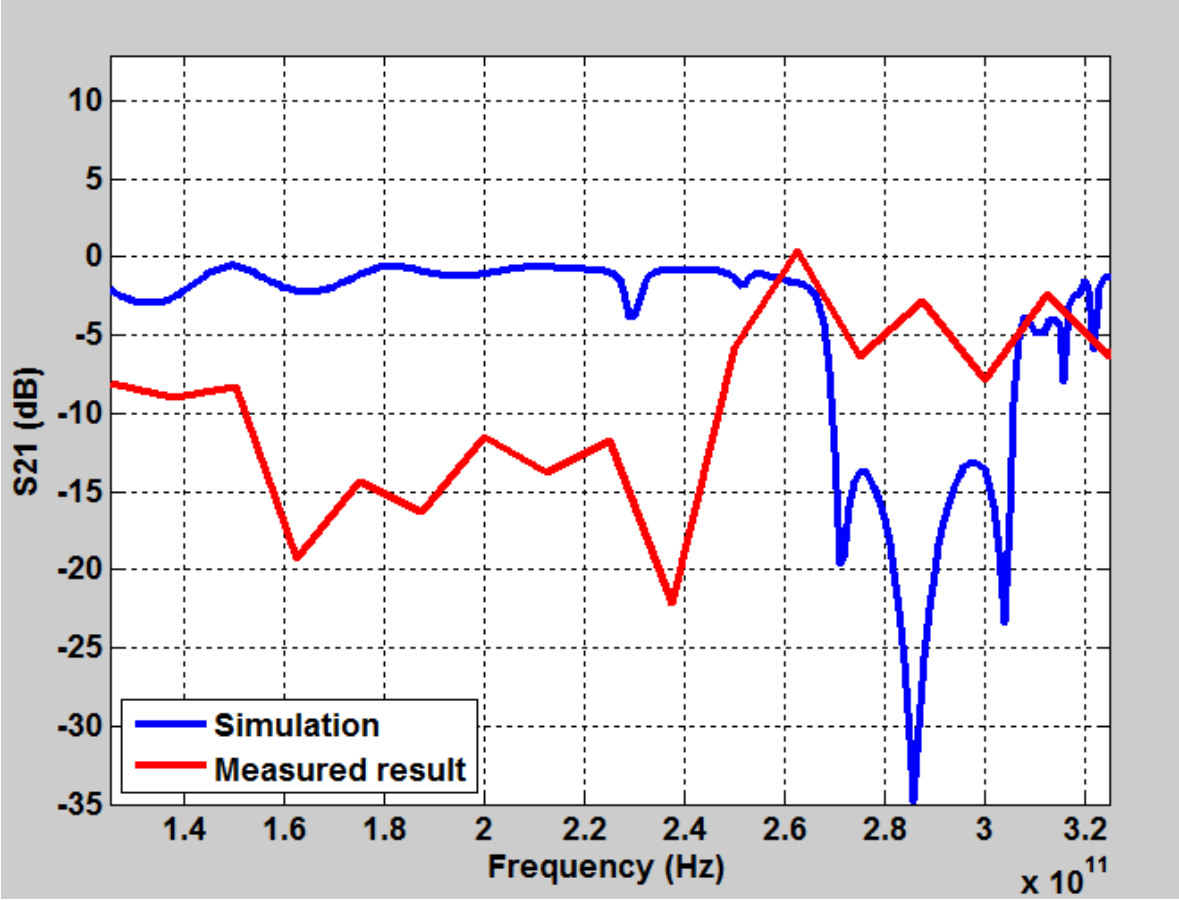

Figure 35. Measured versus simulated transmission coefficient magnitudes

The decrease in intensity of the band gap shown in Figure 35 above is believed to be due to the measurement limitations, the simulation is picking up points every 1GHz while the measured results are being picked up every 12GHz, making it possible for the larger intensity picks to be missed. Finally the loss of the material appears to be greater, this can be explained by the cleaning process, even though nitrogen and a vacuum were used to remove the liquids used to clean the sensor, it is possible that some residue was left behind making the results show as a more lossy material, also dust and oil form hand holding the device could cause this loss. In addition to all of this there is also the systems fluctuation when measuring the transmission explained in chapter 2.

Since for this work there is limitation in measurement, in the 3D printing resolution and materials to be used are limited, the combined restrictions on fabricating and measuring this device are still too great. These measurement challenges by themselves are not an issue to work around but when united with severe fabrication issues such as in the 3D sensor printing case, they become almost too great. In view of these challenges, the structure was not used in carrying out any further improvements. However, it has been clearly demonstrated through simulations that this structure will form a highly sensitive sensor for the characterization of small volumes of samples.

CHAPTER 4

CONCLUSION

Three PC sensors were designed under the same theoretical principles. Each sensor was improved based upon the previous one chronologically. The sensors are sensitive, cost efficient, compact, easy to fabricate and allow for real time monitoring. Material characterization can be carried out from the sensor data as shown in the case of the 1D sensor. The devices were designed to work in the THz frequency range which provides many advantages for characterizing or sensing biomaterials.

In chapter 2, two THz 1D photonic crystal sensing structures have been demonstrated with one being an improvement on the other. The sensors are inexpensive, compact, highly sensitive, and allow for real time monitoring and characterization of materials. The underlying theory behind the sensors, the design and fabrication procedures have been presented. The sensing operation is made possible due to the fact that the transmission coefficient of a wave through the sensor is dependent upon the material filling the gap regions of the device. The effect of different gap filling materials has been examined through calculation and measurement. In order to better understand and gain more information about the material being sensed, a material characterization scheme was developed and tested using synthesized and measured data. The material characterization scheme extracts the dielectric material properties of the unknown gap filling material being interrogated. Future work for the 1D sensor includes carrying out error analysis studies to examine the manufacturing and measurement uncertainties on the sensor and its corresponding material characterization method results. The results of the error analysis study may be used to improve the sensor design and measurement setup. Additionally, sensing and

characterization of biomaterials could be carried out.

In this thesis, the main concentration was to design and improve the sensing capabilities of a PC sensor in the THz frequency range. One goal was to expand on the 1D design and find one that would be more compact and sensitive, would require less test sample volume to be used and will be relatively easy and inexpensive to fabricate. Keeping this in mind, a THz microfluidic 3D PC sensor has been demonstrated in chapter 3. This design has been proven, through simulations, to be more sensitive. In principle, it was shown to be easier to fabricate, in addition to needing smaller sample volumes than the 1D design. The sensing operation is also made possible in this design due to the fact that the transmission coefficient of a wave through the sensor is dependent upon the material filling the gap regions of the device. The effect of different gap filling materials has been examined through calculation and measurement. However, when it comes to measurement and fabrication, more advances need to be made with Terahertz technologies and 3D printing in order for this sensor to be a viable solution for the public at this time. While keeping in mind those limitations, the overall 3D design could be improved by increasing the width of the rods or by using a material with higher dielectric constant.

We have successfully implemented microfluidics, photonic crystal and terahertz all in one design and as technologies with terahertz systems and 3D printing are improved this sensors can become part of everyday industry testing.

APPENDIX

Appendix

Matlab Code

```
% 1D sensor, no defect, Calculated Transmission, Forward Problem
Solution

clc
clear all
close all
format long
%%%forward problem
%%%generating synthesized transmission coefficient

layers=10^-6*[150 315 150 310 150 305 150 302 150 302 150 305
150 310 150 315 150];%thickness of layers (layers start by
solid-air-solid)

%erps=1.8;%other empty layers dielectric constant (real)
%eips=0.01;%other empty layers dielectric constant (imaginary)
erps=1.0;%other empty layers dielectric constant (real)
eips=0.0;%other empty layers dielectric constant (imaginary)


fs=100*(10^9):10*(10^9):500*(10^9);%frequency range
rps=3*ones(1,size(fs,2));%dielectric constant of solid (real
part)
ips=0.15*ones(1,size(fs,2));%dielectric constant of solid
(imaginary part)

for jh=1:size(fs,2)
    realeps=rps(jh);
    imageps=ips(jh);
    empty_layers_realeps=erps;
    empty_layers_imageps=eips;
    freqsa=fs(jh);
    test_response1=
OneD_filter_response_no_defect(layers,realeps,imageps,freqsa,emp
ty_layers_realeps,empty_layers_imageps);
    test_response(jh,1:2)=test_response1;
end

figure
plot((test_response(:,1)),abs((((test_response(:,2))))),'r');
grid
```

```
Tm=test_response(:,2);%calculated


%%%%%%%%%%%%%%%%%%%%%%%%%%%%%%%%%%%%%%%%%%%%%%%%%%%%%%%%%%%%%%%%%%%%%%%%%%%%
%%%%%%%%%%%%%%%%%%%%%%%%%%%%%%%%%%%%%%%%%%%%%%%%%%%%%%%%%%%%%%%%%%%%%%%%%%%%
%%%%%%%%%%%%%%%%%%%%%%%%%%%%%%%%%%%%%%%%%%%%%%%%%%%%%%%%%%%%%%%%%%%%%%%%%%%%

% Function needed to run the code above
resp=OneD_filter_reponse_no_defect(thicknessvector,realeps,image
ps,freqsa,empty_layers_realeps,empty_layers_imageps)


% 1D (Planar) N-Layer P-Polarization (TM) Simulation
% (C) 2009-2010, Collin Meierbachtol, meierbac [at] msu [dot]
edu
% Taken from "Theory of reflection : of electromagnetic and
particle waves"
% by John Lekner, 1987.

format short g

% USER INPUT - System Definitions

t = 0; %Angle of incidence measured from normal [degrees]

%dielectric properties of each layer including the input and
output media
%(air in this case)
eps = [1 complex(realeps,imageps)
complex(empty_layers_realeps,empty_layers_imageps)...
    complex(realeps,imageps)
complex(empty_layers_realeps,empty_layers_imageps)...
    complex(realeps,imageps)
complex(empty_layers_realeps,empty_layers_imageps)...
    complex(realeps,imageps)
complex(empty_layers_realeps,empty_layers_imageps)...
    complex(realeps,imageps)
complex(empty_layers_realeps,empty_layers_imageps)...
        complex(realeps,imageps)
complex(empty_layers_realeps,empty_layers_imageps)...
    complex(realeps,imageps)
complex(empty_layers_realeps,empty_layers_imageps)...
    complex(realeps,imageps)
complex(empty_layers_realeps,empty_layers_imageps)...
    complex(realeps,imageps)...
    1]; %Permittivity matrix - can be complex!
layers=thicknessvector;
```

```
d=[0,layers,0];

% NOTE: first and nth layer assumed to be semi-infinite, so
their thickness is set to zero
% to the total sum is just the layer thicknesses, given in
meters

% Inherent Physical Constants
eps0=8.85e-12; % Permittivity of free space [F/m]
mu0=pi*4e-7; % Permeability of free space [Wb/m]
c=1/sqrt(eps0*mu0); %Speed of light [m/s]
lambdabla=c./freqsa;
%hold on

for lambdavary=1:1:1
    lambda01(lambdavary) = lambdabla(lambdavary);


% Conversions and calculations
[epsr,epsc] = size(eps); %epsc reports number of layers
k0(lambdavary) = 2*pi/lambda01(lambdavary); %Free space incident
wave number
c=1/sqrt(eps0*mu0); %Speed of light [m/s]
omega(lambdavary) = c*k0(lambdavary); %Incident wave frequency
ztot=sum(d); %Total thickness of finite layers

% Generate boundary vector matrix
zsum(1) = 0;
for zj = 2:1:epsc-1;
    zsum(zj) = zsum(zj-1) + d(zj);
end

% MAIN CALCULATION LOOP - DO NOT ALTER!
Mtot = [1 0;0 1];
for n = 1:1:epsc;
    kx = k0(lambdavary)*sin(t*pi/180);
        kz(n) = k0(lambdavary)*sqrt(eps(n) -
eps(1)*(sin(t*pi/180))^2);
        Kz(n) = kz(n)/eps(n);

    if ((n > 1) && (n < epsc))
                M(:,:,n) = [cos(kz(n)*d(n))
sin(kz(n)*d(n))/Kz(n);
            -Kz(n)*sin(kz(n)*d(n)) cos(kz(n)*d(n))];

        Mtot = M(:,:,n)*Mtot;
    end
```

```
end
% Reflection coefficient (often complex)
rp(lambdavary) = -(Kz(1)*Kz(epsc)*Mtot(1,2)+Mtot(2,1)-
i*Kz(epsc)*Mtot(1,1)+i*Kz(1)*Mtot(2,2))/(Kz(1)*Kz(epsc)*Mtot(1,2
)-Mtot(2,1)+i*Kz(epsc)*Mtot(1,1)+i*Kz(1)*Mtot(2,2));

% Transmission coefficient (often complex)
tp(lambdavary) = 2*i*Kz(1)*exp(-
j*kz(epsc)*ztot)/(Kz(1)*Kz(epsc)*Mtot(1,2)-
Mtot(2,1)+i*Kz(epsc)*Mtot(1,1)+i*Kz(1)*Mtot(2,2));

% Reflectance (R+T+A=1)
Rp(lambdavary) = real(conj(rp(lambdavary))*rp(lambdavary));

% Transmittance (R+T+A=1)
Tp(lambdavary) =
real((kz(epsc)/kz(1))*conj(tp(lambdavary))*tp(lambdavary));

% Absorptance (R+T+A=1)
Ap(lambdavary) = 1-(Rp(lambdavary)+Tp(lambdavary));

end

freqresp=[omega'./(2*pi),tp'];
freqresp=flipud(freqresp);
resp=freqresp;

return


%%%%%%%%%%%%%%%%%%%%%%%%%%%%%%%%%%%%%%%%%%%%%%%%%%%%%%%%%%%%%%%%%%%%%%%
%%%%%%%%%%%%%%%%%%%%%%%%%%%%%%%%%%%%%%%%%%%%%%%%%%%%%%%%%%%%%%%%%%%%%%%
%%%%%%%%%%%%%%%%%%%%%%%%%%%%%%%%%%%%%%%%%%%%%%%%%%%%%%%%%%%%%%%%%%%%%%%

%%%%inverse problem solution to find dielectric property of
materials


Tm=test_response(:,2);%calculated transmission.  Although this
transmission came from calculated data, real data can be put in
here instead. In this thesis the code was run for both real and
calculated data.

for jjy=1:size(Tm,1)
cc=0
freqsa=fs(jjy)
if jjy==1
```

```
erpsc=1.7+rand*0.2;
eips=0+0.05*rand;
end
maxit=50;%maximum iterations for Nelder Mead at each frequency
while cc==0
N=2;
alfa=2; %Update with problem
rho=1; %Update with problem
zhi=2;
gamma=0.5;
sigma=1/2;

x0=[erpsc eips];
gama1=(((N+1)^(1/2)+N-1)/(N*sqrt(2)))*alfa
gama2=(((N+1)^(1/2)-1)/(N*sqrt(2)))*alfa

c=erpsc+gama1;
d=eips+gama2;
x1=[c,d]

e=erpsc+gama2;
f=eips+gama1;
x2=[e,f]

for jhk=1:maxit

if jhk==1
 x0new=x0
 x1new=x1
 x2new=x2
end

test_response0new=OneD_filter_response_no_defect(layers,realeps,
imageps,freqsa,x0new(1,1),x0new(1,2));
    Tc0new=test_response0new(:,2);
    aag01=angle(Tc0new);
    aah01=angle(Tm(jjy,1));
    af0=aah01-aag01;
    if abs(af0)>pi && abs(af0)<2*pi
        af0=abs(af0)-2*pi;
    end
    f0=abs(abs(Tm(jjy,1))-abs(Tc0new))+abs(af0);

    test_response1new=
OneD_filter_response_no_defect(layers,realeps,imageps,freqsa,x1n
ew(1,1),x1new(1,2));
    Tc1new=test_response1new(:,2);
```

```
    aag11=angle(Tc1new);
    aah11=angle(Tm(jjy,1));
    af1=aah11-aag11;
    if abs(af1)>pi && abs(af1)<2*pi
        af1=abs(af1)-2*pi;
    end
    f1=abs(abs(Tm(jjy,1))-abs(Tc1new))+abs(af1);


    test_response2new=
OneD_filter_response_no_defect(layers,realeps,imageps,freqsa,x2n
ew(1,1),x2new(1,2));;
        Tc2new=test_response2new(:,2);
           aag21=angle(Tc2new);
    aah21=angle(Tm(jjy,1));
    af2=aah21-aag21;
    if abs(af2)>pi && abs(af2)<2*pi
        af2=abs(af2)-2*pi;
    end
    f2=abs(abs(Tm(jjy,1))-abs(Tc2new))+abs(af2);

if abs(f0)<=0.0001
    x1final=x0new(1,1)
    x2final=x0new(1,2)
    cc=2

erpsc=x1final;
   eipsc=x2final;
    break
end
if abs(f1)<=0.0001
    x1final=x1new(1,1)
    x2final=x1new(1,2)
    cc=2
    erpsc=x1final;
    eipsc=x2final;
    break
end
if abs(f2)<=0.0001
    x1final=x2new(1,1)
    x2final=x2new(1,2)
    cc=2
   erpsc=x1final;
   eipsc=x2final;
    break
end
```

```
F=[f0 f1 f2]
 if std(F)<=0.0000000000001
    if f0<f1 && f0<f2
         x1final=x0new(1,1)
         x2final=x0new(1,2)
         cc=2
    break
    end
    if f1<f0 && f1<f2
       x1final=x1new(1,1)
       x2final=x1new(1,2)
       cc=2
    break
    end
         if f2<f0 && f2<f1
             x1final=x2new(1,1)
     x2final=x2new(1,2)
         cc=2
    break
         end

 end


% %case 5
 if f0>f1 && f1>f2
     xc=(1/N)*(x1new+x2new);
    M1=x0new;
    xr=(1+rho)*xc-(rho*M1);
    test_response_r=
OneD_filter_response_no_defect(layers,realeps,imageps,freqsa,xr(
1,1),xr(1,2));
    Tc_r=test_response_r(:,2)
    aagr1=angle(Tc_r);
    aahr1=angle(Tm(jjy,1));
    afr=aahr1-aagr1;
    if abs(afr)>pi && abs(afr)<2*pi
        afr=abs(afr)-2*pi;
    end
    fr=abs(abs(Tm(jjy,1))-abs(Tc_r))+abs(afr);
 if fr>=f2 && fr<f1
     x0new=xr
    continue
 end
 if fr<f2
     xe=xc+zhi*(xr-xc);
```

```
   test_response_e=
OneD_filter_response_no_defect(layers,realeps,imageps,freqsa,xe(
1,1),xe(1,2));
    Tc_e=test_response_e(:,2);
    aage1=angle(Tc_e);
    aahe1=angle(Tm(jjy,1));
    afe=aahe1-aage1;
    if abs(afe)>pi && abs(afe)<2*pi
        afe=abs(afe)-2*pi;
    end
        fe=abs(abs(Tm(jjy,1))-abs(Tc_r))+abs(afe);
         if fe<fr
         x0new=xe;
         continue
     else
        x0new=xr;
        continue
     end
 end
    if fr>=f1
         if fr>=f1 && fr<f0
             xcon=xc+gamma*(xr-xc);
test_response_con=
OneD_filter_response_no_defect(layers,realeps,imageps,freqsa,xco
n(1,1),xcon(1,2));
    Tc_con=test_response_con(:,2);
    aagcon1=angle(Tc_con);
    aahcon1=angle(Tm(jjy,1));
    afcon=aahcon1-aagcon1;
    if abs(afcon)>pi && abs(afcon)<2*pi
        afcon=abs(afcon)-2*pi;
    end
    fcon=abs(abs(Tm(jjy,1))-abs(Tc_con))+abs(afcon);


         if fcon<=fr
                 x0new=xcon;
                 continue
             end
         end
         if fr>=f0
        xccon=xc-gamma*(xc-x0new);

 test_response_ccon=
OneD_filter_response_no_defect(layers,realeps,imageps,freqsa,xcc
on(1,1),xccon(1,2));
    Tc_ccon=test_response_ccon(:,2);
```

```
        aagccon1=angle(Tc_ccon);
    aahccon1=angle(Tm(jjy,1));
    afccon=aahccon1-aagccon1;
    if abs(afccon)>pi && abs(afccon)<2*pi
        afccon=abs(afccon)-2*pi;
    end

    fccon=abs(abs(Tm(jjy,1))-abs(Tc_ccon))+abs((afccon));
            if fccon<f0
                x0new=xccon;
                 continue
           end
        end
    end
    %start here
    x0new=x2new+sigma*(x0new-x2new);
    x1new=x2new+sigma*(x1new-x2new);
    x2new=x2new;
    continue
end
%%case 1
 if f2>f1 && f1>f0
     xc=(1/N)*(x1new+x0new);
    M1=x2new;
    xr=(1+rho)*xc-(rho*M1);
    test_response_r=
OneD_filter_response_no_defect(layers,realeps,imageps,freqsa,xr(
1,1),xr(1,2));
    Tc_r=test_response_r(:,2);
    aagr1=angle(Tc_r);
    aahr1=angle(Tm(jjy,1));
    afr=aahr1-aagr1;
    if abs(afr)>pi && abs(afr)<2*pi
        afr=abs(afr)-2*pi;
    end
    fr=abs(abs(Tm(jjy,1))-abs(Tc_r))+abs(afr);
 if fr>=f0 && fr<f1
     x2new=xr;
    continue
 end
 if fr<f0
     xe=xc+zhi*(xr-xc);
   test_response_e=
OneD_filter_response_no_defect(layers,realeps,imageps,freqsa,xe(
1,1),xe(1,2));
    Tc_e=test_response_e(:,2);
    aage1=angle(Tc_e);
```

```
    aahe1=angle(Tm(jjy,1));
    afe=aahe1-aage1;
    if abs(afe)>pi && abs(afe)<2*pi
        afe=abs(afe)-2*pi;
    end
        fe=abs(abs(Tm(jjy,1))-abs(Tc_r))+abs(afe);
     if fe<fr
         x2new=xe;
         continue
     else
        x2new=xr;
        continue
     end
 end
    if fr>=f1
         if fr>=f1 && fr<f2
             xcon=xc+gamma*(xr-xc);
test_response_con=
OneD_filter_response_no_defect(layers,realeps,imageps,freqsa,xco
n(1,1),xcon(1,2));
    Tc_con=test_response_con(:,2);
    aagcon1=angle(Tc_con);
    aahcon1=angle(Tm(jjy,1));
    afcon=aahcon1-aagcon1;
    if abs(afcon)>pi && abs(afcon)<2*pi
        afcon=abs(afcon)-2*pi;
    end
    fcon=abs(abs(Tm(jjy,1))-abs(Tc_con))+abs(afcon);

         if fcon<=fr
                 x2new=xcon;
                 continue
             end
         end
         if fr>=f2
        xccon=xc-gamma*(xc-x2new);
 test_response_ccon=
OneD_filter_response_no_defect(layers,realeps,imageps,freqsa,xcc
on(1,1),xccon(1,2));
    Tc_ccon=test_response_ccon(:,2)
        aagccon1=angle(Tc_ccon);
    aahccon1=angle(Tm(jjy,1));
    afccon=aahccon1-aagccon1;
    if abs(afccon)>pi && abs(afccon)<2*pi
        afccon=abs(afccon)-2*pi;
    end
        fccon=abs(abs(Tm(jjy,1))-abs(Tc_ccon))+abs((afccon));
```

```
            if fccon<f2
                x2new=xccon;
                 continue
           end
        end
    end
    %start here
    x2new=x0new+sigma*(x2new-x0new);
    x1new=x0new+sigma*(x1new-x0new);
    x0new=x0new;
    continue
end
%% case 2
 if f1>f2 && f2>f0
     xc=(1/N)*(x2new+x0new);
    M1=x1new;
    xr=(1+rho)*xc-(rho*M1);
    test_response_r=
OneD_filter_response_no_defect(layers,realeps,imageps,freqsa,xr(
1,1),xr(1,2));
    Tc_r=test_response_r(:,2);
    aagr1=angle(Tc_r);
    aahr1=angle(Tm(jjy,1));
    afr=aahr1-aagr1;
    if abs(afr)>pi && abs(afr)<2*pi
        afr=abs(afr)-2*pi;
    end
    fr=abs(abs(Tm(jjy,1))-abs(Tc_r))+abs(afr);
 if fr>=f0 && fr<f2
     x1new=xr;
    continue
 end
 if fr<f0
     xe=xc+zhi*(xr-xc);
   test_response_e=
OneD_filter_response_no_defect(layers,realeps,imageps,freqsa,xe(
1,1),xe(1,2));
    Tc_e=test_response_e(:,2);
    aage1=angle(Tc_e);
    aahe1=angle(Tm(jjy,1));
    afe=aahe1-aage1;
    if abs(afe)>pi && abs(afe)<2*pi
        afe=abs(afe)-2*pi;
    end
    fe=abs(abs(Tm(jjy,1))-abs(Tc_r))+abs(afe);
     if fe<fr
         x1new=xe;
```

```
         continue
      else
         x1new=xr;
         continue
      end
 end
    if fr>=f2
         if fr>=f2 && fr<f1
             xcon=xc+gamma*(xr-xc);
test_response_con=
OneD_filter_response_no_defect(layers,realeps,imageps,freqsa,xco
n(1,1),xcon(1,2));
    Tc_con=test_response_con(:,2);
    aagcon1=angle(Tc_con);
    aahcon1=angle(Tm(jjy,1));
    afcon=aahcon1-aagcon1;
    if abs(afcon)>pi && abs(afcon)<2*pi
        afcon=abs(afcon)-2*pi;
    end
        fcon=abs(abs(Tm(jjy,1))-abs(Tc_con))+abs(afcon);
         if fcon<=fr
                 x1new=xcon;
                 continue
             end
         end
         if fr>=f1
        xccon=xc-gamma*(xc-x1new);

 test_response_ccon=
OneD_filter_response_no_defect(layers,realeps,imageps,freqsa,xcc
on(1,1),xccon(1,2));
    Tc_ccon=test_response_ccon(:,2);
        aagccon1=angle(Tc_ccon);
    aahccon1=angle(Tm(jjy,1));
    afccon=aahccon1-aagccon1;
    if abs(afccon)>pi && abs(afccon)<2*pi
        afccon=abs(afccon)-2*pi;
    end
        fccon=abs(abs(Tm(jjy,1))-abs(Tc_ccon))+abs((afccon));
            if fccon<f1
                x1new=xccon;
                 continue
           end
        end
    end
    %start here
    x1new=x0new+sigma*(x1new-x0new);
```

```
    x2new=x0new+sigma*(x2new-x0new);
    x0new=x0new;
    continue
end
%% case 3
 if f0>f2 && f2>f1
     xc=(1/N)*(x2new+x1new);
    M1=x0new;
    xr=(1+rho)*xc-(rho*M1);
    test_response_r=
OneD_filter_response_no_defect(layers,realeps,imageps,freqsa,xr(
1,1),xr(1,2));
    Tc_r=test_response_r(:,2);
    aagr1=angle(Tc_r);
    aahr1=angle(Tm(jjy,1));
    afr=aahr1-aagr1;
    if abs(afr)>pi && abs(afr)<2*pi
        afr=abs(afr)-2*pi;
    end
    fr=abs(abs(Tm(jjy,1))-abs(Tc_r))+abs(afr);
 if fr>=f1 && fr<f2
     x0new=xr;
    continue
 end
 if fr<f1
     xe=xc+zhi*(xr-xc);
   test_response_e=
OneD_filter_response_no_defect(layers,realeps,imageps,freqsa,xe(
1,1),xe(1,2));
    Tc_e=test_response_e(:,2);
    aage1=angle(Tc_e);
    aahe1=angle(Tm(jjy,1));
    afe=aahe1-aage1;
    if abs(afe)>pi && abs(afe)<2*pi
        afe=abs(afe)-2*pi;
    end
    fe=abs(abs(Tm(jjy,1))-abs(Tc_r))+abs(afe);

     if fe<fr
         x0new=xe;
         continue
     else
        x0new=xr;
        continue
     end
 end
    if fr>=f2
```

```
         if fr>=f2 && fr<f0
             xcon=xc+gamma*(xr-xc);
%             test_response_con=
OneD_filter_response_no_defect(layers,realeps,imageps,freqsa,xco
n(1,1),xcon(1,2));
    Tc_con=test_response_con(:,2);
    aagcon1=angle(Tc_con);
    aahcon1=angle(Tm(jjy,1));
    afcon=aahcon1-aagcon1;
    if abs(afcon)>pi && abs(afcon)<2*pi
        afcon=abs(afcon)-2*pi;
    end

    fcon=abs(abs(Tm(jjy,1))-abs(Tc_con))+abs(afcon);

         if fcon<=fr
                 x0new=xcon;
                 continue
             end
         end
         if fr>=f0
        xccon=xc-gamma*(xc-x0new);

 test_response_ccon=
OneD_filter_response_no_defect(layers,realeps,imageps,freqsa,xcc
on(1,1),xccon(1,2));
    Tc_ccon=test_response_ccon(:,2);
        aagccon1=angle(Tc_ccon);
    aahccon1=angle(Tm(jjy,1));
    afccon=aahccon1-aagccon1;
    if abs(afccon)>pi && abs(afccon)<2*pi
        afccon=abs(afccon)-2*pi;
    end
    fccon=abs(abs(Tm(jjy,1))-abs(Tc_ccon))+abs((afccon));

            if fccon<f0
                x0new=xccon;
                 continue
           end
        end
    end
    %start here
    x0new=x1new+sigma*(x0new-x1new);
    x2new=x1new+sigma*(x2new-x1new);
    x1new=x1new;
    continue
 end
```

```
%%% case 4
 if f2>f0 && f0>f1
     xc=(1/N)*(x0new+x1new);
    M1=x2new;
    xr=(1+rho)*xc-(rho*M1);
    test_response_r=
OneD_filter_response_no_defect(layers,realeps,imageps,freqsa,xr(
1,1),xr(1,2));
    Tc_r=test_response_r(:,2);
    aagr1=angle(Tc_r);
    aahr1=angle(Tm(jjy,1));
    afr=aahr1-aagr1;
    if abs(afr)>pi && abs(afr)<2*pi
        afr=abs(afr)-2*pi;
    end
    fr=abs(abs(Tm(jjy,1))-abs(Tc_r))+abs(afr);
 if fr>=f1 && fr<f0
     x2new=xr;
    continue
 end
 if fr<f1
     xe=xc+zhi*(xr-xc);
   test_response_e=
OneD_filter_response_no_defect(layers,realeps,imageps,freqsa,xe(
1,1),xe(1,2));
    Tc_e=test_response_e(:,2);
    aage1=angle(Tc_e);
    aahe1=angle(Tm(jjy,1));
    afe=aahe1-aage1;
    if abs(afe)>pi && abs(afe)<2*pi
        afe=abs(afe)-2*pi;
    end
    fe=abs(abs(Tm(jjy,1))-abs(Tc_r))+abs(afe);

     if fe<fr
         x2new=xe;
         continue
     else
        x2new=xr;
        continue
     end
 end
    if fr>=f0
         if fr>=f0 && fr<f2
             xcon=xc+gamma*(xr-xc);
```

```
 test_response_con=
OneD_filter_response_no_defect(layers,realeps,imageps,freqsa,xco
n(1,1),xcon(1,2));
    Tc_con=test_response_con(:,2);
    aagcon1=angle(Tc_con);
    aahcon1=angle(Tm(jjy,1));
    afcon=aahcon1-aagcon1;
    if abs(afcon)>pi && abs(afcon)<2*pi
        afcon=abs(afcon)-2*pi;
    end
    fcon=abs(abs(Tm(jjy,1))-abs(Tc_con))+abs(afcon);

         if fcon<=fr
                 x2new=xcon;
                 continue
             end
         end
         if fr>=f2
        xccon=xc-gamma*(xc-x2new);

 test_response_ccon=
OneD_filter_response_no_defect(layers,realeps,imageps,freqsa,xcc
on(1,1),xccon(1,2));
    Tc_ccon=test_response_ccon(:,2);
        aagccon1=angle(Tc_ccon);
    aahccon1=angle(Tm(jjy,1));
    afccon=aahccon1-aagccon1;
    if abs(afccon)>pi && abs(afccon)<2*pi
        afccon=abs(afccon)-2*pi;
    end
    fccon=abs(abs(Tm(jjy,1))-abs(Tc_ccon))+abs((afccon));
            if fccon<f2
                x2new=xccon;
                 continue
           end
        end
    end
    %start here
    x2new=x1new+sigma*(x2new-x1new);
    x0new=x1new+sigma*(x0new-x1new);
    x1new=x1new;
    continue
 end
%% case 6
 if f1>f0 && f0>f2
     xc=(1/N)*(x0new+x2new);
    M1=x1new;
```

```
    xr=(1+rho)*xc-(rho*M1);
    test_response_r=
OneD_filter_response_no_defect(layers,realeps,imageps,freqsa,xr(
1,1),xr(1,2));
    Tc_r=test_response_r(:,2);
    aagr1=angle(Tc_r);
    aahr1=angle(Tm(jjy,1));
    afr=aahr1-aagr1;
    if abs(afr)>pi && abs(afr)<2*pi
        afr=abs(afr)-2*pi;
    end
    fr=abs(abs(Tm(jjy,1))-abs(Tc_r))+abs(afr);
 if fr>=f2 && fr<f0
     x1new=xr;
    continue
 end
 if fr<f2
     xe=xc+zhi*(xr-xc);
   test_response_e=
OneD_filter_response_no_defect(layers,realeps,imageps,freqsa,xe(
1,1),xe(1,2));
    Tc_e=test_response_e(:,2);
    aage1=angle(Tc_e);
    aahe1=angle(Tm(jjy,1));
    afe=aahe1-aage1;
    if abs(afe)>pi && abs(afe)<2*pi
        afe=abs(afe)-2*pi;
    end

    fe=abs(abs(Tm(jjy,1))-abs(Tc_r))+abs(afe);

     if fe<fr
         x1new=xe;
         continue
     else
        x1new=xr;
        continue
     end
 end
    if fr>=f0
         if fr>=f0 && fr<f1
             xcon=xc+gamma*(xr-xc);
%

test_response_con=OneD_filter_response_no_defect(layers,realeps,
imageps,freqsa,xcon(1,1),xcon(1,2));
    Tc_con=test_response_con(:,2);
```

```
    aagcon1=angle(Tc_con);
    aahcon1=angle(Tm(jjy,1));
    afcon=aahcon1-aagcon1;
    if abs(afcon)>pi && abs(afcon)<2*pi
        afcon=abs(afcon)-2*pi;
    end
        fcon=abs(abs(Tm(jjy,1))-abs(Tc_con))+abs(afcon);

         if fcon<=fr
                x1new=xcon;
                continue
            end
         end
         if fr>=f1
        xccon=xc-gamma*(xc-x1new);

 test_response_ccon=
OneD_filter_response_no_defect(layers,realeps,imageps,freqsa,xcc
on(1,1),xccon(1,2));
    Tc_ccon=test_response_ccon(:,2);
        aagccon1=angle(Tc_ccon);
    aahccon1=angle(Tm(jjy,1));
    afccon=aahccon1-aagccon1;
    if abs(afccon)>pi && abs(afccon)<2*pi
        afccon=abs(afccon)-2*pi;
    end
    fccon=abs(abs(Tm(jjy,1))-abs(Tc_ccon))+abs((afccon));
            if fccon<f1
                x1new=xccon;
                 continue
           end
        end
    end
    %start here
    x1new=x2new+sigma*(x1new-x2new);
    x0new=x2new+sigma*(x0new-x2new);
    x2new=x2new;
    continue
end
end
if jhk==maxit
erpsc=1.7+rand*0.2;%guess for dielectric cst- real part of fluid
eips=0+0.05*rand;%guess for dielectric cst- imaginary part of
fluid
end
end
x11final(jjy)=x1final;
```

```
x22final(jjy)=x2final;
if jjy==size(Tm,1)
    break
end

end

figure;plot(fs,x11final)
figure;plot(fs,x22final)

%%%%%%%%%%%%%%%%%%%%%%%%%%%%%%%%%%%%%%%%%%%%%%%%%%%%%%%%%%%%%%%%%%%%%%%%%%%%
%%%%%%%%%%%%%%%%%%%%%%%%%%%%%%%%%%%%%%%%%%%%%%%%%%%%%%%%%%%%%%%%%%%%%%%%%%%%
%%%%%%%%%%%%%%%%%%%%%%%%%%%%%%%%%%%%%%%%%%%%%%%%%%%%%%%%%%%%%%%%%%%%%%%%%%%%
```

%Inverse problem solution from experimental data

```
    circularbackground=textread('circularbackground.txt',
'%s');%loading measured incident signal
    circularbackground=str2double(circularbackground);%changing
string to double

    toluene=textread('toluene.txt', '%s');
    toluene=str2double(toluene);


    j=1;
    for i=1:size(circularbackground,1)%reorganizing data into
two columns, first column is time
        %second column is signal intensity
        if mod(i,2)~=0
            circularbackground_c(j,1)=circularbackground(i,1);
%column 1
            toluene_c(j,1)=toluene(i,1);


        end
        if mod(i,2)==0
            circularbackground_c(j,2)=circularbackground(i,1);
%column 1

            toluene_c(j,2)=toluene(i,1);

            j=j+1;
        end
    end

figure;
```

```
plot(toluene_c(:,1),toluene_c(:,2), 'green');grid

f_circularbackground_c=fft(circularbackground_c(:,2));
f_toluene_c=fft(toluene_c(:,2));


sampling_period=circularbackground_c(2,1)-
circularbackground_c(1,1);
sampling_period4=toluene_c(2,1)-toluene_c(1,1);


sampling_frequency=1/sampling_period;
sampling_frequency4=1/sampling_period4;


freq=0:sampling_frequency/2048:sampling_frequency-
sampling_frequency/2048;

figure;plot(freq,abs(f_toluene_c),'black');grid
joses3=abs(f_toluene_c./f_circularbackground_c);
figure;plot(freq(9:41)*(10^12),joses3(9:41),'green');grid


%%%%%%%%%%%%%%%%%%%%%%%%%%%%%%%%%%%%%%%%%%%%%%%%%%%%%%%%%%%%%%%%%%%%%%%
%%%%%%%%%%%%%%%%%%%%%%%%%%%%%%%%%%%%%%%%%%%%%%%%%%%%%%%%%%%%%%%%%%%%%%%
%%%%%%%%%%%%%%%%%%%%%%%%%%%%%%%%%%%%%%%%%%%%%%%%%%%%%%%%%%%%%%%%%%%%%%%


%clc
%clear all
%close all
format long
%%%forward problem
%%%generating synthesized transmission coefficient

layers=10^-6*[127 274 127 276 127 277 127 278 127 278 127 277
127 276 127 274 127];%thickness of layers (layers start by
solid-air-solid)

fs=freq(9:41)*10^12
%fs=100*(10^9):12.5*(10^9):500*(10^9);%frequency range
rps=3.0*ones(1,size(fs,2));%dielectric constant of solid (real
part)
ips=.15*ones(1,size(fs,2)); dielectric constant of solid
(imaginary part)

for jh=1:size(fs,2)
```

```
   realeps=rps(jh);
   imageps=ips(jh);
    freqsa=fs(jh);
end


Tm=joses3(9:41)

%%%%inverse problem solution

%after jose
for jjy=1:size(Tm,1)
cc=0
freqsa=fs(jjy)
if jjy==1

%erpsc=2.1
%eips=0
erpsc=2+rand*0.2;
eips=0.0+0.2*rand;
end
maxit=50;%maximum iterations for Nelder Mead at each frequency
while cc==0
N=2;
alfa=0.02; %Update with problem
rho=1; %Update with problem
zhi=2;
gamma=0.5;
sigma=1/2;

x0=[erpsc eips];
gama1=(((N+1)^(1/2)+N-1)/(N*sqrt(2)))*alfa
gama2=(((N+1)^(1/2)-1)/(N*sqrt(2)))*alfa

c=erpsc+gama1;
d=eips+gama2;
x1=[c,d]

e=erpsc+gama2;
f=eips+gama1;
x2=[e,f]

for jhk=1:maxit

if jhk==1
 x0new=x0
 x1new=x1
```

```
 x2new=x2
end

test_response0new=OneD_filter_response_no_defect(layers,realeps,
imageps,freqsa,x0new(1,1),x0new(1,2));
    Tc0new=test_response0new(:,2);
    aag01=angle(Tc0new);
    aah01=angle(Tm(jjy,1));
    af0=aah01-aag01;
    if abs(af0)>pi && abs(af0)<2*pi
        af0=abs(af0)-2*pi;
    end
    f0=abs(abs(Tm(jjy,1))-abs(Tc0new))+abs(af0);

    test_response1new=
OneD_filter_response_no_defect(layers,realeps,imageps,freqsa,x1n
ew(1,1),x1new(1,2));
    Tc1new=test_response1new(:,2);
    aag11=angle(Tc1new);
    aah11=angle(Tm(jjy,1));
    af1=aah11-aag11;
    if abs(af1)>pi && abs(af1)<2*pi
        af1=abs(af1)-2*pi;
    end
    f1=abs(abs(Tm(jjy,1))-abs(Tc1new))+abs(af1);


    test_response2new=
OneD_filter_response_no_defect(layers,realeps,imageps,freqsa,x2n
ew(1,1),x2new(1,2));;
        Tc2new=test_response2new(:,2);
           aag21=angle(Tc2new);
    aah21=angle(Tm(jjy,1));
    af2=aah21-aag21;
    if abs(af2)>pi && abs(af2)<2*pi
        af2=abs(af2)-2*pi;
    end
    f2=abs(abs(Tm(jjy,1))-abs(Tc2new))+abs(af2);

if abs(f0)<=0.00001
    x1final=x0new(1,1)
    x2final=x0new(1,2)
    cc=2

erpsc=x1final;
   eipsc=x2final;
    break
```

```
end
if abs(f1)<=0.00001
    x1final=x1new(1,1)
    x2final=x1new(1,2)
    cc=2
    erpsc=x1final;
    eipsc=x2final;
    break
end
if abs(f2)<=0.00001
    x1final=x2new(1,1)
    x2final=x2new(1,2)
    cc=2
   erpsc=x1final;
   eipsc=x2final;
    break
end

F=[f0 f1 f2]
 if std(F)<=0.0000000000001
    if f0<f1 && f0<f2
         x1final=x0new(1,1)
         x2final=x0new(1,2)
         cc=2
    break
    end
    if f1<f0 && f1<f2
       x1final=x1new(1,1)
       x2final=x1new(1,2)
       cc=2
    break
    end
         if f2<f0 && f2<f1
             x1final=x2new(1,1)
     x2final=x2new(1,2)
         cc=2
    break
         end

 end


% %case 5
 if f0>f1 && f1>f2
     xc=(1/N)*(x1new+x2new);
    M1=x0new;
    xr=(1+rho)*xc-(rho*M1);
```

```
    test_response_r=
OneD_filter_response_no_defect(layers,realeps,imageps,freqsa,xr(
1,1),xr(1,2));
    Tc_r=test_response_r(:,2)
    aagr1=angle(Tc_r);
    aahr1=angle(Tm(jjy,1));
    afr=aahr1-aagr1;
    if abs(afr)>pi && abs(afr)<2*pi
        afr=abs(afr)-2*pi;
    end
    fr=abs(abs(Tm(jjy,1))-abs(Tc_r))+abs(afr);
 if fr>=f2 && fr<f1
     x0new=xr
    continue
 end
 if fr<f2
     xe=xc+zhi*(xr-xc);

   test_response_e=
OneD_filter_response_no_defect(layers,realeps,imageps,freqsa,xe(
1,1),xe(1,2));
    Tc_e=test_response_e(:,2);
    aage1=angle(Tc_e);
    aahe1=angle(Tm(jjy,1));
    afe=aahe1-aage1;
    if abs(afe)>pi && abs(afe)<2*pi
        afe=abs(afe)-2*pi;
    end
        fe=abs(abs(Tm(jjy,1))-abs(Tc_r))+abs(afe);
         if fe<fr
         x0new=xe;
         continue
     else
        x0new=xr;
        continue
     end
 end
    if fr>=f1
         if fr>=f1 && fr<f0
             xcon=xc+gamma*(xr-xc);
test_response_con=
OneD_filter_response_no_defect(layers,realeps,imageps,freqsa,xco
n(1,1),xcon(1,2));
    Tc_con=test_response_con(:,2);
    aagcon1=angle(Tc_con);
    aahcon1=angle(Tm(jjy,1));
    afcon=aahcon1-aagcon1;
```

```
    if abs(afcon)>pi && abs(afcon)<2*pi
        afcon=abs(afcon)-2*pi;
    end
    fcon=abs(abs(Tm(jjy,1))-abs(Tc_con))+abs(afcon);

         if fcon<=fr
                 x0new=xcon;
                 continue
             end
         end
         if fr>=f0
        xccon=xc-gamma*(xc-x0new);

 test_response_ccon=
OneD_filter_response_no_defect(layers,realeps,imageps,freqsa,xcc
on(1,1),xccon(1,2));
    Tc_ccon=test_response_ccon(:,2);
        aagccon1=angle(Tc_ccon);
    aahccon1=angle(Tm(jjy,1));
    afccon=aahccon1-aagccon1;
    if abs(afccon)>pi && abs(afccon)<2*pi
        afccon=abs(afccon)-2*pi;
    end
      fccon=abs(abs(Tm(jjy,1))-abs(Tc_ccon))+abs((afccon));
            if fccon<f0
                x0new=xccon;
                 continue
           end
        end
    end
    %start here
    x0new=x2new+sigma*(x0new-x2new);
    x1new=x2new+sigma*(x1new-x2new);
    x2new=x2new;
    continue
end
%%case 1
 if f2>f1 && f1>f0
     xc=(1/N)*(x1new+x0new);
    M1=x2new;
    xr=(1+rho)*xc-(rho*M1);

    test_response_r=
OneD_filter_response_no_defect(layers,realeps,imageps,freqsa,xr(
1,1),xr(1,2));
    Tc_r=test_response_r(:,2);
    aagr1=angle(Tc_r);
```

```
    aahr1=angle(Tm(jjy,1));
    afr=aahr1-aagr1;
    if abs(afr)>pi && abs(afr)<2*pi
        afr=abs(afr)-2*pi;
    end
    fr=abs(abs(Tm(jjy,1))-abs(Tc_r))+abs(afr);
 if fr>=f0 && fr<f1
     x2new=xr;
    continue
 end
 if fr<f0
     xe=xc+zhi*(xr-xc);
   test_response_e=
OneD_filter_response_no_defect(layers,realeps,imageps,freqsa,xe(
1,1),xe(1,2));
    Tc_e=test_response_e(:,2);
    aage1=angle(Tc_e);
    aahe1=angle(Tm(jjy,1));
    afe=aahe1-aage1;
    if abs(afe)>pi && abs(afe)<2*pi
        afe=abs(afe)-2*pi;
    end
    fe=abs(abs(Tm(jjy,1))-abs(Tc_r))+abs(afe);
     if fe<fr
         x2new=xe;
         continue
     else
        x2new=xr;
        continue
     end
 end
    if fr>=f1
         if fr>=f1 && fr<f2
             xcon=xc+gamma*(xr-xc);
test_response_con=
OneD_filter_response_no_defect(layers,realeps,imageps,freqsa,xco
n(1,1),xcon(1,2));
    Tc_con=test_response_con(:,2);
    aagcon1=angle(Tc_con);
    aahcon1=angle(Tm(jjy,1));
    afcon=aahcon1-aagcon1;
    if abs(afcon)>pi && abs(afcon)<2*pi
        afcon=abs(afcon)-2*pi;
    end

    fcon=abs(abs(Tm(jjy,1))-abs(Tc_con))+abs(afcon);
```

```
          if fcon<=fr
                  x2new=xcon;
                  continue
              end
          end
          if fr>=f2
         xccon=xc-gamma*(xc-x2new);
 test_response_ccon=
OneD_filter_response_no_defect(layers,realeps,imageps,freqsa,xcc
on(1,1),xccon(1,2));
    Tc_ccon=test_response_ccon(:,2)
        aagccon1=angle(Tc_ccon);
    aahccon1=angle(Tm(jjy,1));
    afccon=aahccon1-aagccon1;
    if abs(afccon)>pi && abs(afccon)<2*pi
        afccon=abs(afccon)-2*pi;
    end
    fccon=abs(abs(Tm(jjy,1))-abs(Tc_ccon))+abs((afccon));

            if fccon<f2
                x2new=xccon;
                 continue
           end
        end
    end
    %start here
    x2new=x0new+sigma*(x2new-x0new);
    x1new=x0new+sigma*(x1new-x0new);
    x0new=x0new;
    continue
end
%% case 2
 if f1>f2 && f2>f0
     xc=(1/N)*(x2new+x0new);
    M1=x1new;
    xr=(1+rho)*xc-(rho*M1);
%     fr=(1-xr(1,1))^2+(1.5-xr(1,2))^2
    test_response_r=
OneD_filter_response_no_defect(layers,realeps,imageps,freqsa,xr(
1,1),xr(1,2));
    Tc_r=test_response_r(:,2);
    aagr1=angle(Tc_r);
    aahr1=angle(Tm(jjy,1));
    afr=aahr1-aagr1;
    if abs(afr)>pi && abs(afr)<2*pi
        afr=abs(afr)-2*pi;
    end
```

```
    fr=abs(abs(Tm(jjy,1))-abs(Tc_r))+abs(afr);
 if fr>=f0 && fr<f2
     x1new=xr;
    continue
 end
 if fr<f0
     xe=xc+zhi*(xr-xc);

   test_response_e=
OneD_filter_response_no_defect(layers,realeps,imageps,freqsa,xe(
1,1),xe(1,2));
    Tc_e=test_response_e(:,2);
    aage1=angle(Tc_e);
    aahe1=angle(Tm(jjy,1));
    afe=aahe1-aage1;
    if abs(afe)>pi && abs(afe)<2*pi
        afe=abs(afe)-2*pi;
    end
    fe=abs(abs(Tm(jjy,1))-abs(Tc_r))+abs(afe);

     if fe<fr
         x1new=xe;
         continue
     else
        x1new=xr;
        continue
     end
 end
    if fr>=f2
         if fr>=f2 && fr<f1
             xcon=xc+gamma*(xr-xc);
test_response_con=
OneD_filter_response_no_defect(layers,realeps,imageps,freqsa,xco
n(1,1),xcon(1,2));
    Tc_con=test_response_con(:,2);
    aagcon1=angle(Tc_con);
    aahcon1=angle(Tm(jjy,1));
    afcon=aahcon1-aagcon1;
    if abs(afcon)>pi && abs(afcon)<2*pi
        afcon=abs(afcon)-2*pi;
    end

    fcon=abs(abs(Tm(jjy,1))-abs(Tc_con))+abs(afcon);

         if fcon<=fr
                 x1new=xcon;
                 continue
```

```
            end
         end
         if fr>=f1
        xccon=xc-gamma*(xc-x1new);

 test_response_ccon=
OneD_filter_response_no_defect(layers,realeps,imageps,freqsa,xcc
on(1,1),xccon(1,2));
    Tc_ccon=test_response_ccon(:,2);
        aagccon1=angle(Tc_ccon);
    aahccon1=angle(Tm(jjy,1));
    afccon=aahccon1-aagccon1;
    if abs(afccon)>pi && abs(afccon)<2*pi
        afccon=abs(afccon)-2*pi;
    end
    fccon=abs(abs(Tm(jjy,1))-abs(Tc_ccon))+abs((afccon));

            if fccon<f1
                x1new=xccon;
                 continue
           end
        end
    end
    %start here
    x1new=x0new+sigma*(x1new-x0new);
    x2new=x0new+sigma*(x2new-x0new);
    x0new=x0new;
    continue
end
%% case 3
 if f0>f2 && f2>f1
     xc=(1/N)*(x2new+x1new);
    M1=x0new;
    xr=(1+rho)*xc-(rho*M1);
    test_response_r=
OneD_filter_response_no_defect(layers,realeps,imageps,freqsa,xr(
1,1),xr(1,2));
    Tc_r=test_response_r(:,2);
    aagr1=angle(Tc_r);
    aahr1=angle(Tm(jjy,1));
    afr=aahr1-aagr1;
    if abs(afr)>pi && abs(afr)<2*pi
        afr=abs(afr)-2*pi;
    end
    fr=abs(abs(Tm(jjy,1))-abs(Tc_r))+abs(afr);
 if fr>=f1 && fr<f2
     x0new=xr;
```

```
    continue
 end
 if fr<f1
     xe=xc+zhi*(xr-xc);
   test_response_e=
OneD_filter_response_no_defect(layers,realeps,imageps,freqsa,xe(
1,1),xe(1,2));
    Tc_e=test_response_e(:,2);
    aage1=angle(Tc_e);
    aahe1=angle(Tm(jjy,1));
    afe=aahe1-aage1;
    if abs(afe)>pi && abs(afe)<2*pi
        afe=abs(afe)-2*pi;
    end
    fe=abs(abs(Tm(jjy,1))-abs(Tc_r))+abs(afe);
     if fe<fr
         x0new=xe;
         continue
     else
        x0new=xr;
        continue
     end
 end
    if fr>=f2
         if fr>=f2 && fr<f0
             xcon=xc+gamma*(xr-xc);
test_response_con=
OneD_filter_response_no_defect(layers,realeps,imageps,freqsa,xco
n(1,1),xcon(1,2));
    Tc_con=test_response_con(:,2);
    aagcon1=angle(Tc_con);
    aahcon1=angle(Tm(jjy,1));
    afcon=aahcon1-aagcon1;
    if abs(afcon)>pi && abs(afcon)<2*pi
        afcon=abs(afcon)-2*pi;
    end
        fcon=abs(abs(Tm(jjy,1))-abs(Tc_con))+abs(afcon);

         if fcon<=fr
                 x0new=xcon;
                 continue
             end
         end
         if fr>=f0
        xccon=xc-gamma*(xc-x0new);
```

```
 test_response_ccon=
OneD_filter_response_no_defect(layers,realeps,imageps,freqsa,xcc
on(1,1),xccon(1,2));
    Tc_ccon=test_response_ccon(:,2);
        aagccon1=angle(Tc_ccon);
    aahccon1=angle(Tm(jjy,1));
    afccon=aahccon1-aagccon1;
    if abs(afccon)>pi && abs(afccon)<2*pi
        afccon=abs(afccon)-2*pi;
    end

    fccon=abs(abs(Tm(jjy,1))-abs(Tc_ccon))+abs((afccon));
            if fccon<f0
                x0new=xccon;
                 continue
           end
        end
    end
    %start here
    x0new=x1new+sigma*(x0new-x1new);
    x2new=x1new+sigma*(x2new-x1new);
    x1new=x1new;
    continue
 end
%%% case 4
 if f2>f0 && f0>f1
     xc=(1/N)*(x0new+x1new);
    M1=x2new;
    xr=(1+rho)*xc-(rho*M1);
    test_response_r=
OneD_filter_response_no_defect(layers,realeps,imageps,freqsa,xr(
1,1),xr(1,2));
    Tc_r=test_response_r(:,2);
    aagr1=angle(Tc_r);
    aahr1=angle(Tm(jjy,1));
    afr=aahr1-aagr1;
    if abs(afr)>pi && abs(afr)<2*pi
        afr=abs(afr)-2*pi;
    end
    fr=abs(abs(Tm(jjy,1))-abs(Tc_r))+abs(afr);
 if fr>=f1 && fr<f0
     x2new=xr;
    continue
 end
 if fr<f1
     xe=xc+zhi*(xr-xc);
```

```
   test_response_e=
OneD_filter_response_no_defect(layers,realeps,imageps,freqsa,xe(
1,1),xe(1,2));
    Tc_e=test_response_e(:,2);
    aage1=angle(Tc_e);
    aahe1=angle(Tm(jjy,1));
    afe=aahe1-aage1;
    if abs(afe)>pi && abs(afe)<2*pi
        afe=abs(afe)-2*pi;
    end
    fe=abs(abs(Tm(jjy,1))-abs(Tc_r))+abs(afe);
     if fe<fr
         x2new=xe;
         continue
     else
        x2new=xr;
        continue
     end
 end
    if fr>=f0
         if fr>=f0 && fr<f2
             xcon=xc+gamma*(xr-xc);
test_response_con=
OneD_filter_response_no_defect(layers,realeps,imageps,freqsa,xco
n(1,1),xcon(1,2));
    Tc_con=test_response_con(:,2);
    aagcon1=angle(Tc_con);
    aahcon1=angle(Tm(jjy,1));
    afcon=aahcon1-aagcon1;
    if abs(afcon)>pi && abs(afcon)<2*pi
        afcon=abs(afcon)-2*pi;
    end
        fcon=abs(abs(Tm(jjy,1))-abs(Tc_con))+abs(afcon);


         if fcon<=fr
                 x2new=xcon;
                 continue
             end
         end
         if fr>=f2
        xccon=xc-gamma*(xc-x2new);

 test_response_ccon=
OneD_filter_response_no_defect(layers,realeps,imageps,freqsa,xcc
on(1,1),xccon(1,2));
    Tc_ccon=test_response_ccon(:,2);
```

```
        aagccon1=angle(Tc_ccon);
    aahccon1=angle(Tm(jjy,1));
    afccon=aahccon1-aagccon1;
    if abs(afccon)>pi && abs(afccon)<2*pi
        afccon=abs(afccon)-2*pi;
    end
    fccon=abs(abs(Tm(jjy,1))-abs(Tc_ccon))+abs((afccon));

            if fccon<f2
                x2new=xccon;
                 continue
           end
        end
    end
    %start here
    x2new=x1new+sigma*(x2new-x1new);
    x0new=x1new+sigma*(x0new-x1new);
    x1new=x1new;
    continue
 end
%% case 6
 if f1>f0 && f0>f2
     xc=(1/N)*(x0new+x2new);
    M1=x1new;
    xr=(1+rho)*xc-(rho*M1);
    test_response_r=
OneD_filter_response_no_defect(layers,realeps,imageps,freqsa,xr(
1,1),xr(1,2));
    Tc_r=test_response_r(:,2);
    aagr1=angle(Tc_r);
    aahr1=angle(Tm(jjy,1));
    afr=aahr1-aagr1;
    if abs(afr)>pi && abs(afr)<2*pi
        afr=abs(afr)-2*pi;
    end
    fr=abs(abs(Tm(jjy,1))-abs(Tc_r))+abs(afr);
 if fr>=f2 && fr<f0
     x1new=xr;
    continue
 end
 if fr<f2
     xe=xc+zhi*(xr-xc);

   test_response_e=
OneD_filter_response_no_defect(layers,realeps,imageps,freqsa,xe(
1,1),xe(1,2));
    Tc_e=test_response_e(:,2);
```

```
    aage1=angle(Tc_e);
    aahe1=angle(Tm(jjy,1));
    afe=aahe1-aage1;
    if abs(afe)>pi && abs(afe)<2*pi
        afe=abs(afe)-2*pi;
    end

    fe=abs(abs(Tm(jjy,1))-abs(Tc_r))+abs(afe);
         if fe<fr
         x1new=xe;
         continue
     else
        x1new=xr;
        continue
     end
 end
    if fr>=f0
         if fr>=f0 && fr<f1
             xcon=xc+gamma*(xr-xc);


test_response_con=OneD_filter_response_no_defect(layers,realeps,
imageps,freqsa,xcon(1,1),xcon(1,2));
    Tc_con=test_response_con(:,2);
    aagcon1=angle(Tc_con);
    aahcon1=angle(Tm(jjy,1));
    afcon=aahcon1-aagcon1;
    if abs(afcon)>pi && abs(afcon)<2*pi
        afcon=abs(afcon)-2*pi;
    end

    fcon=abs(abs(Tm(jjy,1))-abs(Tc_con))+abs(afcon);

         if fcon<=fr
                 x1new=xcon;
                 continue
             end
         end
         if fr>=f1
        xccon=xc-gamma*(xc-x1new);

 test_response_ccon=
OneD_filter_response_no_defect(layers,realeps,imageps,freqsa,xcc
on(1,1),xccon(1,2));
    Tc_ccon=test_response_ccon(:,2);
        aagccon1=angle(Tc_ccon);
    aahccon1=angle(Tm(jjy,1));
```

```
    afccon=aahccon1-aagccon1;
    if abs(afccon)>pi && abs(afccon)<2*pi
        afccon=abs(afccon)-2*pi;
    end
    fccon=abs(abs(Tm(jjy,1))-abs(Tc_ccon))+abs((afccon));


            if fccon<f1
                x1new=xccon;
                 continue
           end
        end
    end
    %start here
    x1new=x2new+sigma*(x1new-x2new);
    x0new=x2new+sigma*(x0new-x2new);
    x2new=x2new;
    continue
end
end
if jhk==maxit
rpsc=2.0+rand*0.2;%guess for dielectric cst- real part of fluid
eips=0.0+0.2*rand;%guess for dielectric cst- imaginary part of
fluid
end
end
x11final(jjy)=x1final;
x22final(jjy)=x2final;
if jjy==size(Tm,1)
    break
end

end

figure;plot(fs,x11final)
figure;plot(fs,x22final)


%%%%%%%%%%%%%%%%%%%%%%%%%%%%%%%%%%%%%%%%%%%%%%%%%%%%%%%%%%%%%%%%%%%%%%%%%%%%
%%%%%%%%%%%%%%%%%%%%%%%%%%%%%%%%%%%%%%%%%%%%%%%%%%%%%%%%%%%%%%%%%%%%%%%%%%%%
%%%%%%%%%%%%%%%%%%%%%%%%%%%%%%%%%%%%%%%%%%%%%%%%%%%%%%%%%%%%%%%%%%%%%%%%%%%%

%Forward Problem solution with defect:

clc
clear all
close all
```

```
format long
%%%forward problem
%%%generating synthesized transmission coefficient

layers=10^-6*[127 254 127 254 127 254 127 635 127 254 127 254
127 254 127];%thickness of layers (layers start by solid-air-
solid)

erps=1;%other empty layers dielectric constant (real)
eips=0.0;%other empty layers dielectric constant (imaginary)

der=1.0;%other empty layers dielectric constant (real)
dei=0.001;%other empty layers dielectric constant (imaginary)

fs=100*(10^9):10*(10^9):500*(10^9);%frequency range
rps=3*ones(1,size(fs,2));%dielectric constant of solid (real
part)
ips=0.12*ones(1,size(fs,2));%rps.*(0.01*2:(0.034*2-
0.01*2)/(size(fs,2)-1):0.034*2);%dielectic constant of solid
(imaginary part)

for jh=1:size(fs,2)
    realeps=rps(jh);
    imageps=ips(jh);
    empty_layers_realeps=erps;
    empty_layers_imageps=eips;
    defect_layers_realeps=der;
    defect_layers_imageps=dei;
    freqsa=fs(jh);
    test_response1=
OneD_filter_response_defect(layers,realeps,imageps,freqsa,empty_
layers_realeps,empty_layers_imageps,defect_layers_realeps,defect
_layers_imageps);
    test_response(jh,1:2)=test_response1;
end

%figure
plot((test_response(:,1)),abs((((test_response(:,2))))),'blue');

%%%%%%%%%%%%%%%%%%%%%%%%%%%%%%%%%%%%%%%%%%%%%%%%%%%%%%%%%%%%%%%%%
%%%%%%%%%%%%%%%%%%%%%%%%%%%%%%%%%%%%%%%%%%%%%%%%%%%%%%%%%%%%%%%%%
%%%%%%%%%%%%%%%%%%%%%%%%%%%%%%%%%%%%%%%%%%%%%%%%%%%%%%%%%%%%%%%%%

%Function needed for code above

function
resp=OneD_filter_reponse_defect(thicknessvector,realeps,imageps,
```

```
freqsa,empty_layers_realeps,empty_layers_imageps,defect_layers_r
ealeps,defect_layers_imageps)


% 1D (Planar) N-Layer P-Polarization (TM) Simulation
% (C) 2009-2010, Collin Meierbachtol, meierbac [at] msu [dot]
edu
% Taken from "Theory of reflection : of electromagnetic and
particle waves"
% by John Lekner, 1987.

format short g

% USER INPUT - System Definitions

t = 0; %Angle of incidence measured from normal [degrees]

%dielectric properties of each layer including the input and
output media
%(air in this case)
eps = [1 complex(realeps,imageps)
complex(empty_layers_realeps,empty_layers_imageps)...
    complex(realeps,imageps)
complex(empty_layers_realeps,empty_layers_imageps)...
    complex(realeps,imageps)
complex(empty_layers_realeps,empty_layers_imageps)...
    complex(realeps,imageps)...
    complex(defect_layers_realeps,defect_layers_imageps)...
        complex(realeps,imageps)
complex(empty_layers_realeps,empty_layers_imageps)...
    complex(realeps,imageps)
complex(empty_layers_realeps,empty_layers_imageps)...
    complex(realeps,imageps)
complex(empty_layers_realeps,empty_layers_imageps)...
    complex(realeps,imageps)...
    1]; %Permittivity matrix - can be complex!
layers=thicknessvector;
d=[0,layers,0];

% NOTE: first and nth layer assumed to be semi-infinite, so
their thickness is set to zero
% to the total sum is just the layer thicknesses, given in
meters

% Inherent Physical Constants
eps0=8.85e-12; % Permittivity of free space [F/m]
mu0=pi*4e-7; % Permeability of free space [Wb/m]
```

```
c=1/sqrt(eps0*mu0); %Speed of light [m/s]
lambdabla=c./freqsa;
%hold on

for lambdavary=1:1:1
%     lambda01(lambdavary) = (lambda0)+5e-6*(lambdavary-1);
    lambda01(lambdavary) = lambdabla(lambdavary);


% Conversions and calculations
[epsr,epsc] = size(eps); %epsc reports number of layers
k0(lambdavary) = 2*pi/lambda01(lambdavary); %Free space incident
wave number
c=1/sqrt(eps0*mu0); %Speed of light [m/s]
omega(lambdavary) = c*k0(lambdavary); %Incident wave frequency
ztot=sum(d); %Total thickness of finite layers

% Generate boundary vector matrix
zsum(1) = 0;
for zj = 2:1:epsc-1;
    zsum(zj) = zsum(zj-1) + d(zj);
end

% MAIN CALCULATION LOOP - DO NOT ALTER!
Mtot = [1 0;0 1];
for n = 1:1:epsc;
    kx = k0(lambdavary)*sin(t*pi/180);
        kz(n) = k0(lambdavary)*sqrt(eps(n) -
eps(1)*(sin(t*pi/180))^2);
        Kz(n) = kz(n)/eps(n);

    if ((n > 1) && (n < epsc))
                M(:,:,n) = [cos(kz(n)*d(n))
sin(kz(n)*d(n))/Kz(n);
            -Kz(n)*sin(kz(n)*d(n)) cos(kz(n)*d(n))];

        Mtot = M(:,:,n)*Mtot;
    end
end
% Reflection coefficient (often complex)
rp(lambdavary) = -(Kz(1)*Kz(epsc)*Mtot(1,2)+Mtot(2,1)-
i*Kz(epsc)*Mtot(1,1)+i*Kz(1)*Mtot(2,2))/(Kz(1)*Kz(epsc)*Mtot(1,2
)-Mtot(2,1)+i*Kz(epsc)*Mtot(1,1)+i*Kz(1)*Mtot(2,2));

% Transmission coefficient (often complex)
```

```
tp(lambdavary) = 2*i*Kz(1)*exp(-
j*kz(epsc)*ztot)/(Kz(1)*Kz(epsc)*Mtot(1,2)-
Mtot(2,1)+i*Kz(epsc)*Mtot(1,1)+i*Kz(1)*Mtot(2,2));

% Reflectance (R+T+A=1)
Rp(lambdavary) = real(conj(rp(lambdavary))*rp(lambdavary));

% Transmittance (R+T+A=1)
Tp(lambdavary) =
real((kz(epsc)/kz(1))*conj(tp(lambdavary))*tp(lambdavary));

% Absorptance (R+T+A=1)
Ap(lambdavary) = 1-(Rp(lambdavary)+Tp(lambdavary));

end

freqresp=[omega'./(2*pi),tp'];
freqresp=flipud(freqresp);
resp=freqresp;

return

%%%%%%%%%%%%%%%%%%%%%%%%%%%%%%%%%%%%%%%%%%%%%%%%%%%%%%%%%%%%%%%%%%%%%%%
%%%%%%%%%%%%%%%%%%%%%%%%%%%%%%%%%%%%%%%%%%%%%%%%%%%%%%%%%%%%%%%%%%%%%%%
%%%%%%%%%%%%%%%%%%%%%%%%%%%%%%%%%%%%%%%%%%%%%%%%%%%%%%%%%%%%%%%%%%%%%%%


%3D (and 1D )sensor experimental data extraction (The same code
is used for all experimental data extractions, including the 1D
sensors, the only difference being that for the 1D data the
result is not in dB therefore absolutes and absolutes1 are
directly plotted without using ydb and xdb.

    background=textread('background.txt', '%s');%loading
measured incident signal
   background=str2double(background);%changing string to double


    sensor=textread('sensor.txt', '%s');%loading measured
incident signal
    sensor=str2double(sensor);

    j=1;
    for i=1:size(background,1)%reorganizing data into two
columns, first column is time
        %second column is signal intensity
```

```
        if mod(i,2)~=0
            background_c(j,1)=background(i,1); %column 1
%
            sensor_c(j,1)=sensor(i,1);


        end
        if mod(i,2)==0
            background_c(j,2)=background(i,1); %column 1
%
           sensor_c(j,2)=sensor(i,1);



            j=j+1;
        end
    end


f_background_c=fft(background_c(:,2));
f_sensor_c=fft(sensor_c(:,2));

sampling_period=background_c(2,1)-background_c(1,1);
sampling_period2=sensor_c(2,1)-sensor_c(1,1);

sampling_frequency=1/sampling_period;
sampling_frequency2=1/sampling_period2;


freq=0:sampling_frequency/1024:sampling_frequency-
sampling_frequency/1024;


absolutes=abs(f_sensor_c./f_background_c);
absolutes1=abs(f_sensor_c./f_background_c);
ydb = mag2db(absolutes)
xdb= mag2db(absolutes1)
%figure;
plot(freq(11:29)*(10^12),xdb(11:29),'red');grid
```

BIBLIOGRAPHY

BIBLIOGRAPHY

[1] B. Ferguson and X.-C. Zhang, "Materials for terahertz science and technology," Nat Mater, vol. 1, pp. 26-33, 09//print 2002.

[2] D. Graham-Rowe, "Terahertz takes to the stage," Nat Photon, vol. 1, pp. 75-77, 02//print 2007.

[3] V. P. Wallace, E. MacPherson, J. A. Zeitler, and C. Reid, "Three-dimensional imaging of optically opaque materials using nonionizing terahertz radiation," Journal of the Optical Society of America A, vol. 25, pp. 3120-3133, 2008/12/01 2008.

[4] B. S. Alexandrov, V. Gelev, A. R. Bishop, A. Usheva, and K. Ø. Rasmussen, "DNA breathing dynamics in the presence of a terahertz field," Physics Letters A, vol. 374, pp. 1214-1217, 2/22/ 2010.

[5] Masayoshi Tonouchi, Cutting-edge terahertz technology Nature pthotonics, Vol. 1, February 2007, www.nature.com/naturephotonics

[6] Peter H. Siegel, Terahertz Technology, IEEE Transactions on microwave theory and techniques, VOL. 50, NO. 3, March 2002

[7] P. H. Siegel, "Terahertz technology in biology and medicine," in Microwave Symposium Digest, 2004 IEEE MTT-S International, 2004, pp. 1575-1578 Vol.3.

[8] L. Lianhe, C. Li, Z. Jingxuan, J. Freeman, P. Dean, A. Valavanis, et al., "Terahertz quantum cascade lasers with >1 W output powers," Electronics Letters, vol. 50, pp. 309-311, 2014.

[9] M. Johnston, “Bridging the terahertz gap with novel sources and sensors”, SPIE Newsroom, April 2006.

[10] W. Qi and X.-C. Zhang, "Design and characterization of traveling-wave electrooptic terahertz sensors," Selected Topics in Quantum Electronics, IEEE Journal of, vol. 2, pp. 693-700, 1996.

[11] D. M. Mittleman, R. H. Jacobsen, R. Neelamani, R. G. Baraniuk, and M. C. Nuss, "Gas sensing using terahertz time-domain spectroscopy," Applied Physics B, vol. 67, pp. 379-390, 1998/09/01 1998

[12] H.-B. Liu, G. Plopper, S. Earley, Y. Chen, B. Ferguson, and X. C. Zhang, "Sensing minute changes in biological cell monolayers with THz differential time-domain spectroscopy," Biosensors and Bioelectronics, vol. 22, pp. 1075-1080, 1/15/ 2007

[13] Kyoung Youl Park, Nophadon Wiwatcharagoses, Cecilia Acosta Silveira, and Prem Chahal, Plastic Injection Micromolding of THz Circuits and Microfluidic Sensors, Electronic Components and Technology Conference (ECTC), 2012 IEEE 62nd, June 1, 2012

[14] Kurt, Hamza and Citrin, D. S., "Photonic crystals for biochemical sensing in the terahertz region", Applied Physics Letters, 87, 041108 (2005).

[15] MNagel,M F¨orst and H Kurz, "THz biosensing devices: fundamentals and technology", J. Phys.: Condens. Matter 18 (2006) S601–S618.

[16] J.Hejase, "Terahertz time domain methods for material characterization of layered dielectric media", PhD Dissertation, Department of Computer and Electrical Engineering, Michigan State University, Dissertation, 2012

[17] J. Joannopoulos, S. Johnson, J. Winn, and R. Meade, Photonic Crystals: Molding the Flow of Light (Second Edition): Princeton University Press, 2008.

[18] S.G. Johnson.(2003). Photonic Crystals: Periodic Surprises in Electromagnetism [online]. Available at FTP: http://ab-initio.mit.edu/photons/tutorial/L2-defects.pdf

[19] E. Yablonovitch, "Photonic crystals: semiconductors of light," Scientific American, vol. 285, pp. 46-55, 2001.

[20] B. Troia, A. Paolicelli, F. De Leonardis, and V. M. N. Passaro, "Photonic Crystals for Optical Sensing: A Review," 2013.

[21] F. Villa, L. E. Regalado, F. Ramos-Mendieta, J. Gaspar-Armenta, and T. Lopez-Ríos, "Photonic crystal sensor based on surface waves for thin-film characterization," Optics letters, vol. 27, pp. 646-648, 2002.

[22] P. Liu, J. He, Y. He, and Z. Hong, "THz gas sensor based on one-dimensional photonic crystal," pp. 833011-833011.

[23] Němec, H. and Duvillaret, L. and Garet, F. and Kužel, P. and Xavier, P. and Richard, J. and Rauly, D., "Thermally tunable filter for terahertz range based on a one-dimensional photonic crystal with a defect" Journal of Applied Physics, 96, 4072-4075 (2004).

[24] H. Nemec, P. Kuzel, L. Duvillaret, A. Pashkin, M. Dressel, and M. Sebastian, "Highly tunable photonic crystal filter for the terahertz range," Opt. Lett. 30, 549-551 (2005).

[25] L. C. A. Silveira, J. A. Hejase, and P. Chahal, "A Terahertz Photonic Crystal Structure for Sensing Applications.", Antennas and Propagation Society International Symposium (APSURSI), 2012 IEEE , vol., no., pp.1,2, 8-14 July 2012.

[26] C. C. Cheng, A. Scherer, R.-C. Tyan, Y. Fainman, G. Witzgall, and E. Yablonovitch, "New fabrication techniques for high quality photonic crystals," Journal of Vacuum Science & Technology B, vol. 15, pp. 2764-2767, 1997.

[27] E. Chow, A. Grot, L. W. Mirkarimi, M. Sigalas, and G. Girolami, "Ultracompact biochemical sensor built with two-dimensional photonic crystal microcavity," Optics letters, vol. 29, pp. 1093-1095, 2004.

[28] M. Huang, A. A. Yanik, T.-Y. Chang, and H. Altug, "Sub-wavelength nanofluidics in photonic crystal sensors," Optics express, vol. 17, pp. 24224-24233, 2009.

[29] Zhongping Jian, "Terahertz photonic crystals", PhD Dissertation, Rice University, Houston, Texas. April 2006.

[30] Jukam, Nathan and Sherwin, Mark S., "Two-dimensional terahertz photonic crystals fabricated by deep reactive ion etching in Si", Applied Physics Letters, 83, 21-23 (2003).

[31]. Z. Jian, J. Pearce, and D. M. Mittleman, “Defect modes in photonic crystal slabs studied using terahertz time-domain spectroscopy,” Optics Letters, vol. 29, No. 17, Sep, 2004.

[32] Nathan T Jukam, “Terahertz Photonic Crystal”, PhD dissertation, Physics, University of California, Santa Barbara.

[33] E. Ozbay, E. Michel, G. Tuttle, R. Biswas, M. Sigalas, and K. M. Ho, "Micromachined millimeter-wave photonic band-gap crystals," Applied Physics Letters, vol. 64, pp. 2059-2061, 1994.

[34] H. Liu, J. Yao, D. Xu, and P. Wang, "Characteristics of photonic band gaps in woodpile three-dimensional terahertz photonic crystals," Optics express, vol. 15, pp. 695-703, 2007.

[35] Takagi, Kenta and Seno, Kazunori and Kawasaki, Akira, “Fabrication of a three-dimensional terahertz photonic crystal using monosized spherical particles”, Applied Physics Letters, 85, 3681-3683 (2004).

[36] A. Chelnokov, S. Rowson, J.-M. Lourtioz, L. Duvillaret and J.-I,. Coutaz, “Terahertz characterisation of mechanically machined 3D photonic crystal”, Electronic Letters, 6th November 1997 Vol. 33 No. 23

[37] Yong Zhao, Ya-Nan Zhang, Qi Wang, Research advances of photonic crystal gas and liquid sensors, Sensors and Actuators B: Chemical, Volume 160, Issue 1, 15 December 2011, Pages 1288-1297, ISSN 0925-4005, http://dx.doi.org/10.1016/j.snb.2011.09.064.

[38] Jan B. Markowski, “Photonic Crystal Sensors”, ES 530B: Research project, March 17, 2008

[39] S. Noda, K. Tomoda, N. Yamamoto, and A. Chutinan, "Full three-dimensional photonic bandgap crystals at near-infrared wavelengths," Science, vol. 289, pp. 604-606, 2000.

[40] D. Biallo, A. D’Orazio, M. De Sario, V. Marrocco and V. Petruzzelli, “Photonic Crystal Sensors,” Int. Conf. Transparent Optical Networks, Nottingham, England, 2006, pp. 44 – 48

[41] P. S. Dittrich and A. Manz, "Lab-on-a-chip: microfluidics in drug discovery," Nature Reviews Drug Discovery, vol. 5, pp. 210-218, 2006.

[42] H. Kurt and D. S. Citrin, "Photonic crystals for biochemical sensing in the terahertz region," Applied Physics Letters, vol. 87, p. 041108, 2005.

[43] M. Huang, A. A. Yanik, T.-Y. Chang, and H. Altug, "Sub-wavelength nanofluidics in photonic crystal sensors," Optics express, vol. 17, pp. 24224-24233, 2009.

[44] H. Shafiee, E. A. Lidstone, M. Jahangir, F. Inci, E. Hanhauser, T. J. Henrich, et al., "Nanostructured Optical Photonic Crystal Biosensor for HIV Viral Load Measurement," Scientific reports, vol. 4, 2014.

[45] Jiusheng Li, "Terahertz modulator using photonic crystals, Optics Communications", Volume 269, Issue 1, 1 January 2007, Pages 98-101.

[46] H. Nemec, P. Kuzel, L. Duvillaret, A. Pashkin, M. Dressel, and M. T. Sebastian, "Highly tunable photonic crystal filter for the terahertz range," Optics letters, vol. 30, pp. 549-551, 2005.

[47] H. Němec, L. Duvillaret, F. Garet, P. Kužel, P. Xavier, J. Richard, et al., "Thermally tunable filter for terahertz range based on a one-dimensional photonic crystal with a defect," Journal of applied physics, vol. 96, pp. 4072-4075, 2004.

[48] A. Benz, C. Deutsch, M. Brandstetter, A. M. Andrews, P. Klang, H. Detz, et al., "Terahertz active photonic crystals for condensed gas sensing," Sensors, vol. 11, pp. 6003-6014, 2011.

[49] H.Kurt, D. S. Citrin, "Analysis of Photonic crystals for biochemical sensing in the terahertz region using the finite-difference time-domain method with recursive convolution", School of Electrical and Computer Engineering, Georgia Institute of Technology.

[50] Fan, W.-H. Gu, X.-H. Wang, and S.-J. Chang, "Real-time quantitative terahertz microfluidic sensing based on photonic crystal pillar array," Applied Physics Letters, vol. 102, p. 121113, 2013.

[51] W. C. Chew, "Planar Layered Media," in Waves and Fields in Inhomogeneous Media, 1st ed. New York: VNR, 1990, ch. 2, sec. 1, pp.48–49.

[52] L. C. Acosta Silveira, J. A. Hejase, and P. Chahal, "A Terahertz Photonic Crystal Structure for Sensing Applications." Antennas and Propagation Society International Symposium, 2012 IEEE , vol., no., pp.1,2, 8-14 July 2012

[53] Hejase, J.A.; Paladhi, P.R.; Chahal, P., "Terahertz Characterization of Dielectric Substrates for Component Design and Nondestructive Evaluation of Packages," Components, Packaging and Manufacturing Technology, IEEE Transactions on , vol.1, no.11, pp.1685,1694, Nov. 2011

[54] M. Naftaly and R. E. Miles, "Terahertz time-domain spectroscopy for material characterization," Proc. IEEE, vol. 95, no. 8, pp. 1658–1665, Aug, 2007.

[55] A. Podzorov and G. Gallot, "Low-loss polymers for terahertz applications," Appl. Opt., vol. 47, no. 18, pp. 3254–3257, Jun. 2008.

[56] S. Wietzke, C. Jansen, T. Jung, M. Reuter, B. Baudrit, M. Bastian, S. Chatterjee, and M. Koch, "Terahertz time-domain spectroscopy as a tool to monitor the glass transition in polymers," Opt. Exp., vol. 17, no. 21, pp. 19006–19014, Oct. 2009.

[57] J. Balakrishnan, B. M. Fischer, and D. Abbot, "Sensing the hygroscopicity of polymer and copolymer materials using terahertz time-domain spectroscopy," Appl. Opt., vol. 48, no. 12, pp. 2262–2266, Apr. 2009.

[58] A. J. Baragwanath, G. P. Swift, D. Dai, A. J. Gallant, and J. M. Chamberlain, "Silicon based microfluidic cell for terahertz frequencies," Journal of Applied Physics, vol. 108, p. 013102, 2010)

[59] A. Ravindran, K.M. Ragsdell, and G.V. Reklaitis, "Engineering Optimization: Methods and Applications" (Wiley, 2006)

[60] J J. C. Lagarias, J. A. Reeds, M. H. Wright, and P. E. Wright, "Convergence properties of the Nelder--Mead simplex method in low dimensions," SIAM Journal on Optimization, vol. 9, pp. 112-147, 1998

[61] J. A. Nelder and R. Mead, "A simplex method for function minimization," Computer journal, vol. 7, pp. 308-313, 1965.

[62] Zanforlin, L., "Permittivity Measurements of Lossy Liquids at Millimeter-Wave Frequencies," Microwave Theory and Techniques, IEEE Transactions on , vol.31, no.5, pp.417,419, May 1983

[63] Meriakri, V. V. "Beam Waveguide Spectroscopy of Materials in Millimetre and Submillimetre Waves Ranges."

[64] J. Crossley, S. W. Tucker, and S. Walker, "Dielectric studies. Part 5.—Two relaxation processes of cyclopentanone, tetrahydrofuran and thiacyclopentane," Trans. Faraday Soc., vol. 62, pp. 576-584, 1966.

[65] L. Huan, Y. Jian-Quan, L. En-Bang, W. Wu-Qi, Z. Qiang, and W. Peng, "Theoretical analysis of optimum parameters for complete forbidden bands of three-dimensional photonic crystals with typical lattice structures,", Acta Phys. Sin. 55, 230-238, 2006.

[66] S. Fan, P. R. Villeneuve, and J. D. Joannopoulos, "Theoretical investigation of fabrication-related disorder on the properties of photonic crystals," Journal of applied physics, vol. 78, pp. 1415-1418, 1995.

[67] P. Kopperschmidt, "Tetragonal photonic woodpile structures," Applied Physics B, vol. 76, pp. 729-734, 2003.

[68] J. Wu, D. Day, and M. Gu, "A microfluidic refractive index sensor based on an integrated three-dimensional photonic crystal," Applied Physics Letters, vol. 92, p. 071108, 2008

[69] E. Özbay, A. Abeyta, G. Tuttle, M. Tringides, R. Biswas, C. T. Chan, et al., "Measurement of a three-dimensional photonic band gap in a crystal structure made of dielectric rods," Physical Review B, vol. 50, p. 1945-1948, 1994.

[70] E. Özbay, J. Bostak, D. M. Bloom, E. Michel, G. Tuttle, R. Biswas, et al., "Terahertz spectroscopy of three-dimensional photonic band-gap crystals," Optics letters, vol. 19, pp. 1155-1157, 1994.

[71] S.-y. Lin, J. G. Fleming, D. L. Hetherington, B. K. Smith, R. Biswas, K. M. Ho, et al., "A three-dimensional photonic crystal operating at infrared wavelengths," Nature, vol. 394, pp. 251-253, 1998.

[72] K. Y. Park, N. Wiwatcharagoses, and P. Chahal, “Wafer-level Integration of Micro-Lens for THz Focal Plane Array Application”, IEEE 63rd Electronic Components and Technology Conf. Proc., Las Vegas, NV, May, 2013

[73] S.D. Gedney, “Periodic Structures and Floquet’s Theorem,” University of Kentucky, Lexington, Kentucky, Spring 2007, Lecture. http://www.engr.uky.edu/~gedney/courses/ee625/